SLAC-PUB-7930
October 1998

The Standard Model and Why We Believe It

J. L. Hewett

Invited talk presented at Theoretical Advanced Study Institute in Elementary Particle Physics (TASI 97): Supersymmetry, Supergravity, and Supercolliders, 6/1/97—6/7/97, Boulder, CO, USA

Stanford Linear Accelerator Center, Stanford University, Stanford, CA 94309

Work supported by Department of Energy contract DE–AC03–76SF00515.

SLAC-PUB-7930

THE STANDARD MODEL AND WHY WE BELIEVE IT *†

J.L. HEWETT
Stanford Linear Accelerator Center, Stanford, CA 94309

The principle components of the Standard Model and the status of their experimental verification are reviewed.

1 The Standard Model

The Standard Model (SM), which combines the $SU(2)_L \times U(1)_Y$ Glashow - Weinberg - Salam theory of electroweak interactions [1] together with Quantum Chromodynamics,[2] constitutes a remarkable achievement. The formulation of the theory as a renormalizable quantum theory preserves its predictive power beyond tree-level computations and allows for the probing of quantum effects. An array of experimental results confirm every feature of the theory to a high degree of precision, at the level of testing higher order perturbation theory. In fact, at present there are no compelling pieces of evidence that are in conflict with the SM. In these lectures I will review the components of the SM and the extent to which they have been tested.

The strong interactions are described by Quantum Chromodynamics [2] (QCD), which is a non-abelian gauge theory based on SU(3). Each quark flavor is a color triplet in the fundamental representation of $SU(3)_{\rm Color}$ and the SU(3) gauge fields, *i.e.*, the gluons, lie in the adjoint representation $\underline{\mathbf{8}}$. All other particles are color singlets and don't experience strong interactions. The QCD Lagrangian may be written as

$$\mathcal{L}_{QCD} = -\frac{1}{4}\hat{F}^a_{\mu\nu}\hat{F}^{\mu\nu}_a + \bar{\psi}_i(i\gamma^\mu \hat{D}_\mu - m)\psi_i \,, \tag{1}$$

with

$$\hat{F}^a_{\mu\nu} = \partial_\mu G^a_\nu - \partial_\nu G^a_\mu + g_s f^{abc} G_{b\mu} G_{c\nu} \tag{2}$$

being the gluon field tensor and the covariant derivative is defined by $\hat{D}_\mu = \partial_\mu \delta - i g_s T_a G^a_\mu$. Here g_s represents the strong coupling and the indices are summed over color with $a = 1 - 8$ and $i = 1, 2, 3$. T_a and f_{abc} are the SU(3)

*Lectures given at *TASI97: Supersymmetry, Supergravity, and Supercolliders*, Boulder, CO, June 1997.

†Work supported by the Department of Energy, Contract DE-AC03-76SF00515

generators and structure constants, respectively, which obey the usual commutation relation

$$[T_a, T_b] = i f_{abc} T_c \,. \tag{3}$$

The generators are related to the 3×3 Gell-Mann matrices[3] by $T_a = \lambda_a/2$. The Lagrangian is invariant under infinitesimal local gauge transformations. Note that in the limit of equal mass quarks, the QCD Lagrangian possesses a global $\mathrm{SU(N)}_f$ flavor symmetry, and in the limit of massless quarks an $\mathrm{SU(N)}_L \times \mathrm{SU(N)}_R$ chiral symmetry is present. SU(3) gauge invariance ensures that the gluons are massless.

The Standard Model of electroweak interactions [1] is based on the gauge group $\mathrm{SU(2)}_L \times \mathrm{U(1)}_Y$, where the generators of $\mathrm{SU(2)}_L$ correspond to the three components of weak isospin T_i and the $\mathrm{U(1)}_Y$ generator to the weak hypercharge Y. These are related to the electric charge by $Q = T_3 + Y/2$. The Lagrangian describing the electroweak interactions is

$$\begin{aligned}\mathcal{L}_{EW} = & -\frac{1}{4} F^a_{\mu\nu} F_a^{\mu\nu} - \frac{1}{4} G_{\mu\nu} G^{\mu\nu} + i \bar{\psi}_j \gamma^\mu D_\mu \psi_j \\ & + (D_\mu \Phi)(D^\mu \Phi)^\dagger - \mu^2 \Phi^\dagger \Phi - \lambda (\Phi^\dagger \Phi)^2 \\ & + \lambda_{e_k} \bar{L}_{L_k} \Phi e_{R_k} + \lambda_{u_{jk}} \bar{Q}_{L_j} \tilde{\Phi} u_{R_k} + \lambda_{d_{jk}} \bar{Q}_{L_j} \Phi d_{R_k} + h.c.\,,\end{aligned} \tag{4}$$

with the field strength tensors

$$\begin{aligned} F^a_{\mu\nu} &= \partial_\mu B^a_\nu - \partial_\nu B^a_\mu + g \epsilon^{abc} B_{b\mu} B_{c\nu} \,, \\ G_{\mu\nu} &= \partial_\mu C_\nu - \partial_\nu C_\mu \,, \end{aligned} \tag{5}$$

for the three non-abelian fields of $\mathrm{SU(2)}_L$ and the single abelian gauge field associated with $\mathrm{U(1)}_Y$, respectively. The covariant derivative is

$$D_\mu = \partial_\mu - i g T_a B^a_\mu - i g' \frac{Y}{2} C_\mu \,, \tag{6}$$

with $g\,, g'$ being the $\mathrm{SU(2)}_L$, $\mathrm{U(1)}_Y$ coupling strength, respectively. The SU(2) generators obey the usual relation $[T_a, T_b] = i\epsilon_{abc} T_c$ and are related to the Pauli spin matrices by $T_a = \tau_a/2$. This Lagrangian is invariant under the infinitesimal local gauge transformations for $\mathrm{SU(2)}_L$ and $\mathrm{U(1)}_Y$ independently. Being in the adjoint representation, the $\mathrm{SU(2)}_L$ massless gauge fields form a weak isospin triplet with the charged fields being defined by $W^\pm_\mu = (B_1 \mp i B_2)_\mu/\sqrt{2}$. The neutral component of B_a mixes with the abelian gauge field to form the physical states

$$\begin{aligned} Z_\mu &= B^3_\mu \cos\theta_w + C_\mu \sin\theta_w \,, \\ A_\mu &= C_\mu \cos\theta_w - B^3_\mu \sin\theta_w \,, \end{aligned} \tag{7}$$

where $\tan\theta_w = g'/g$ is the weak mixing angle.

To generate the left-handed structure of the weak charged current interactions, the SU(2) symmetry is applied to left-handed fermion fields only. The fermion fields are thus given by

$$\psi_L: \quad L_{L_k} = \frac{1}{2}(1-\gamma_5)\begin{pmatrix}\nu_k\\ e_k\end{pmatrix}, \qquad Q_{L_k} = \frac{1}{2}(1-\gamma_5)\begin{pmatrix}u_k\\ d_k\end{pmatrix}, \tag{8}$$

for the $\mathrm{SU}(2)_L$ left-handed doublets and

$$\psi_R: \quad e_{R_k} = \frac{1}{2}(1+\gamma_5)e\,, \quad u_{R_k} = \frac{1}{2}(1+\gamma_5)u\,, \quad d_{R_k} = \frac{1}{2}(1+\gamma_5)d\,, \tag{9}$$

for the right-handed singlets, with $k = 1-3$ being a generation index. The usual convention is that right-handed neutrinos are not introduced. With quarks having three colors, the quantum numbers for this set of fermions ensures the cancellation of divergent chiral anomaly diagrams. The λ_i in Eq. (4) above are the Yukawa couplings of the quarks and leptons.

Masses for the non-abelian gauge fields and fermions are generated by the Higgs mechanism [4] via spontaneous symmetry breaking (SSB) which preserves [5] the renormalizability of the gauge theory. The Higgs fields are complex scalar iso-doublets (ϕ^+, ϕ^0) with electroweak interactions described by the second line in Eq. (4). For the choice $\mu^2 < 0$, the ground state of the theory is obtained when the neutral member of the Higgs doublet acquires a vacuum expectation value (vev),

$$\langle\Phi\rangle = \begin{pmatrix}0\\ \frac{v}{\sqrt{2}}\end{pmatrix}, \tag{10}$$

where v is given by $v^2 = -\mu^2/\lambda$. This non-vanishing vev selects a preferred direction in $\mathrm{SU}(2)_L\times\mathrm{U}(1)_Y$ space and spontaneously breaks the theory, leaving the $\mathrm{U}(1)_{\mathrm{em}}$ subgroup intact. $\mathrm{U}(1)_{\mathrm{em}}$ would be broken as well if the ϕ^+ field were also allowed to obtain a vev. ϕ^0 is then redefined by $\phi^0 = (H+v)/\sqrt{2}$, such that the physical field H has a vanishing vev and positive mass squared. The remaining degrees of freedom, *i.e.*, the Goldstone bosons, are gauged away from the scalar sector, but essentially reappear in the gauge sector, providing the longitudinal modes for the W and Z bosons. An examination of the v^2 terms in the kinetic piece of the scalar Lagrangian reveals the mass terms for the physical gauge bosons,

$$M_W = \frac{1}{2}gv\,, \qquad M_Z = \frac{v}{2}\sqrt{g^2+g'^2}\,, \qquad M_A = 0\,. \tag{11}$$

In order to obtain Quantum Electrodynamics (QED) the massless A_μ is identified with the photon and $e \equiv g \sin\theta_w$. The QED and weak charged and neutral currents become

$$\begin{aligned} J_\mu^{em} &= \bar{\psi}\gamma_\mu Q \psi \,, \\ J_\mu^{CC} &= \bar{\psi}\gamma_\mu T_L^{\pm} \psi \,, \\ J_\mu^{NC} &= \bar{\psi}(T_{3L} - x_w Q)\psi \,, \end{aligned} \tag{12}$$

with the interaction terms being

$$\mathcal{L} = e J_\mu^{em} A^\mu + \frac{g}{\sqrt{2}} J_\mu^{CC} W^\mu + \frac{g}{\cos\theta_w} J_\mu^{NC} Z^\mu \,. \tag{13}$$

Here, $x_w \equiv \sin^2\theta_w$ and the $T_L^{\pm} \equiv (T_1 \pm i T_2)_L/\sqrt{2} = \tau^{\pm}/2$ operations act on the left-handed isodoublets ψ_L, and vanish on ψ_R. Comparison with the Fermi theory of weak interactions yields the relation

$$\frac{G_F}{\sqrt{2}} = \frac{g^2}{8 M_W^2} \,, \tag{14}$$

where G_F is the Fermi constant and is well determined from μ decay. Eq. (11) relates the gauge bosons masses by $M_Z = M_W/\cos\theta_w$. A commonly used parameter, defined by

$$\rho = \frac{M_W^2}{M_Z^2 \cos^2\theta_w} \,, \tag{15}$$

measures the ratio of the charged to neutral current strengths. It is unity at tree-level in the SM with one Higgs doublet. For a more general set of Higgs representations with weak isospin T_i and vev's v_i it is given by

$$\rho = \frac{\sum_i [T_i(T_i+1) - T_{i3}^2] v_i^2}{\sum_i 2 T_{i3}^2 v_i^2} \,. \tag{16}$$

After SSB, the last line of Eq. (4) gives the physical Higgs - fermion interactions and generates masses for the fermions, $m_f = \lambda_f v/\sqrt{2}$. Diagonalization of the masses in the quark sector introduces the weak mixing, or Cabibbo-Kobayashi-Maskawa (CKM) matrix,[6] which then appears in the hadronic weak charged current.

Having briefly introduced the essential ingredients of the SM, we now pause to examine its general features and success as a theory. Three principle assumptions went into the building of the theory:

- The gauge group is $\mathrm{SU}(3)_C \times \mathrm{SU}(2)_L \times \mathrm{U}(1)_Y$

- There is one Higgs doublet
- The fermion representations are left-handed weak isodoublets and right-handed singlets

In addition to these assumptions the theory contains 21 *a priori* free parameters:

- 3 coupling constants
- 12 fermion masses
- 4 fermion mixing parameters
- 1 Higgs mass
- 1 independent gauge boson mass

These parameters are inserted into the framework of the SM by hand. The missing ingredients of the model are, of course, the Higgs boson which has yet to be discovered, and the τ-neutrino for which there is only indirect evidence at present. However, since experiment is now sensitive to loop-level effects, indirect constraints on the Higgs boson mass have been obtained. These bounds will be discussed at length below. The successes of the SM as a theory can be listed as:

- Renormalizability
- Unitarity
- Unification of the electromagnetic and weak forces
- Prediction of a specific relationship between W and Z boson masses
- The weak charged and neutral current structure agrees with experiment
- All aspects have impressive agreement with all experimental data

Despite these successes there remain a number of important questions which the SM does not address. These include:

- The fermion masses and mixings and the nature of CP-violation
- Neutrino masses and oscillations
- The number of generations

- Parity violation in the weak interactions
- Suppression of strong CP phase
- What is the electroweak symmetry breaking mechanism (is there really a light Higgs doublet, or do the gauge bosons become strongly interacting at the TeV scale) and how is the hierarchy maintained
- Unification with the strong and gravitational forces
- Charge quantization, *i.e.*, why does $Q_e = -Q_p$
- Origin of dark matter
- Baryogensis
- Cosmological constant
- Why is spacetime 4 dimensional?

This list of unanswered questions provides the principle motivation for consideration of physics beyond the SM. Numerous theories are studied in the hope that they will address at least one of these issues. However, no single theory has been invented that successfully addresses all of these questions simultaneously. Unfortunately, since all data agree with the SM, there is not one shred of experimental evidence to provide guidance for extending the theory, or to indicate that physics beyond the SM exists.

For the remainder of these lectures, I will discuss the theoretical predictions of the SM at the quantum level, and the experimental techniques and accuracy by which the elements of the SM have been determined. Here, it is interesting to provide a short historical perspective. In the mid 1980's, when I was a student at TASI, the elements of the SM which still awaited experimental confirmation were:

- Verify the multiplet structure of fermions (find top!)
- Demonstrate asymptotic freedom over a wide range of Q^2
- Confirm universality
- Extract $\sin^2\theta_w$ from numerous experiments and compare
- Measure the W and Z boson properties
- Prove it's a gauge theory (measure self-interactions)

- Find the Higgs

Except for discovering the Higgs, this list of measurements has now been completed at various levels of sensitivity. For example, $\sin^2\theta_w$ is now determined to the level of 0.1% (!), whereas we are just now entering the era where the gauge self-interactions are being probed at an interesting level. It is clear that we have made substantial progress verifying the SM in the last decade, however, it is time to move on (experimentally and theoretically) to what lies beyond.

2 Tests of QCD

The basic building blocks of the strong interactions have been presented in the previous section and here we focus on the experimental verification of the various components of the QCD Lagrangian. Due to the principle of asymptotic freedom, which we discuss below, the renormalized strong coupling is small only at high energies. Hence perturbation theory is only valid and precision experimental tests can only be performed in this domain. Although much progress has recently been made [7] in quantifying QCD predictions in the non-perturbative region via lattice gauge theory or for soft hadronic processes, we will concentrate solely on the perturbative regime.

The basic perturbative processes responsible for the production of hadronic final states in a variety of interactions are schematically represented in Fig. 1. In contrast to the other reactions, we see that in e^+e^- annihilation all hadronic activity is confined, by construction, to the final state; there are no beam remnants to consider, the hadronic center of mass frame coincides with the lab frame, there are no parton density uncertainties, and there are fewer Feynman diagrams to compute at a given order in perturbation theory. Electron-positron colliders thus provide a clean and less complicated laboratory for precise QCD studies, both from the experimental and theoretical points of view, and our review is biased in this direction.

We now discuss the principle features of QCD and the experimental evidence which supports QCD as being the underlying theory of the strong interactions.[8] We first list these features:

- Quarks exist as spin 1/2 color triplets
- Gluons exist as spin 1 color octets
- The $q\bar{q}g$ coupling exists
- The non-abelian triple and quartic gluon couplings exist
- Asymptotic Freedom

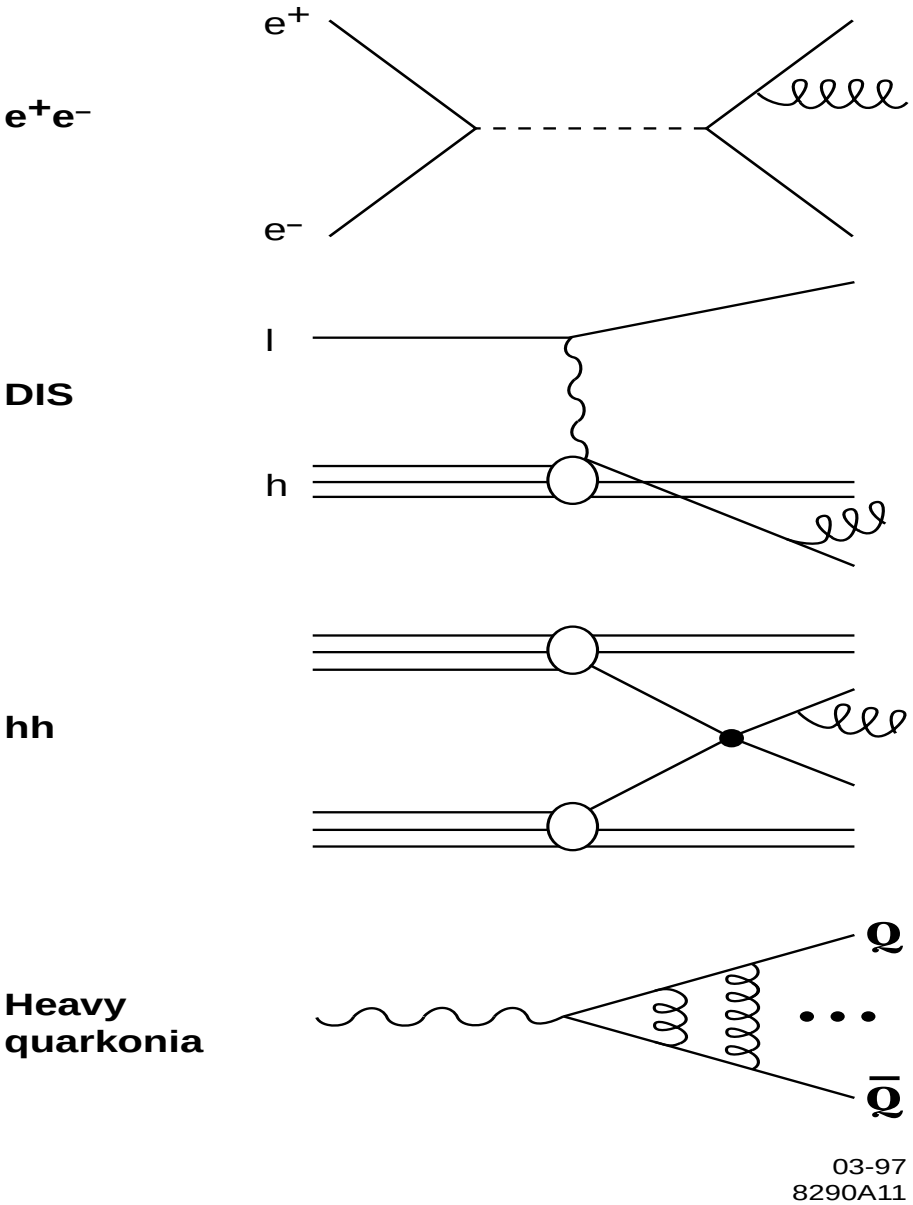

Figure 1: Diagrams representing the basic processes of hadronic production in e^+e^- annihilation, deep inelastic lepton-hadron scattering, hadronic collisions, and heavy quarkonia production and decay.

- Flavor independence of α_s,

and then demonstrate their validity by concentrating on n-jet events in e^+e^- annihilation.

2.1 2-jet Events

The first direct evidence for the existence of quarks came from deep inelastic electron-nucleon scattering at SLAC in the 1960s, which established that the electrons were scattering off of point-like particles in the nucleus. Jet production was first observed in e^+e^- annihilation via $e^+e^- \to q\bar{q}$ by the Mark I experiment at SPEAR. At higher energies, the quark-parton model suggests that the transverse momenta of quark fragmentation products remains small since it arises mainly from soft processes, whereas the longitudinal momenta increases with quark energy, leading to jet production. In order to describe the degree of jet-like behavior, event shape variables, which characterize the spatial distribution of particles in hadronic events, were introduced. One such variable, which describes the extent of isotropy in the particle flow, is sphericity,

$$S = \frac{3}{2} \frac{\text{Min}\left[\sum_i (p_{Ti})^2\right]}{\sum_i p_i^2}\,, \tag{17}$$

where the sum is carried out over all the final state particles in an event, and the subscript T denotes the transverse momentum component. The axis which minimizes the sum in the numerator is known as the sphericity axis. Sphericity lies in the range $0 \leq S \leq 1$, where 0 represents perfectly collimated back-to-back jets, and $S = 1$ corresponds to completely isotropic or spherical events. The sphericity distributions from Mark I [9] are presented in Fig. 2. A marked shift towards lower sphericity with increasing center of mass energy is clearly present, indicating the onset of jet production. These observations have since been corroborated at higher energy, such as on the Z-pole where the jets are almost perfectly collimated.

Although sphericity is an experimentally useful variable, it is not directly calculable in perturbation theory, essentially due to its quadratic form. At higher order in perturbation theory a quark can split into a collinear quark-gluon pair which not only results in an divergence in the massless limit, but also gives substantially different contributions to the quadratic function than that of the original quark. Monte Carlo simulations of the fragmentation process must then be performed, introducing additional uncertainties. One means around this is to integrate the cross section over finite ranges of energy and angles. Sterman and Weinberg [10] computed the cross section for the case where a fraction of $1 - \epsilon$ or more of the total energy is emitted within two

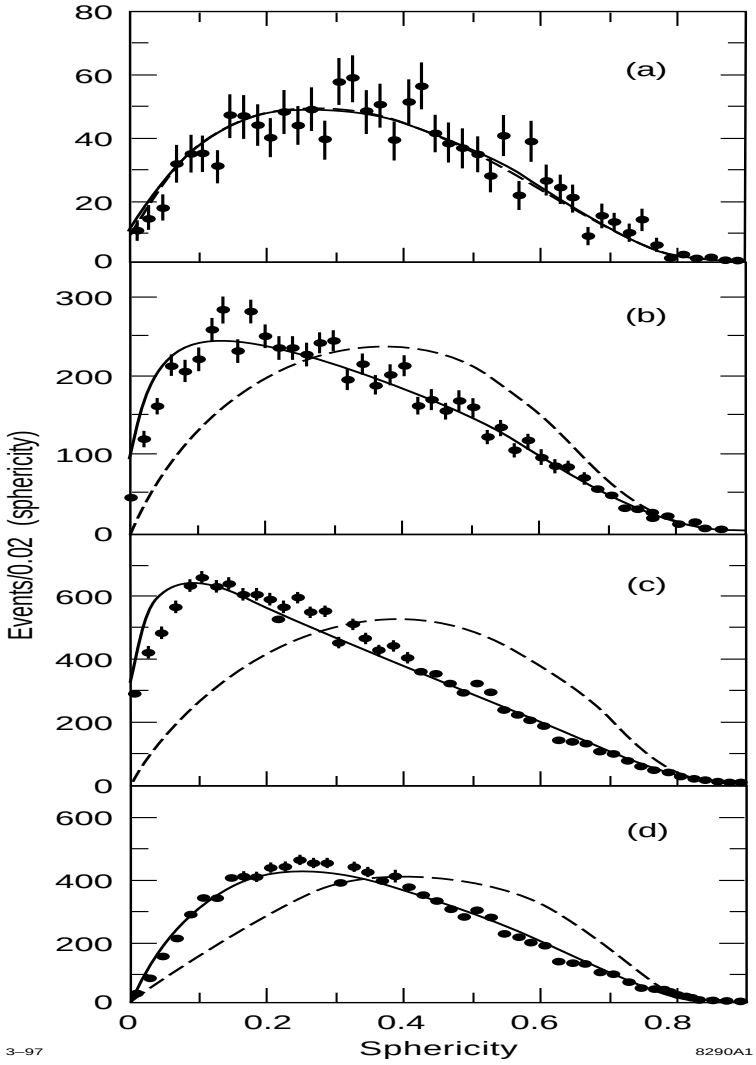

Figure 2: Sphericity distributions from Mark I [9] measured at $\sqrt{s}$ = (a) 3.0 GeV, (b) 6.2 GeV, and (c) 7.4 GeV. (d) Distribution at 7.4 GeV for a subset of events with particles having scaled momentum $2p/Q < 0.4$. The dashed curves represent the expectations for a phase space model of hadron production, while the solid curves correspond to parton model jet production.

oppositely directed cones of half-angle δ, making an angle θ with respect to the beam axis. In this case the collinear singularities approximately cancel to a given order in perturbation theory as long as $\epsilon, \delta \ll 1$. Another way to avoid the problems associated with collinear splittings is to introduce jet variables which are based on linear sums of particle momenta. Three such collinear and infrared safe shape variables that are commonly used are thrust, acoplanarity, and spherocity, defined by

$$\begin{aligned} T &= \text{Max} \left[\frac{\sum_i |\mathbf{p}_i \cdot \mathbf{n}|}{\sum_i |\mathbf{p}_i|} \right] , \\ A &= 4\,\text{Min} \left[\frac{\sum_i |\mathbf{p}_i \cdot \mathbf{n}'|}{\sum_i |\mathbf{p}_i|} \right]^2 , \\ S' &= \frac{16}{\pi^2}\,\text{Min}\, \frac{\left[\sum_i E_i |\sin\theta_i|\right]^2}{E_{tot}^2} . \end{aligned} \tag{18}$$

Here $\mathbf{n}(\mathbf{n}')$ is a unit vector chosen to maximize (minimize) the numerator and define the thrust axis (event plane), and θ_i is the angle between $\mathbf{p}_i$ and $\mathbf{n}$. These variables have the ranges, $1/2 \le T \le 1$, $0 \le A, S' \le 1$. The thrust distribution becomes narrower and more peaked towards unity as the total energy increases, while the acoplanarity defines the flatness of an event.

In e^+e^- collisions the spin of the quark was determined by examining the angular distributions of the sphericity and thrust axes. A fit to the functional forms (where P is the degree of transverse polarization that built up at SPEAR due to a synchrotron radiation effect)

$$\begin{aligned} \frac{dN}{d\cos\theta} &\propto 1 + \alpha\cos^2\theta + P^2\alpha\sin^2\theta\cos 2\phi\,, \\ \frac{dN}{d\cos\theta} &\propto 1 + a_{S,T}\cos^2\theta_{S,T}\,, \end{aligned} \tag{19}$$

yielded $\alpha = 0.78 \pm 0.12$ at 7.4 GeV from Mark I [11] and $a_S = 1.03 \pm 0.07$ and $a_T = 1.01 \pm 0.06$ at 35 GeV from TASSO.[12] These fits are all close to unity, which is what is expected [13] for the pair production of fermions.

That fact that quarks are color triplets was established experimentally in e^+e^- annihilation by the R-ratio, *i.e.*, the ratio of the hadronic cross section to the point cross section,

$$R^{(0)} = \frac{\sigma(e^+e^- \to \text{hadrons})}{\sigma_{QED}(e^+e^- \to \mu^+\mu^-)} = N_c \sum_f Q_f^2\,, \tag{20}$$

where we have given the leading order parton model expectation at values of s not close to quark thresholds, with Q_f being the charge of the quark flavor f.

A summary of measurements of the R-ratio below the Z boson resonance from Ref. [14] is shown in Fig. 3. We see that the leading order quark parton model prediction is consistent with the data only if each quark flavor has 3 colors. The excess in the R-ratio over the these parton model predictions provides support for QCD radiative corrections; this additional contribution arises from gluon emission. The higher-order corrections have been calculated to 3-loops [15] and can be expressed as

$$R = R^{(0)} \left[1 + \frac{\alpha_s}{\pi} + C_2 \left(\frac{\alpha_s}{\pi} \right)^2 + C_3 \left(\frac{\alpha_s}{\pi} \right)^3 + \cdots \right] , \tag{21}$$

with $C_2 = 1.411$ and $C_3 = -12.8$. From looking at the figure, we also see that the relative size of this excess tends to decrease, roughly logarithmically, with Q^2; this is a consequence of asymptotic freedom, which will be discussed further below. Production cross sections in e^+e^- annihilation are often quoted in units of R, where R represents the point cross section for μ pair production in QED, *i.e.* the denominator in Eq. (20) above. $1\,R = 4\pi\alpha^2/3s = 87\text{fb}/s(\text{TeV}^2)$.

Of course, the fact that quarks are color triplets is also required by the quark parton model in order not to violate the Pauli exclusion principle when forming the spin-3/2 baryon states such as the Δ^{++} and the Ω^-.

2.2 Three-jet events

The existence of the gluon and its coupling to quarks was established by the observation of 3-jet events at $\sqrt{s} \approx 30$ GeV at PETRA [16]. These events were interpreted in terms of the process $e^+e^- \to q\bar{q}g$ and provided direct evidence for the $q\bar{q}g$ coupling. Simply by event counting, it was determined that [17]

$$\frac{\text{Number } (3-\text{jet events})}{\text{Number } (2-\text{jet events})} \approx 0.15 \tag{22}$$

at this center of mass energy. At lowest order in perturbative QCD, this ratio is just the probability of gluon emission and thus provided a first direct measurement of the strong coupling constant α_s.

The spin of the gluon can be determined by analyzing the jet energy and angular distributions of three-jet events. It is common practice to label the three jet energies in terms of the ordering $E_1 > E_2 > E_3$ and to define the scaled jet energies $x_i \equiv 2E_i/Q$ such that the relation $x_1 + x_2 + x_3 = 2$ holds. Performing a Lorentz boost into the rest frame of jets 2 and 3, the Ellis-Karliner angle [18] can be defined as the angle between jets 1 and 2 in this frame. At lowest order with massless partons, we have

$$\cos\theta_{EK} = \frac{x_2 - x_3}{x_1} . \tag{23}$$

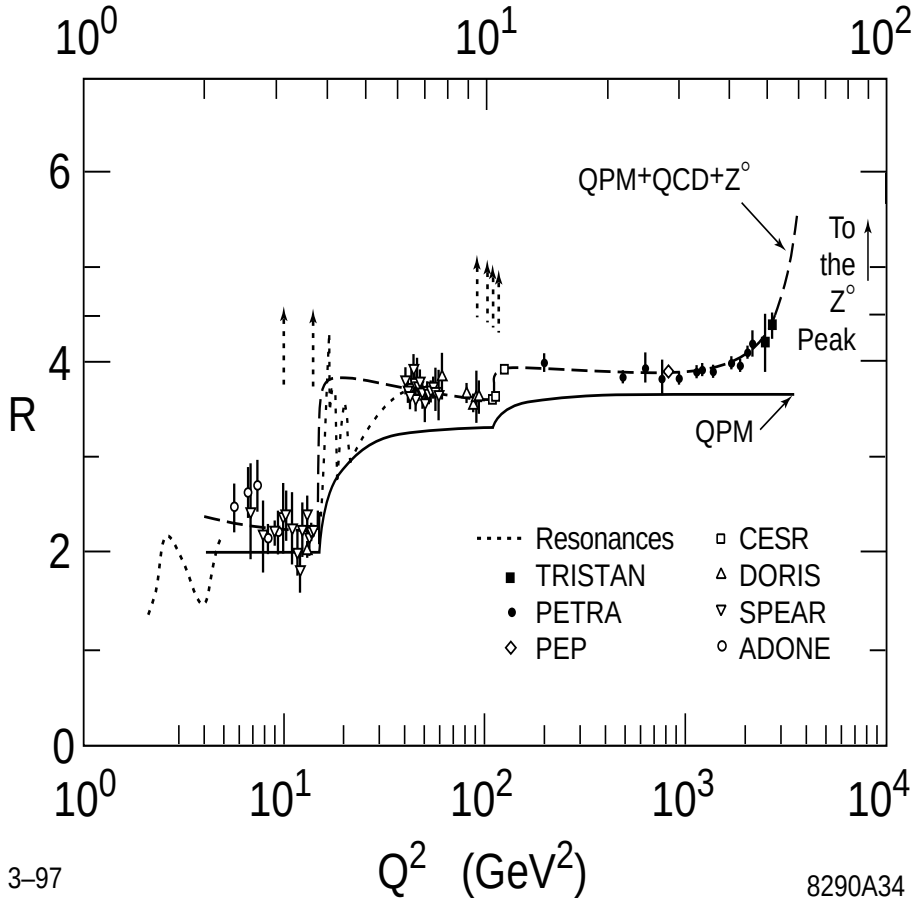

Figure 3: Summary of measurements of the R-ratio as a function of center of mass energy. The expectations of the quark parton model alone and including QCD and electroweak radiative corrections are given by the solid and dashed curves, respectively. The dashed arrows represent onset of the charmonium and upsilon resonances.

This angle is particularly sensitive to the spin of the gluon. Figure 4 displays the x_i and Ellis-Karliner angle distributions for 3-jet events as determined [19] by SLD at $\sqrt{s} = M_Z$. In this figure, the data is compared with expectations for the distributions from leading-order vector, scalar, and tensor gluon models; it is clear that the data prefer the vector case.

We now return to the subject of collinear singularities in 3-jet events, which we briefly discussed above. The leading order normalized differential cross section for $e^+e^- \to q\bar{q}g$ in the massless limit is

$$\frac{1}{\sigma_{\rm total}} \frac{d\sigma}{dx_1 dx_2} = \frac{2\alpha_s}{3\pi} \frac{x_1^2 + x_2^2}{(1-x_1)(1-x_2)} \,. \tag{24}$$

Here, the indices 1 and 2 now label the scaled jet energies of the quark and anti-quark. This expression is clearly singular when $x_i \to 1$; this behavior is exhibited in two distinct physical situations. (i) Infrared divergences occur when the gluon is soft, *i.e.*, when both $x_1, x_2 \sim 1$. (ii) Collinear singularities occur when the gluon is emitted parallel to either of the quark jets, *i.e.*, either x_1 or $x_2 \sim 1$. These singularities are cancelled by terms higher order in perturbation theory. However, in practice a real-life detector cannot resolve 3-jet events if the gluon is very soft or collinear. The procedure introduced by Sterman-Weinberg [10] is sometimes employed. The definition of the 3-jet fraction is then

$$\begin{aligned} (1-f) &= \frac{\sigma_{3-\rm jet}}{\sigma_{\rm total}} \\ &= \int_{\epsilon,\delta} \frac{1}{\sigma_{\rm total}} \frac{d^2\sigma_{3-\rm jet}}{dx_1 dx_2} \\ &= \frac{4\alpha_s}{3\pi} [4 \ln\delta \ln 2\epsilon + 3\ln\delta + \frac{\pi^2}{3} - \frac{7}{4}] \,, \end{aligned} \tag{25}$$

where ϵ and δ are as defined in the previous section, and f represents the fraction of total cross section in which all but ϵ of the total energy is deposited into two cones of opening angle δ.

An alternative approach in defining the 3-jet cross section which has become more popular is to introduce the variable $y_{\rm cut}$. At the parton level for $e^+e^- \to q(p_1) + \bar{q}(p_2) + g(p_3)$, one demands that the invariant mass of any pair of final state momenta be greater than some minimum value, *i.e.*, $(p_i + p_j)^2/s \geq y_{\rm cut}$. With this requirement, the integration over the infrared and collinear divergences is rendered finite, since all jet (*i.e.*, parton) energies are now required to exceed $y_{\rm cut}\sqrt{s}$ and the opening angle between two partons

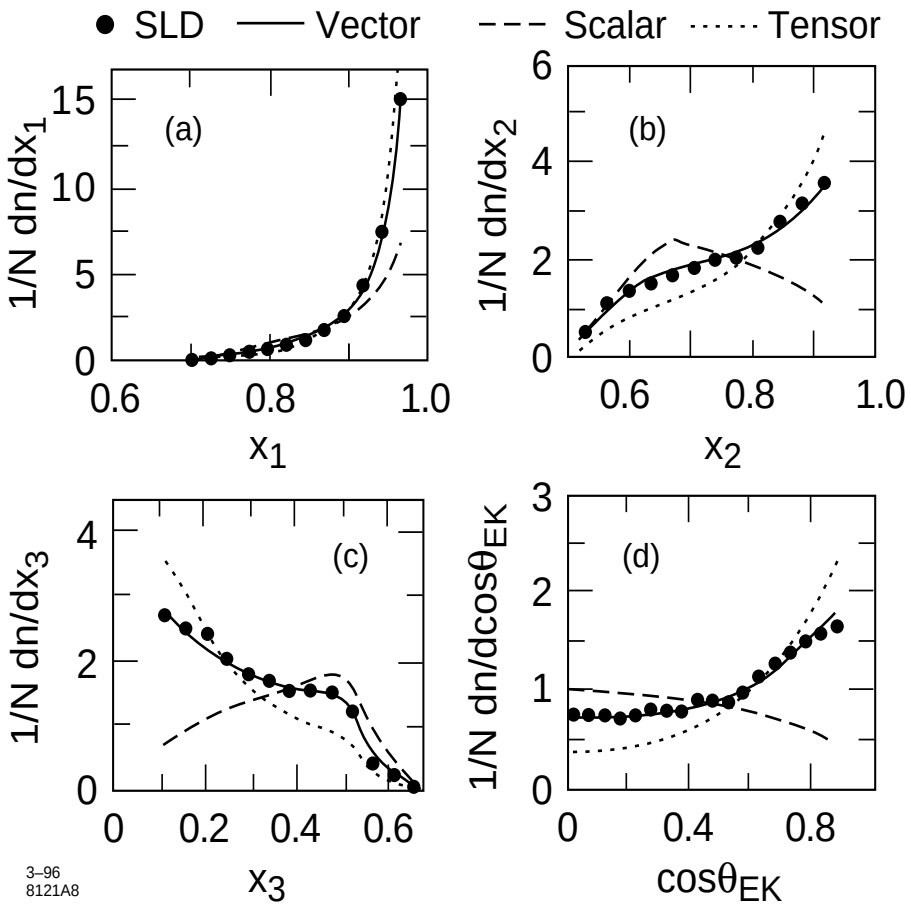

Figure 4: Scaled jet energy and Ellis-Karliner angle distributions in 3-jet events as measured by SLD. Also shown are the predictions from leading-order vector, scalar, and tensor gluon models. From [19].

satisfies $x_i x_j (1 - \cos\theta_{ij}) \geq 2y_{\rm cut}$. In this case one obtains

$$\frac{\sigma_{3-\rm jet}}{\sigma_{\rm total}} = \int_{2y_{\rm cut}}^{1-y_{\rm cut}} dx_1 \int_{1+y_{\rm cut}-x_1}^{1-y_{\rm cut}} dx_2 \, \frac{1}{\sigma_{\rm total}} \frac{d^2\sigma_{3-\rm jet}}{dx_1 dx_2} \, . \tag{26}$$

Another property of QCD that can be verified in 3-jet events is that the strong coupling between quarks and gluons be independent of quark flavor. This is required by gauge invariance and renormalizability. While theoretical and experimental uncertainties, such as those discussed above, limit the absolute precision to which α_s can be determined in such events, the ratio of the couplings for different quark flavors can provide an accurate test of flavor independence as most of the uncertainties cancel in the ratio. The first such comparisons [20] were performed at PETRA with the limited precision of $\delta\alpha_s^c/\alpha_s^{\rm all} = 0.41$ and $\delta\alpha_s^b/\alpha_s^{\rm all} = 0.57$; these measurements were hampered by low statistics and poor heavy quark tagging capabilities. Much better accuracy has recently been obtained at the Z-boson resonance due to the large available data sample and the use of micro-vertex detectors for improved heavy quark tagging. For example, the SLD Collaboration finds [21]

$$\begin{aligned}
\alpha_s^{uds}/\alpha_s^{\rm all} &= 0.987 \pm 0.010(stat)^{+0.012}_{-0.010}(sys)^{+0.009}_{-0.008}(theory) \, , \\
\alpha_s^{c}/\alpha_s^{\rm all} &= 1.023 \pm 0.034(stat)^{+0.032}_{-0.036}(sys)^{+0.018}_{-0.014}(theory) \, , \\
\alpha_s^{b}/\alpha_s^{\rm all} &= 0.993 \pm 0.016(stat)^{+0.020}_{-0.023}(sys)^{+0.019}_{-0.027}(theory) \, ,
\end{aligned} \tag{27}$$

which is consistent with the strong coupling being independent of quark flavor.

2.3 Multi-Jet Events

The non-abelian triple gluon vertex and the Casimir classification of the tree-level QCD couplings can be probed in 4-jet production in e^+e^- annihilation. The tree-level Feynman diagrams responsible for 4-jet production are displayed in Fig. 5. Figures 5(a) and (b) correspond to double bremsstrahlung diagrams, and have the characteristic that the primary jets originating from the q and $\bar{q}$ are the most energetic. Figure 5(d) illustrates the gluon splitting into a quark pair; here the radiated $q\bar{q}$ tend to be produced along the axis normal to the primary $q\bar{q}$ plane. Figure 5(c) represents the non-abelian triple gluon vertex. In this case the gg pair tend to be produced in the plane of the primary $q\bar{q}$ pair. This diagram has no analog in QED.

In any general gauge group obeying a Lie algebra the couplings of the fermions to the gauge fields and of the gauge self-interactions in the non-abelian case are determined by the coupling constant and the Casimir operators of the gauge group. The Casimir operators are invariant operators which commute

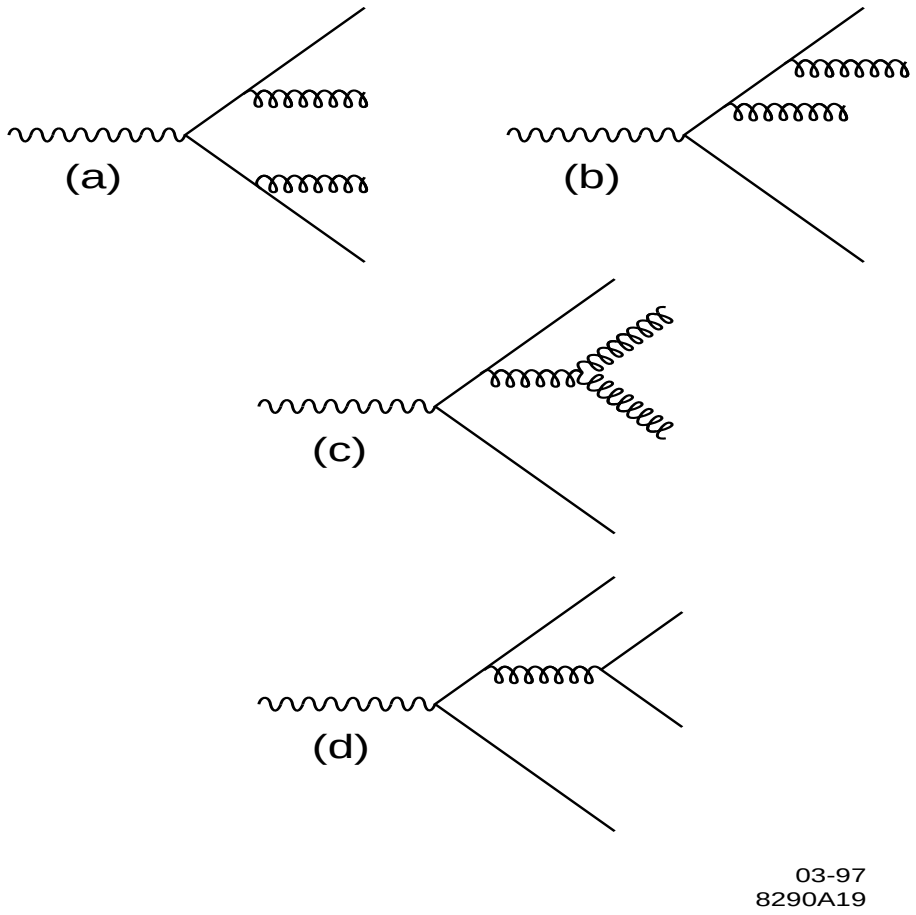

Figure 5: Set of tree-level diagrams responsible for 4-jet production in e^+e^- collisions.

Group	C_A	C_F	T_F
U(1)	0	1	1
$U(1)_3$	0	1	3
SU(N)	N	$(N^2-1)/2N$	1/2
SU(3)	3	4/3	1/2

Table 1: Casimir factors for some common gauge groups. $U(1)_3$ represents the abelian gluon model.

with the generators of the gauge group. Determination of the eigenvalues of these operators probes the underlying structure of the theory in a gauge invariant manner. The relations

$$\begin{aligned} \sum_a (T^a T^{\dagger a})_{ij} &= \delta_{ij} C_F \,, \\ \sum_{a,b} (f^{abc} f^{*abd}) &= \delta^{cd} C_A \,, \\ \sum_{ij} T^a_{ij} T^{\dagger b}_{ji} &= \delta^{ab} T_F \,, \end{aligned} \tag{28}$$

define the eigenvalues $C_F\,, C_A\,, T_F$, which are the color factors of QCD. The Casimir factors for various gauge groups, including $SU(3)_C$, are listed in Table 1. The tree-level couplings present in QCD can be classified in terms of the eigenvalues of the Casimir operators as illustrated in Fig. 6. Note that the direction of momentum flow is relevant in these diagrams.

How well can these color factors be probed in 4-jet events? To answer this, one must first compute the 4-jet production cross section to a consistent order in perturbation theory. To lowest order, this entails computing the tree-level diagrams in Fig. 5 as well as the 2- and 3-jet amplitudes to a consistent order in perturbation theory. The terms which correspond to 4-jet production can then be identified in a gauge consistent manner, and yield the expression

$$\begin{aligned} \frac{1}{\sigma_0} d\sigma^{(4)} = \left(\frac{\alpha_s C_F}{\pi}\right)^2 \Bigg[& F_A + \left(1 - \frac{C_A}{2C_F}\right) F_B + \frac{C_A}{C_F} F_C \\ & + \frac{T_F}{C_F} N_f F_D + \left(1 - \frac{C_A}{2C_F}\right) F_E \Bigg] \,, \end{aligned} \tag{29}$$

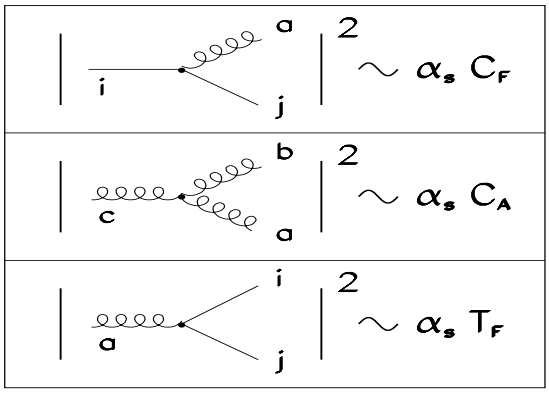

Figure 6: Casimir classification of the tree-level couplings present in QCD.

where $F_{A...E}$ are kinematical functions. We note that the complete next-to-leading (NLO) 4-jet production cross section has recently been computed [22] and that it is in excellent agreement with experiment. We see that the kinematical distributions of the above cross section depend on the ratios C_A/C_F and T_F/C_F, as well as the number of flavors N_f, which in principle can then be determined by experiment. In fact, numerous 4-jet event shape observables have been proposed which are sensitive to these ratios of color factors. A determination [23] of these ratios by ALEPH is presented in Fig. 7; also shown in the figure are the expectations from several potential gauge groups. We see that only the groups SU(3), SU(4), SP(4), and SP(6) are consistent with the data. However, the latter three groups, SU(4), SP(4), and SP(6), do not contain 3 degrees of freedom for the quark color representation, leaving SU(3) as the only viable gauge theory for QCD. We also note that the observation of a nonzero value of C_A/C_F provides evidence for the existence of the gluon three-point function. In order that the theory of QCD be gauge-invariant and self-consistent, this implies that the quartic gluon self-interaction must also

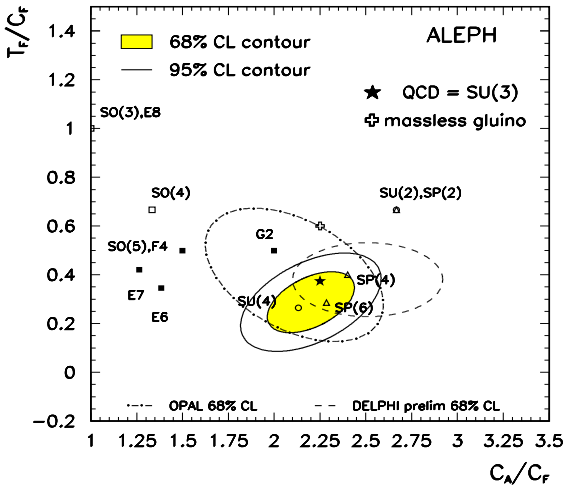

Figure 7: Measurement of the QCD color factors from Ref. [23].

exist.

However, it should come as no surprise that direct experimental verification of the quartic gluon vertex requires 5-jet production in e^+e^- annihilation! Performing a computation of the 5-jet cross section similar to that above for 4jets, which is gauge invariant and consistent in perturbation theory, schematically yields

$$\frac{1}{\sigma_0} d\sigma^{(5)} = \frac{1}{\sigma_0} d\sigma^{2q3g} + \frac{1}{\sigma_0} d\sigma^{4q1g} \,. \tag{30}$$

The first term contributes approximately 85% of the total cross section and can be written as

$$\frac{1}{\sigma_0} d\sigma^{2q3g} = \left(\frac{\alpha_s C_F}{\pi}\right)^3 \left[G_A + \frac{C_A}{C_F} G_B + \left(\frac{C_A}{C_F}\right)^2 G_C\right] , \tag{31}$$

where $G_{A,B,C}$ are again kinematical functions. It is the last term in this expression which corresponds to the quartic gluon coupling. In principle a set of 5-jet event shape observables can be analogously defined, however, the data is not yet sufficient to show statistically significant evidence for the quartic gluon term.[23]

2.4 Renormalization of the Strong Coupling and Asymptotic Freedom

When evaluating processes beyond tree-level it is necessary to define a renormalized coupling constant. Loop-level diagrams contain divergent integrals over the loop momenta which must be regularized by some procedure that re-expresses the divergences in a well defined manner. The regularized divergences are then removed by absorbing them into the definitions of physical quantities via renormalization. This procedure is performed by a specified prescription, of which many are available, and introduces a new scale, μ. All renormalized quantities depend on this scale, however different prescriptions must lead to the same observable amplitudes.

As an example, consider a single particle irreducible Green's function Γ, which cannot be disconnected by a cut on any single internal line. The introduction of an ultra-violet cut-off, Λ, in the loop momentum integrals controls the divergences and yields the unrenormalized Green's function $\Gamma_U(p_i, g_0, \Lambda)$, where p_i represents the momenta of the external particles and g_0 is the bare coupling. In a renormalizable theory it is possible to define a renormalized Green's function

$$\Gamma_R(p_i, g, \mu) = Z_\Gamma(g_0, \Lambda/\mu)\Gamma_U(p_i, g_0, \Lambda)\,, \tag{32}$$

such that Γ_R is then finite in the limit $\Lambda \to \infty$, but depends on the prescription parameter μ and the renormalized coupling g. The function Z_Γ is a product of renormalization factors, with one factor for each external particle. Now, the unrenormalized Green's function is independent of μ and thus

$$\frac{d\Gamma_U}{d\mu} = 0\,, \tag{33}$$

giving

$$\left(\mu\frac{\partial}{\partial\mu} + \beta\frac{\partial}{\partial g} + \gamma\right)\Gamma_R(p_i, g, \mu) = 0\,, \tag{34}$$

with Λ being held constant and then taking the subsequent limit $\Lambda \to \infty$. Here the beta-function $\beta(g)$ and the anomalous dimension γ are defined by

$$\beta = \mu\frac{\partial g}{\partial\mu}\,, \qquad \gamma = \frac{\mu}{Z_\Gamma}\frac{\partial Z_\Gamma}{\partial\mu}\,. \tag{35}$$

The beta-function is universal, but the anomalous dimension clearly depends on the Green's function. In the case where there is a single large momentum scale, Q, all momenta p_i can be expressed as a fixed fraction x_i of Q. Then introducing a momentum dependent, or 'running' coupling via the integral equation

$$t \equiv \int_{g(0)}^{g(t)} \frac{dg'}{\beta(g')}\,, \tag{36}$$

where $t = (1/2)\ln(Q^2/\mu^2)$, yields the general solution

$$\Gamma(t, g(0), x_i) = \Gamma(0, g(t), x_i) \exp \int_{g(0)}^{g(t)} dg' \frac{\gamma(g')}{\beta(g')} \tag{37}$$

to the Renormalization Group Equation (RGE) of Eq. (34). This explicitly demonstrates that the entire dependence of Γ on the scale Q arises through the running coupling $g(t)$.

The renormalization scale dependence of the QCD effective coupling $\alpha_s = g^2/4\pi$ is determined by the beta-function. Expanding this function in a power series in α_s gives

$$\beta = \mu \frac{\partial \alpha_s}{\partial \mu} = -\frac{\beta_0}{2\pi}\alpha_s^2 - \frac{\beta_1}{4\pi^2}\alpha_s^3 - \frac{\beta_2}{64\pi^3}\alpha_s^4 - \cdots \tag{38}$$

with

$$\begin{aligned} \beta_0 &= 11 - \frac{2}{3}N_f\,, \\ \beta_1 &= 51 - \frac{19}{3}N_f\,, \\ \beta_2 &= 2857 - \frac{5033}{9}N_f + \frac{325}{27}N_f^2\,, \end{aligned} \tag{39}$$

where N_f is the number of flavors with mass less than the scale μ. The solution to the differential equation (38) introduces a constant of integration; this constant is scheme (or prescription) dependent and must be determined from experiment. The conventional prescription choice [24] for QCD is the modified minimal subtraction scheme, $\overline{\rm MS}$, (which is discussed in the next section) and results in (to third order)

$$\begin{aligned} \alpha_s(\mu) = \frac{4\pi}{\beta_0 \ln(\mu^2/\Lambda^2)} \Bigg[1 - \frac{2\beta_1}{\beta_0^2} \frac{\ln[\ln(\mu^2/\Lambda^2)]}{\ln(\mu^2/\Lambda^2)} + \frac{4\beta_1^2}{\beta_0^4 \ln^2(\mu^2/\Lambda^2)} \\ \times \left(\left[\ln[\ln(\mu^2/\Lambda^2)] - \frac{1}{2} \right]^2 + \frac{\beta_2 \beta_0}{8\beta_1^2} - \frac{5}{4} \right) \Bigg]\,. \end{aligned} \tag{40}$$

This equation demonstrates the principle of asymptotic freedom, that is that the running coupling $\to 0$ as $\mu \to \infty$. This property allows for the RGE-improved perturbative calculations at large values of μ. We note that the expression for β_2 above (39) is scheme dependent and assumes $\overline{\rm MS}$.

We stress again that all physical quantities or observables are independent of the renormalization scheme. However, our calculations are truncated at some order in perturbation theory, and this termination of the perturbation series introduces a residual renormalization scheme dependence. The magnitude of this leftover scheme dependence can be sizeable since the expansion parameter, α_s, is large. This introduces a source of uncertainty in comparing QCD predictions to data, which can only be reduced by higher order computations.

A quantitative test of QCD and the property of asymptotic freedom is given by the measurement of α_s in a variety of processes at numerous scales Q. Determinations of α_s have been obtained from tests of sum rules in low-energy Deep Inelastic Scattering (DIS), hadronic τ decays, neutrino DIS, high-energy DIS at HERA, lattice QCD calculations, heavy quarkonium decays, hadronic cross sections and event shape observables in e^+e^- annihilation, and jet, prompt photon, and $b\bar{b}$ production in hadronic collisions. The corresponding scales for these processes range from $1 \lesssim Q \lesssim 500$ GeV and the theoretical computation for each process has been performed at least to order NLO, and in some cases to (next-)next-to-leading order (NNLO), in perturbation theory. A review of the procedure by which α_s is extracted in each case, as well as a discussion of the associated theoretical errors is given in the Particle Data Book.[24] An up-to-date summary of this information from the 1998 summer conferences[25] is reproduced here in Table 2. We that in many cases, the dominant source of error is theoretical. This is related to the residual scheme dependence discussed above, and can be resolved only by performing higher order calculations. Due to the large data sample available at the Z boson resonance, it has become conventional to use the scale $Q = M_Z$ as the standard candle by which to compare the various measurements. This is shown graphically in Fig. 8. It is apparent that the measurements are all consistent within the uncertainties. The present world average value of $\alpha_s(M_Z)$ is

$$\alpha_s(M_Z) = 0.1190 \pm 0.0058\,, \tag{41}$$

which implies

$$\begin{aligned} \Lambda^{(5)}_{\overline{\rm MS}} &= 220^{+78}_{-63}\,{\rm MeV}\,, \\ \Lambda^{(4)}_{\overline{\rm MS}} &= 305^{+94}_{-79}\,{\rm MeV}\,. \end{aligned} \tag{42}$$

Finally, demonstration that the property of asymptotic freedom is experimentally verified is given in Fig. 9 from Bethke.[8]

2.5 Inclusive Jet Cross Sections in Hadronic Collisions

Hadronic collisions have also provided several valuable tests of QCD, but a detailed review [26] will not be given here. Perhaps the most impressive confirmation of QCD is given by the spectacular agreement of the inclusive jet cross section with the NLO predictions of QCD. Numerous parton-level subprocesses, involving all the interactions present in the QCD Lagrangian, contribute to this cross section. At leading order, this cross section is described by all $2 \to 2$ QCD reactions initiated with $gg, g^{(}\bar{q}^{)}, q^{(}\bar{q}^{)}$ scattering, while higher order QCD subprocesses give more elaborate configurations of partons. The radiative corrections have been computed [27] to NLO and the $O(\alpha_s^2)$ parton cross section is convoluted with the initial parton distributions. The inclusive differential cross section for jet production measured by CDF [28] for jet transverse energies from 15 to 440 GeV in the central pseudorapidity region $0.1 \leq |\eta| \leq 0.7$ is displayed in the insert of Fig. 10. The pseudorapidity of a final state particle or jet is defined as $\eta \equiv -\ln\tan(\theta/2)$ with $\cos\theta = p_z/p$. We see that the agreement between theory and experiment is very good, both in the shape and the normalization of the distribution, spanning over many orders of magnitude of the falling cross section. This agreement establishes the QCD Lagrangian of Eq. (1) as the correct theory of the strong interactions at perturbative energies. It also illustrates the existence of all the initial scattering states, directly showing that the gluon gauge symmetry is non-abelian, and demonstrates the importance of the Q^2 evolution of the parton density functions. The remainder of the figure shows the percentage difference between the CDF measurement and the expectations of NLO QCD, for various parameterizations of the parton densities, as a function of the jet transverse energy. The error bars represent uncertainties uncorrelated from point to point. The apparent disagreement at high values of the jet transverse energy has not been explicitly corroborated by measurements from D0,[29] and can be easily explained by modifying the gluon distribution inside the proton.[30]

3 QED

Quantum electrodynamics is a renormalizable local gauge theory. The QED Lagrangian is invariant under the local gauge transformation

$$\psi(x) \to \exp[ieQ\Lambda(x)]\psi(x)\,,$$

Process	Q GeV	$\alpha_s(Q)$	$\alpha_s(M_Z)$	$\Delta\alpha_s(M_Z)$ expt.	$\Delta\alpha_s(M_Z)$ theor.	Theory
DIS [pol. strct. fun.]	$0.7-8$		$0.120^{+0.010}_{-0.008}$	$^{+0.004}_{-0.005}$	$^{+0.009}_{-0.006}$	NLO
DIS [Bj-SR]	1.58	$0.375^{+0.062}_{-0.081}$	$0.121^{+0.005}_{-0.009}$	–	–	NNLO
DIS [GLS-SR]	1.73	$0.295^{+0.092}_{-0.073}$	$0.114^{+0.010}_{-0.012}$	$^{+0.005}_{-0.006}$	$^{+0.009}_{-0.010}$	NNLO
τ Decays	1.78	0.339 ± 0.021	0.120 ± 0.003	0.001	0.003	NNLO
DIS [ν; F_2 and F_3]	5.0	0.215 ± 0.016	0.119 ± 0.005	0.002	0.004	NLO
DIS [μ; F_2]	7.1	0.180 ± 0.014	0.113 ± 0.005	0.003	0.004	NLO
DIS [HERA; F_2]	$2-10$		0.120 ± 0.010	0.005	0.009	NLO
DIS [HERA; jets]	$10-100$		0.118 ± 0.008	0.003	0.008	NLO
DIS [HERA; ev. shps]	$7-100$		$0.118^{+0.007}_{-0.006}$	0.001	$^{+0.007}_{-0.006}$	NLO
$Q\bar{Q}$ states	4.1	0.223 ± 0.009	0.117 ± 0.003	0.000	0.003	LGT
Υ Decays	4.13	0.220 ± 0.027	0.119 ± 0.008	0.001	0.008	NLO
e^+e^- [$\sigma_{\rm had}$]	10.52	0.20 ± 0.06	$0.130^{+0.021}_{-0.029}$	$^{+0.021}_{-0.029}$	–	NNLO
e^+e^- [ev. shapes]	22.0	$0.161^{+0.016}_{-0.011}$	$0.124^{+0.009}_{-0.006}$	0.005	$^{+0.008}_{-0.003}$	resum
e^+e^- [$\sigma_{\rm had}$]	34.0	$0.146^{+0.031}_{-0.026}$	$0.123^{+0.021}_{-0.019}$	$^{+0.021}_{-0.019}$	–	NLO
e^+e^- [ev. shapes]	35.0	$0.145^{+0.012}_{-0.007}$	$0.123^{+0.008}_{-0.006}$	0.002	$^{+0.008}_{-0.005}$	resum
e^+e^- [ev. shapes]	44.0	$0.139^{+0.010}_{-0.007}$	$0.123^{+0.008}_{-0.006}$	0.003	$^{+0.007}_{-0.005}$	resum
e^+e^- [ev. shapes]	58.0	0.132 ± 0.008	0.123 ± 0.007	0.003	0.007	resum
$p\bar{p} \to b\bar{b}X$	20.0	$0.145^{+0.018}_{-0.019}$	0.113 ± 0.011	$^{+0.007}_{-0.006}$	$^{+0.008}_{-0.009}$	NLO
$p\bar{p}$, $pp \to \gamma X$	24.2	$0.137^{+0.017}_{-0.014}$	$0.111^{+0.012}_{-0.008}$	0.006	$^{+0.010}_{-0.005}$	NLO
$\sigma(p\bar{p} \to \text{jets})$	$30-500$		0.121 ± 0.009	0.001	0.009	NLO
e^+e^- [$\Gamma(Z \to \text{had})$]	91.2	0.122 ± 0.004	0.122 ± 0.004	0.004	0.003	NNLO
e^+e^- [ev. shapes]	91.2	0.122 ± 0.006	0.122 ± 0.006	0.001	0.006	resum
e^+e^- [ev. shapes]	133.0	0.111 ± 0.008	0.117 ± 0.008	0.004	0.007	resum
e^+e^- [ev. shapes]	161.0	0.105 ± 0.007	0.114 ± 0.008	0.004	0.007	resum
e^+e^- [ev. shapes]	172.0	0.102 ± 0.007	0.111 ± 0.008	0.004	0.007	resum
e^+e^- [ev. shapes]	183.0	0.109 ± 0.005	0.121 ± 0.006	0.002	0.006	resum

Table 2: World summary of measurements of α_s. Abbreviations: DIS= deep inelastic scattering; GLS-SR=Gross-Llewellyn-Smith sum rules; Bj-SR= Bjorken sum rules; (N)NLO=(next)next-to-leading order; LGT= lattice gauge theory; resum= resummed NLO. From [25].

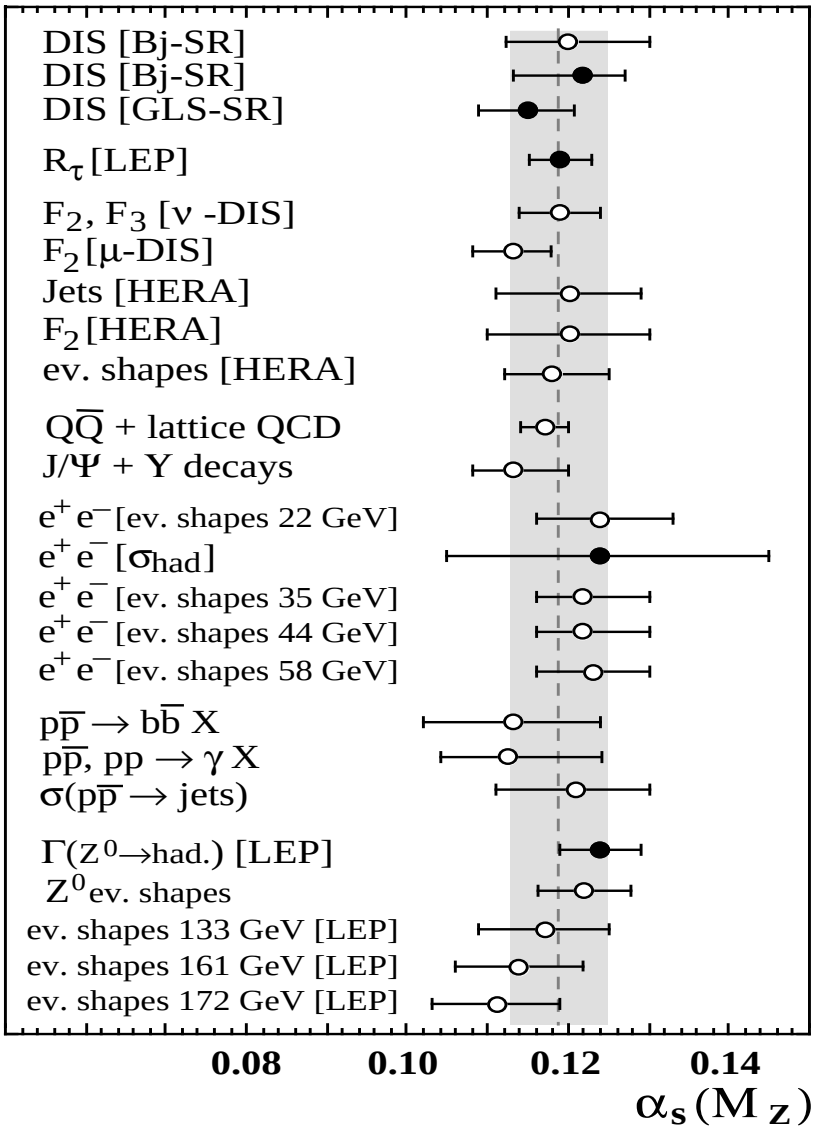

Figure 8: Summary of the various determinations of α_s, evaluated at the scale $\mu = M_Z$. From Bethke [8].

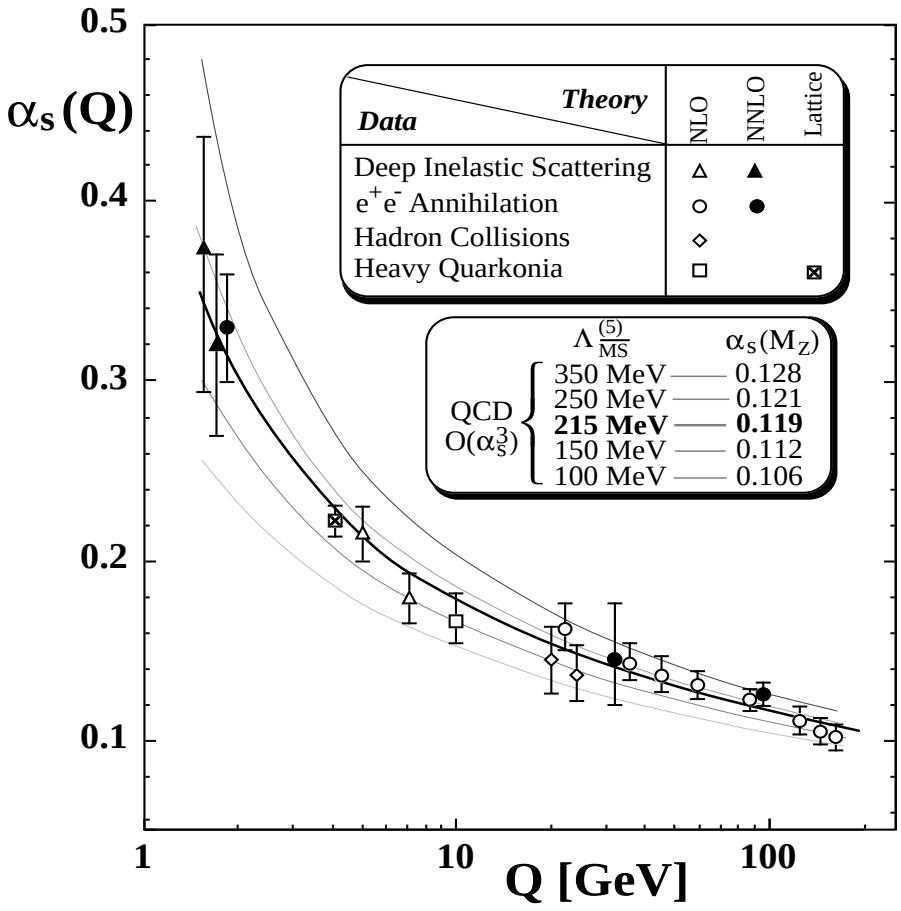

Figure 9: Demonstration of the property of asymptotic freedom via comparison of data from various processes as labeled with the theoretical predictions for several values of $\Lambda^{(5)}_{\overline{MS}}$ as labeled. The best fit is indicated by the thick solid line. From Bethke[8].

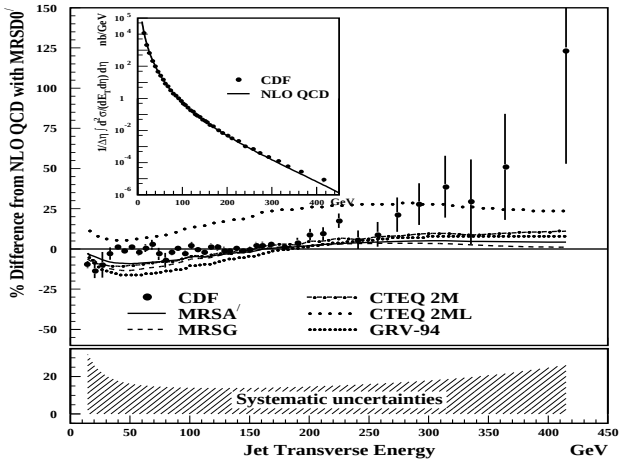

Figure 10: Percentage difference between the CDF inclusive jet cross section and the predictions of NLO QCD for various parton densities as indicated. The error bars represent the uncorrelated uncertainties, while the shaded region at the bottom indicates the quadratic sum of the correlated systematic errors. The differential cross section is shown in the insert. From [28].

$$A_\mu(x) \to A_\mu(x) + \partial\Lambda(x)/\partial x_\mu \,, \tag{43}$$

with $\Lambda(x)$ being arbitrary and the phase factor originating from the symmetry group U(1) with generator Q. The photon must remain massless to preserve exact gauge invariance. The electromagnetic current (12) is conserved, *i.e.*, $\partial_\mu J^\mu_{em} = 0$, implying conservation of electric charge. The success of QED as the first and simplest gauge theory made it a starting point in forming gauge theories for the strong and weak interactions.

3.1 Renormalization of the QED Coupling

As discussed in the introduction, in addition to the boson and fermion masses and CKM mixings, the SM has three *a priori* free parameters which are inserted into the theory and must be used as input into all calculations. Due to their

precise experimental determination two of these are taken to be $\alpha_{QED} \equiv e^2/4\pi$ and G_F, which play fundamental roles in many tests of the SM. The fact that QED is renormalizable and hence α can be treated as a 'running' coupling is essential in analyzing SM radiative corrections. It is instructive to briefly review this concept.

Consider the process $e^+e^- \to \gamma \to \mu^+\mu^-$ at $s = q^2 \gg m_e^2, m_\mu^2$. At lowest order the amplitude can be written schematically as

$$A_0 \sim e^2 J_\sigma^e \cdot \frac{-ig^{\sigma\lambda}}{q^2} \cdot J_\lambda^\mu \,, \tag{44}$$

where $J^{e,\mu}$ are the conserved electron and muon electromagnetic currents. At the next order in perturbation theory there is a correction due to the 1-loop vacuum polarization (or photon self-energy) diagram of Fig. 11. This yields the 1-loop amplitude

$$A_1 \sim e^2 J_\sigma^e \frac{-ig^{\sigma\alpha}}{q^2} \Pi_{\alpha\beta}(q^2) \frac{-ig^{\beta\lambda}}{q^2} J_\lambda^\mu \,, \tag{45}$$

where

$$\Pi_{\alpha\beta}(q^2) = -e^2 Q_f^2 \int \frac{d^n k}{(2\pi)^n} (\mu^2)^{2-n/2} \frac{Tr[\gamma_\alpha(\not{k} + m_f)\gamma_\beta(\not{k} - \not{q} + m_f)]}{(k^2 - m_f^2)\left((k-q)^2 - m_f^2\right)} \tag{46}$$

using dimensional regularization with k representing the loop momenta of the fermion. Here the log divergent integral over k has been regulated by performing the integration in n dimensions and the factor $\mu^(2 - n/2)$ has been introduced to keep e dimensionless in n dimensions. Due to electromagnetic gauge invariance we can write this as

$$\Pi_{\alpha\beta}(q^2) = -ie^2(q_\alpha q_\beta - g_{\alpha\beta} q^2)\Pi(q^2) \tag{47}$$

so that the scattering amplitude becomes

$$A = A_0 + A_1 \sim e^2[1 + e^2\Pi(q^2)] J_\sigma^e \frac{-ig^{\sigma\lambda}}{q^2} J_\lambda^\mu \,. \tag{48}$$

The bubble string of a series of vacuum polarization contributions depicted in Fig. 12 forms a geometric series and can be resummed so that

$$A = \frac{e^2}{1 - e^2\Pi(q^2)} J_\sigma^e \frac{-ig^{\sigma\lambda}}{q^2} J_\lambda^\mu \,, \tag{49}$$

and the factor $e^2/[1-e^2\Pi(q^2)]$ can be thought of as an effective charge. However, $\Pi(q^2)$ is divergent and must be renormalized before using this definition. One explicitly obtains

$$\Pi(q^2) = \frac{Q_f^2}{12\pi^2}\left\{\frac{1}{2-n/2} + \ln 4\pi - \gamma_E \right. \\ \left. +6\int_0^1 dx\; x(1-x)\ln\left[\frac{\mu^2}{m_f^2 - q^2x(1-x)}\right]\right\}. \qquad (50)$$

Here the first term clearly diverges as $n \to 4$ and γ_E denotes the Euler-Mascheroni constant.

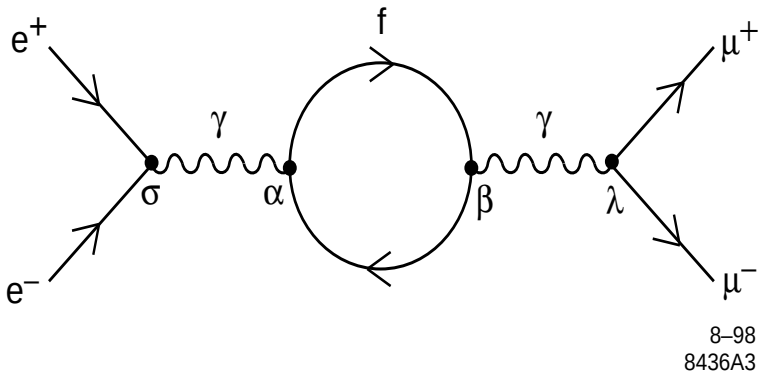

Figure 11: Feymann diagram for the photon self-energy.

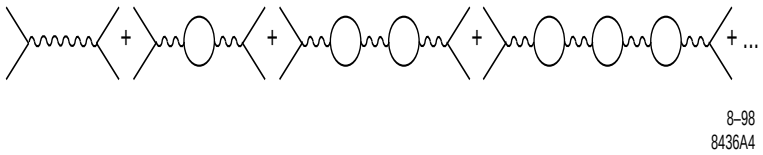

Figure 12: Bubble string contributing to the photon self-energy.

There are several renormalization schemes that can be employed. The two most popular are the on-shell scheme (OS) (upon which we concentrate here) and the $\overline{\rm MS}$ scheme. In the OS scheme e^2 is defined to be the quantity determined by low-energy experiments such as Thompson scattering and the

Josephson Junction [24] or Quantum Hall Effect.[31] In this case $\Pi(q^2)$ is renormalized such that $\Pi(q^2=0)=0$, giving

$$\Pi_{\rm OS}(q^2) = \frac{Q_f^2}{2\pi^2}\int_0^1 dx\; x(1-x)\ln\left[\frac{m_f^2}{m_f^2 - q^2x(1-x)}\right] . \tag{51}$$

Note that if the fermion is heavy, $4m_f^2 \gg q^2$, then $\Pi_{\rm OS}$ exhibits decoupling, *i.e.*, contributions to the integral are highly suppressed by powers of q^2/m_f^2. In this case we obtain

$$\Pi_{\rm OS}(q^2 \ll 4m_f^2) \simeq \frac{-Q_f^2}{60\pi^2}\left[\frac{q^2}{m_f^2} + \frac{3}{28}\frac{q^4}{m_f^4}\right] . \tag{52}$$

In the opposite limit of $q^2 \gg 4m_f^2$ one must be careful if q^2 is time-like as $\Pi_{\rm OS}$ develops an imaginary, or absorptive, part in this case. However, the real part can be written as

$$\mathcal{R}e\Pi_{\rm OS}(q^2 \gg 4m_f^2) \simeq \frac{Q_f^2}{12\pi^2}\left[\ln\frac{q^2}{m_f^2} - \frac{5}{3} - 6\frac{m_f^2}{q^2} + \cdots\right] . \tag{53}$$

Since e^2 is real, convention dictates that only $\mathcal{R}e\Pi(q^2)$ is used to define the renormalized coupling. For example, taking $M_Z^2 = q^2 \gg 4m_f^2$, the fermion contribution is

$$\alpha_{\rm OS}(M_Z^2) = \frac{\alpha(0)}{1-\Delta\alpha_{\rm OS}(M_Z^2)} \tag{54}$$

with

$$\Delta\alpha_{\rm OS}(M_Z^2) \simeq \frac{\alpha}{3\pi}Q_f^2\left[\ln\frac{M_Z^2}{m_f^2} - \frac{5}{3} - 6\frac{m_f^2}{M_Z^2}\right] . \tag{55}$$

Similarly, in keeping with the philosophy of the OS scheme and performing perturbative expansions in terms of physical observables (such as α), the renormalized masses of particles in this scheme correspond to the positions of propagator poles and are the actual physical masses of the particles.

In contrast, in the $\overline{\rm MS}$ scheme one subtracts the $1/(2-n/2) + \ln 4\pi - \gamma_E$ piece in $\Pi(q^2)$ leaving a logarithmically dependent quantity, as can be seen from Eq. (50). This is then absorbed into the definition of the running coupling. In this case, $\alpha_{\overline{\rm MS}}(\mu^2)$ and the corresponding running masses $m_f(\mu^2)$ are not directly related to physical quantities but are more easily dealt with in perturbation theory.

Before proceeding further we note that the summing of the geometric bubble series above leads to a summation of all of the large logarithms of the form

$(\alpha \ln q^2)^n$ that appear in $\Delta\alpha(M_Z^2)$. This is known as the leading-log approximation (LLA). To go beyond this approximation two-loop (and higher order) graphs, such as that depicted in Fig. 13, need to be considered. These higher order diagrams lead to sub-leading terms of order $\alpha(\alpha \ln q^2)^n$ in $\Delta\alpha(M_Z^2)$. The summation of these terms provides the next-to-leading logarithmic (NLL) estimate of $\Delta\alpha(M_Z^2)$.

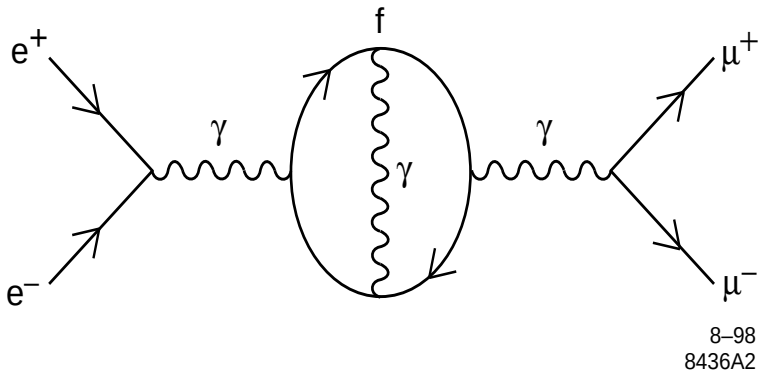

Figure 13: Higher order QED corrections to the photon vacuum polarization.

Given the results above, it would appear that a calculation of $\Delta\alpha(M_Z^2)$ in the OS scheme would be rather straightforward. It is instructive, however, to decompose $\Delta\alpha$ in terms of the various loop contributions given by $\Delta\alpha_{lept}$, $\Delta\alpha_{had}^{(5)}$, and $\Delta\alpha_{top}$. For leptons, which only have electroweak interactions, it is straightforward to obtain

$$\Delta\alpha_{lept}(M_Z^2) = \frac{\alpha}{3\pi}\sum_{\ell}\left[\ln\frac{M_Z^2}{m_\ell^2} - \frac{5}{3} - 6\frac{m_\ell^2}{M_Z^2} + O\left(\frac{m_\ell^4}{M_Z^4}\right)\right] + O(\alpha^2) + O(\alpha^3)\,, \tag{56}$$

where both the $O(\alpha^2)$ and $O(\alpha^3)$ terms have been recently computed,[32] resulting in

$$\Delta\alpha_{lept}(M_Z^2) = 314.97686 \times 10^{-4}. \tag{57}$$

For the top-quark contribution, the QCD corrections are expected to be relatively small and calculable in perturbation theory due to the large top-quark mass. Rescaling the result in Eq. (52) for the $4m_f^2 \gg q^2$ limit, taking $Q_t = 2/3$, and noting that the top-quark is a color triplet, we obtain

$$\Delta\alpha_{top}(M_Z^2) = \frac{-4\alpha M_Z^2}{45\pi m_t^2}\left[a + b\frac{3}{28}\frac{M_Z^2}{m_t^2} + \cdots\right], \tag{58}$$

with the coefficients a, b representing a power series in the QCD coupling. These coefficients are now evaluated through $O(\alpha_s^2)$,[33] so that

$$\Delta\alpha_{top}(M_Z^2) \simeq (-0.71 \pm 0.05) \times 10^{-4} \tag{59}$$

for $m_t = 173.8 \pm 5.0$ GeV.

In computing the corrections for the light quark (u, d, s, c, b) contributions, $\Delta\alpha_{had}^{(5)}$, the problem arises that perturbation theory is no longer reliable since scales of order 1 GeV or less are involved. To handle this situation, dispersion relations are employed to obtain

$$\Delta\alpha_{had}^{(5)} = \frac{-\alpha M_Z^2}{3\pi} \mathcal{R}e \int_{4m_\pi^2}^{\infty} ds \frac{R(s)}{s(s - M_Z^2) - i\epsilon}\,, \tag{60}$$

where $R(s)$ represents the ratio of hadronic to μ pair cross sections in e^+e^- annihilation, as discussed in section 2.1. As we will see in the next section, a similar situation occurs for the hadronic contribution to the anomalous $(g-2)$ of the electron or muon. In this case one finds

$$a_\mu^{had} = \frac{\alpha^2}{3\pi^2} \mathcal{R}e \int_{4m_\pi^2}^{\infty} ds \frac{K(s)}{s} R(s)\,, \tag{61}$$

where $K(s)$ is a known QED determined weight function. Over the last three years, a large effort has been performed on modelling $R(s)$ using both low-energy and τ decay data as well as sophisticated QCD calculations. A summary, from [34], of the results from the various analyses is presented in Fig. 14. The most recent analyses by Davier and Höcker [34] and by Kühn and Steinhauser [32] give essentially identical results:

$$\begin{aligned} \Delta\alpha_{top} + \Delta\alpha_{had}^{(5)} &= (276.3 \pm 1.6) \times 10^{-4} \quad [\mathrm{DH}]\,, \\ &= (277.4 \pm 1.7) \times 10^{-4} \quad [\mathrm{KS}]\,. \end{aligned} \tag{62}$$

When combined with $\Delta\alpha_{lept}(M_Z^2)$ these yield the predictions

$$\alpha^{-1}(M_Z) = \begin{cases} 128.933 \pm 0.021 \quad [\mathrm{DH}]\,, \\ 128.928 \pm 0.023 \quad [\mathrm{KS}]\,. \end{cases} \tag{63}$$

It is important to remember that new physics may also contribute to $\Delta\alpha$ even though new massive states apparently decouple reasonably rapidly. This possibility is usually neglected due to the assumption that the electroweak SM and QCD correctly describe the data below the Z pole. However, one can

imagine some new scenarios which would have an effect, *e.g.* a new Z' boson could modify $R(s)$ somewhat in this energy region and lead to an apparent shift in $\Delta\alpha$.

Better measurements of $R(s)$ in the $\sqrt{s} \sim 1$ GeV region and improved theoretical analyses may lead to a further reduction in the uncertainties in $\alpha(M_Z^2)$.

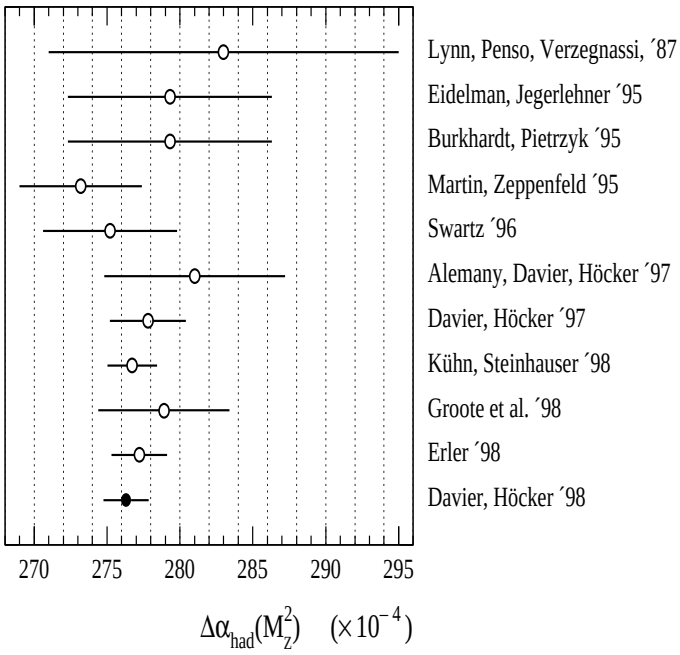

Figure 14: Summary of recent analyses for $\Delta\alpha^{(5)}_{had}$. From [34].

3.2 $g-2$ of the electron and muon

The previous discussion of QED and the renormalization of α naturally leads to the related topic of the anomalous magnetic moment of leptons, $a_{e,\mu} \equiv \frac{1}{2}(g-2)_{e,\mu}$, which are the most precisely calculated quantities in QED.[35] They

can be expressed in terms of the various contributions

$$a_\ell^{Th} = a_\ell^{QED} + a_\ell^{had} + a_\ell^{EW} \,. \tag{64}$$

The first term is given by the usual QED expansion,

$$a_\ell^{QED} = \sum_n c_n^\ell \left(\frac{\alpha}{\pi}\right)^n \,, \tag{65}$$

which is known to $n = 4$ for electrons and $n = 5$ for muons. Results for a_ℓ^{had} are obtained from vacuum polarization contributions and light-by-light scattering involving hadrons, while the perturbative SM electroweak contributions to a_ℓ^{EW} are computed to two-loops.[36] For electrons, these two contributions are quite small,

$$a_e^{had} = 1.635 \times 10^{-12} \,, \qquad a_e^{EW} = 0.030 \times 10^{-12} \,. \tag{66}$$

Using the value of α from Ref. [31], the theoretical expectation for a_e is

$$a_e^{Th} = 1159652156.4(1.2)(22.9) \times 10^{-12}, \tag{67}$$

where the first (last) error arises from uncertainties from higher orders (in α itself). The latest experimental result [37] is given by

$$a_e^{exp} = 1159652188.2(3.0) \times 10^{-12} \,, \tag{68}$$

and agrees within 1σ of the theoretical calculation. Since the electroweak contributions are so small it is doubtful that new physics can make a significant impact here.

For muons, using the results of [34,36] one obtains

$$\begin{aligned} a_\mu^{QED} &= 116584705(2) \times 10^{-11} \,, \\ a_\mu^{had} &= 6739(67) \times 10^{-11} \,, \\ a_\mu^{EW} &= 151(4) \times 10^{-11} \,, \end{aligned} \tag{69}$$

or

$$a_\mu^{Th} = 11659159.6(6.7) \times 10^{-10} \,. \tag{70}$$

Note that the uncertainties in a_μ^{had} are much larger than those for the QED and EW contributions. As discussed in the previous section, these arise from the non-perturbative nature of QCD in the ~ 1 GeV region, where dispersion relations must be employed in the evaluation of these contributions. A compilation, from [34], of recent analyses of the hadronic contributions to a_μ is shown in Fig. 15, where we see that the calculations are becoming more precise.

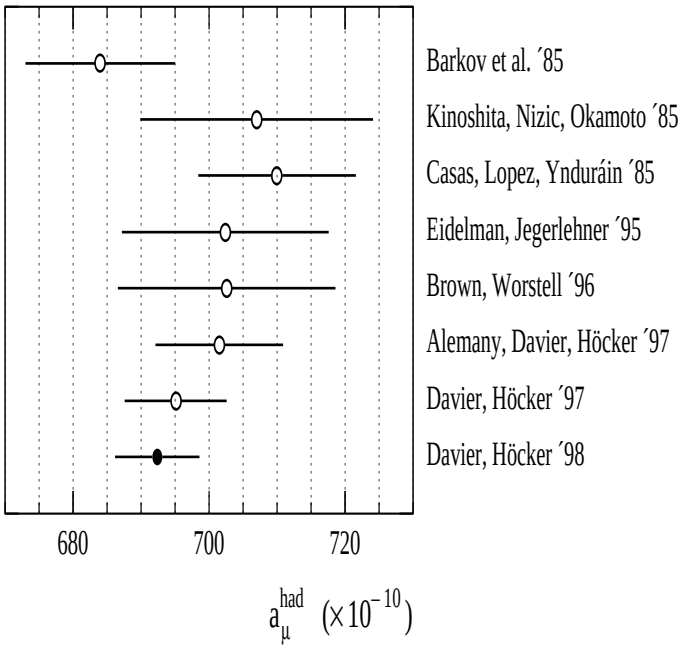

Figure 15: Comparison of the evaluations of a_μ^{had}. From [34].

On the experimental side, the Particle Data Group [24] gives the world average result $a_\mu^{PDG} = 11659230(84.0) \times 10^{-10}$ and a new result from BNL E821 [38] yields $11659250(153.0) \times 10^{-10}$ to give $a_\mu^{exp} = 1165923.5(7.4) \times 10^{-10}$. The difference is then found to be

$$\Delta a_\mu = a_\mu^{exp} - a_\mu^{Th} = (75.4 \pm 74.3) \times 10^{-10}\,, \tag{71}$$

which is approximately 1σ high, leaving room for potential new physics contributions at the same level (or larger) than the SM.[35,39] Future running of the E821 experiment may lower the error by a further factor of ~ 20, which would render new electroweak contributions visible if they are at least half as large as those corresponding to the SM.

4 Electroweak Interactions

As discussed in the introduction, the Standard Model of electroweak interactions has been probed at the quantum level. Presently, precision electroweak measurements at the Z-pole have tested the SM at the $\sim 0.1\%$ level, while low-energy measurements are at the $\sim 1\%$ level. In this section we first review the main aspects of the computation of raditative corrections in the SM, and then examine the comparison between the predictions of the perturbatively corrected theory and the data.

4.1 μ Decay

The constant G_F is defined by the μ lifetime, $\tau_\mu \equiv \Gamma_\mu^{-1}$, as calculated within the local Fermi theory which is finite to first order in G_F and to all orders in α.[40] This implies that Γ_μ may be written as $\Gamma_\mu = \Gamma_0(1+\Delta)$ where Δ is a power series in α,

$$\Delta = \sum_n \alpha^n \Delta_n \,, \tag{72}$$

and Γ_0 is the usual tree-level expression $\Gamma_0 = G_F^2 m_\mu^5/192\pi^3$. The lowest order term Δ_0 arises due to finite $x = m_e^2/m_\mu^2$ phase space corrections (assuming massless neutrinos) and W-boson mass corrections, and is given by

$$\Delta_0 = -8x - 12x^2 \ln x + 8x^3 - x^4 + \frac{3m_\mu^2}{5M_W^2} + O\left(\frac{m_\mu^4}{M_W^4}\right) . \tag{73}$$

Similarly,[41] the higher order terms originate from the n^{th}-loop pure QED corrections, which are found to be

$$\Delta_1 = \frac{\alpha(m_\mu)}{2\pi}\left[\frac{25}{4} - \pi^2\right] + O(\alpha(m_\mu) x \ln x) \,, \tag{74}$$

and the recently computed [42]

$$\Delta_2 = (6.701 \pm 0.002)\left(\frac{\alpha(m_\mu)}{\pi}\right)^2 , \tag{75}$$

where the $\overline{\rm MS}$ scheme is employed [42] in evaluating $\alpha(m_\mu)$,

$$\alpha(m_\mu) = \frac{\alpha}{1 + \frac{\alpha}{3\pi}\ln x} - \frac{\alpha^3}{4\pi^2}\ln x \,. \tag{76}$$

This result contains all corrections of $O(\alpha^2)$, $O(\alpha^3 \ln x)$ and $O(\alpha^n \ln^{n-1} x)$ for $n \geq 2$. Using the PDG [24] values for m_μ, m_e, and $\tau_\mu^{-1} = (2.19703 \pm 0.00004)\mu s$, one obtains

$$G_F = (1.16637 \pm 0.00001) \times 10^{-5}\,\mathrm{GeV}^2\,. \tag{77}$$

This has shifted from the previous value of $G_F = (1.16639 \pm 0.00002) \times 10^{-5}\,\mathrm{GeV}^2$ computed before the above Δ_2 corrections were known. With this recent higher order result, the theory error is now of $O(10^{-8})$. Hence the main uncertainty in G_F now arises solely from the measurement of τ_μ. A factor of 10 improvement in the determination of τ_μ may be achieved in proposed experiments at BNL, PSI, and RIKEN.

4.2 Lorentz Structure of the Weak Interactions

The Lorentz structure of the charged current weak interactions may be cleanly tested in the absence of hadronic interference by the leptonic decays $\ell^- \to \nu_\ell \ell'^- \bar{\nu}_{\ell'}$. For this purpose it is sufficient to consider these reactions at the Born level. Since the momentum transfer carried by the W-boson is very small compared to M_W in this case, the vector boson propagator can be reduced to a contact interaction. Assuming $V-A$ interactions this gives the usual effective Hamiltonian

$$\mathcal{H}_{eff} = \frac{G_F}{\sqrt{2}} \bar{\nu}_\ell \gamma^\alpha (1-\gamma_5) \ell \bar{\ell}' \gamma_\alpha (1-\gamma_5) \nu_{\ell'}\,. \tag{78}$$

The couplings can be determined by the final state lepton energy spectrum, which is easily calculated for $V-A$ interactions with massless neutrinos to be

$$\frac{1}{\Gamma_0}\frac{d\Gamma_0}{dx} = 2x^2(3-2x)\,, \tag{79}$$

with $0 \leq x = 2p_{\ell'} \cdot p_\ell / m_\ell^2 \leq 1$. Deviations from this behavior would indicate new physics arising from new gauge or scalar boson exchange or from modifications in the SM W-boson couplings. Giving up the assumption of $V-A$ interactions yields the most general Lorentz invariant effective Hamiltonian (assuming non-derivative couplings)

$$\mathcal{H}_{eff} = \frac{G_F}{\sqrt{2}} \sum_{\gamma,\epsilon,\omega} g^\gamma_{\epsilon\omega} \langle \bar{\ell}'_\epsilon | \Gamma^\gamma | \nu_{\ell'} \rangle \langle \bar{\nu}_\ell | \Gamma_\gamma | \ell_\omega \rangle\,, \tag{80}$$

where Γ^γ represents either a scalar (I), vector (γ_α), or tensor ($\sigma_{\alpha\beta}/\sqrt{2}$) interaction and $\epsilon, \omega = L, R$ denote the chiralities of the two charged leptons. Tensor interactions exist only if the charged leptons have opposite chiralities. Here we have assumed that neutrinos are massless. This leads to 10 complex coupling

constants, $g^{\gamma}_{\epsilon,\omega}$, for which the SM predicts $g^{V}_{LL} = 1$ with all others vanishing. The inclusion of these additional interactions modifies the decay lepton energy spectrum, which then takes the general form

$$\frac{d\Gamma}{x^2 dx d\cos\theta} = (3-2x) + (\frac{4}{3}\rho - 1)(4x-3) + 12\eta(\frac{m_{\ell'}}{m_\ell}x)(1-x) \\ -[(2x-1) + (\frac{4}{3}\delta - 1)(4x-3)]\xi\cos\theta\,, \tag{81}$$

with θ being the angle between the direction of the momentum of the final state lepton and the spin vector of the decaying lepton. We remind the reader that the spin vector is given by $\vec{s} = (\vec{p}/m,\, E\vec{p}/m|\vec{p}|)$. Note that only four combinations of the coupling constants, ρ, η, ξ, and δ, determine the shape of the lepton energy spectra. These four parameters are known as the Michel parameters,[43] which are defined by

$$\begin{aligned}
\rho &= \frac{3}{4}|g^{V}_{LL}|^2 + \frac{3}{4}|g^{V}_{RR}|^2 + \frac{3}{16}|g^{S}_{LL}|^2 + \frac{3}{16}|g^{S}_{LR}|^2 + \frac{3}{16}|g^{S}_{RL}|^2 + \frac{3}{16}|g^{S}_{RR}|^2 \\
&\quad + \frac{3}{4}|g^{T}_{LR}|^2 + \frac{3}{4}|g^{T}_{RL}|^2 - \frac{3}{4}\mathcal{R}e\,(g^{S}_{LR}g^{T*}_{LR}) - \frac{3}{4}\mathcal{R}e\,(g^{S}_{RL}g^{T*}_{RL})\,, \\
\eta &= \frac{1}{2}\mathcal{R}e\,\left[g^{V}_{LL}g^{S*}_{RR} + g^{V}_{RR}g^{S*}_{LL} + g^{V}_{RL}(g^{S*}_{LR} + 6g^{T*}_{LR}) + g^{V}_{LR}(g^{S*}_{RL} + 6g^{T*}_{RL})\right]\,, \\
\xi &= |g^{V}_{LL}|^2 + 3|g^{V}_{LR}|^2 - 3|g^{V}_{RL}|^2 - |g^{V}_{RR}|^2 + 5|g^{T}_{LR}|^2 - 5|g^{T}_{RL}|^2 \\
&\quad \frac{1}{4}|g^{S}_{LL}|^2 - \frac{1}{4}|g^{S}_{LR}|^2 + \frac{1}{4}|g^{S}_{RL}|^2 - \frac{1}{4}|g^{S}_{RR}|^2 + 4\mathcal{R}e\,(g^{S}_{LR}g^{T*}_{LR}) - 4\mathcal{R}e\,(g^{S}_{RL}g^{T*}_{RL})\,, \\
\xi\delta &= \frac{3}{4}|g^{V}_{LL}|^2 - \frac{3}{4}|g^{V}_{RR}|^2 + \frac{3}{16}|g^{S}_{LL}|^2 - \frac{3}{16}|g^{S}_{LR}|^2 + \frac{3}{16}|g^{V}_{RL}|^2 - \frac{3}{16}|g^{V}_{RR}|^2 \\
&\quad - \frac{3}{4}|g^{T}_{LR}|^2 + \frac{3}{4}|g^{T}_{RL}|^2 + \frac{3}{4}\mathcal{R}e\,(g^{S}_{LR}g^{T*}_{RL}) - \frac{3}{4}\mathcal{R}e\,(g^{S}_{RL}g^{T*}_{RL})\,.
\end{aligned} \tag{82}$$

The SM and experimentally determined [24] values of these parameters are given in Table 3. We see that both the $V-A$ structure of the weak charged current and lepton universality are confirmed at this level of sensitivity.

4.3 Radiative Corrections I: M_W, $\sin^2\theta_w$, Δr

As discussed in the introduction, the SM contains a number of natural tree-level relationships between the lowest order parameters

1. $\sin^2\theta_0 = e_0^2/g_0^2$,
2. $\sin^2\theta_0 = 1 - (M_W^0/M_Z^0)^2$, assuming only Higgs Doublets,

	$V-A$	$\mu \to e$	$\tau \to e$	$\tau \to \mu$
ρ	$\frac{3}{4}$	0.7518 ± 0.0026	0.745 ± 0.012	0.741 ± 0.030
η	0	-0.007 ± 0.013	0.01 ± 0.07	-0.10 ± 0.18
$\xi\delta$	$\frac{3}{4}$	0.7506 ± 0.0074	0.733 ± 0.033	0.78 ± 0.05
ξ	1	1.0027 ± 0.0085	0.98 ± 0.05	1.07 ± 0.08

Table 3: The SM predictions and world average measured values[24] for the Michel parameters.

3. $G_F/\sqrt{2} = g_0^2/8(M_W^0)^2 = e_0^2/8s_0^2(M_W^0)^2$.

When radiative corrections are included it is impossible to simultaneously maintain all of these relationships; the choice of which to keep and which to surrender then defines the renormalization scheme. The OS scheme in its absolute form selects $\alpha\,, M_W\,, M_Z$ (together with all the fermion as well as Higgs masses) to be the input parameters. However, since G_F is much more precisely determined, it is usually traded for M_W as one of the input parameters, with the relationship $x = \sin^2\theta_w = 1 - M_W^2/M_Z^2$ (*i.e.*, the second relation above) being maintained to all orders. In order to use G_F as an input parameter, the third relation above must be employed, together with the definition of G_F from μ-decay. From this discussion we recall that G_F was defined within the local Fermi theory including QED corrections up to $O(\alpha^2)$. In the full electroweak theory however, μ decay proceeds through W exchange, and the higher order corrections involve many more diagrams than the simple QED vertex and bremsstrahlung diagrams.

Figure 16 displays all of the one-loop SM diagrams which mediate μ-decay. These can be separated into several classes beyond those associated with the pure QED contributions in the local theory limit. As can be seen from the figure, these involve corrections to the $\bar{\nu}_e eW$ and $\nu_\mu \mu W$ vertices, W-boson self-energies, box diagrams involving Z exchange, and γ emission off the exchanged W-boson. Since the definition of G_F given in Section 4.1 only included the local QED terms, it is clear that the third relation above is modified and becomes

$$\frac{G_F}{\sqrt{2}} = \frac{e^2}{8xM_W^2}(1+\Delta r)\,, \tag{83}$$

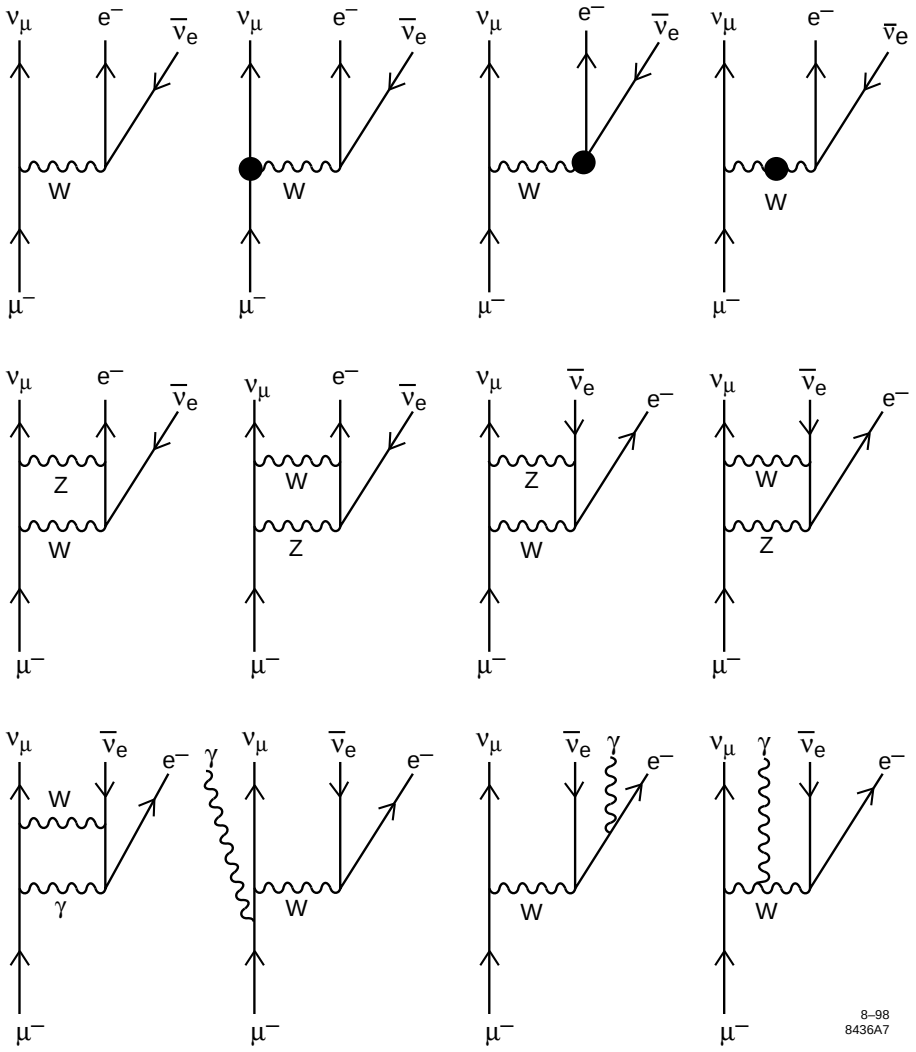

Figure 16: Complete set of Feymann diagrams to order α^3 for μ decay.

where $e^2 = e^2(0)$, M_W is the on-shell value, and Δr represents the non-QED corrections to μ decay. Employing $x \equiv 1 - M_W^2/M_Z^2$, gives

$$x(1-x) = \frac{A}{M_Z^2}(1+\Delta r)\,, \tag{84}$$

with $A \equiv \pi\alpha/\sqrt{2}G_F = (37.2805\,\mathrm{GeV})^2$.

In the $\overline{\rm MS}$ scheme, the relationship between M_W and M_Z is surrendered while $\hat{e}^2 = \hat{g}^2 \sin^2\hat{\theta}$ is maintained, such that $M_W^2 = \hat{c}^2\hat{\rho}M_Z^2$ holds for the physical $M_{W,Z}$, where $\hat{c}^2 = 1 - \hat{s}^2$. In this case the value of $\hat{x} \equiv \hat{s}^2(M_Z^2)$ is given by

$$\hat{x}(1-\hat{x}) = \frac{\hat{A}}{\hat{\rho}M_Z^2}(1+\Delta\hat{r})\,, \tag{85}$$

where $\hat{A} = \pi\hat{\alpha}(M_Z^2)/\sqrt{2}G_F$ with $\hat{\alpha}(M_Z^2)$ being the $\overline{\rm MS}$ running α defined at the Z scale, and $\Delta\hat{r}$ evaluates the diagrams in Fig. 16 in the $\overline{\rm MS}$ scheme. Both of the OS and $\overline{\rm MS}$ schemes do equally well at describing radiative corrections in the SM provided the known two-loop and higher order corrections are included.[44] For example, the OS and $\overline{\rm MS}$ predictions for M_W differ by only $2-3$ MeV which is more than an order of magnitude smaller than the anticipated sensitivity of LEPII and the Tevatron.

In order to consider these higher order corrections it is instructive to first contemplate what lies within the self-energy blob in the W-boson propagator (shown in Fig. 16), evaluated at $q^2 = 0$, *i.e.*, $\Sigma^W(0)$. In the SM the dominant contribution arises from the top-bottom quark and Higgs loops depicted in Fig. 17. These are of order m_t^2/M_W^2 and $\ln m_h/M_W$, respectively, whereas light fermion contributions are small being of order m_f^2/M_W^2. The pure gauge boson loops are also suppressed. This implies that new physics contributions to Δr can occur if the new interactions yield sizeable contributions to the gauge boson self-energies. (New interactions[45] could occur in the box graphs as well, with *e.g.*, $Z \to Z'$ or a SM box being replaced by a supersymmetric box.) To isolate the large terms in Δr we note from Fig. 16 that we can schematically write

$$\frac{G_F}{\sqrt{2}} = \frac{e_0^2}{8s_0^2(M_W^0)^2}\left[1 + \frac{\Sigma^W(0)}{M_W^2} + \text{box and vertex graphs}\right]\,, \tag{86}$$

where the $1/M_W^2$ factor represents an extra W propagator suppression in the $q^2 = 0$ limit. At the one-loop level one must make the replacements[46]

$$e_0^2 \to (e+\delta e)^2 = e^2(1 + \frac{2\delta e}{e})\,,$$

$$(M_W^0)^2 \to M_W^2(1+\frac{\delta M_W^2}{M_W^2})\,, \tag{87}$$
$$s_0^2 \to 1-\frac{M_W^2+\delta M_W^2}{M_Z^2+\delta M_Z^2} = s^2+c^2\left(\frac{\delta M_Z^2}{M_Z^2}-\frac{\delta M_W^2}{M_W^2}\right)\,,$$

which then yield

$$\frac{G_F}{\sqrt{2}} = \frac{e^2}{8s^2M_W^2}\left[1+2\frac{\delta e}{e}-\frac{c^2}{s^2}\left(\frac{\delta M_Z^2}{M_Z^2}-\frac{\delta M_W^2}{M_W^2}\right)+\frac{\Sigma^W(0)-\delta M_W^2}{M_W^2}\right.$$
$$\left.+(\text{vertex}+\text{box graphs})\right]\,, \tag{88}$$
$$= \frac{e^2}{8s^2M_W^2}(1+\Delta r)\,. \tag{89}$$

Here $2\delta e/e = \Delta\alpha$, which is given above in the OS scheme, and $\delta M_i^2 = \mathcal{R}e\,\Sigma^i(M_i^2)$ are the usual mass counterterms. The vertex and box corrections are found to be small as are the light fermion contributions. We then can write

$$\Delta r = \Delta\alpha - \frac{c^2}{s^2}\Delta\rho + \Delta r_{\rm rem}\,. \tag{90}$$

The $\Delta\rho$ term arises from the (t,b) contribution to the W and Z self-energies and can be written to one-loop as the familiar relation [47] (neglecting terms of order m_b^2/m_t^2)

$$\Delta\rho = \frac{3\alpha}{16\pi s^2c^2}\frac{m_t^2}{M_Z^2} \approx \frac{3G_Fm_t^2}{8\sqrt{2}\pi^2}\,. \tag{91}$$

$\Delta r_{\rm rem}$ contains the remaining contributions, which are generally not enhanced, including those due to the Higgs boson. The $\Delta\alpha$ and $\Delta\rho$ terms give the largest contributions to Δr; for $m_t \sim 175$ GeV and a light Higgs they take on the values ≈ 0.0582 and ≈ -0.0322, respectively, while the $\Delta r_{\rm rem}$ pieces are $\lesssim 0.005-0.010$. Note that for this value of m_t the two dominant terms tend to cancel. This makes it very important to understand $\Delta\alpha$ as well as possible, and to calculate $\Delta\rho$ and $\Delta r_{\rm rem}$ to higher-order in order to obtain a firm a set of predictions for M_W and $\sin^2\theta_w$.

As discussed previously $\Delta\alpha$ is now relatively well-known in comparison to just a few years ago with $\delta(\Delta\alpha)_{1998} \lesssim 0.2\delta(\Delta\alpha)_{1995}$. Indeed most terms in Δr have now been computed beyond the level of one-loop, although a complete two-loop calculation has not yet been performed. For example, in the case of $\Delta\rho$ two- and three-loop QCD corrections have been calculated, as have the two-loop Higgs exchange terms. The full $G_F^2m_t^4$ and $G_F^2m_t^2M_Z^2$ two-loop

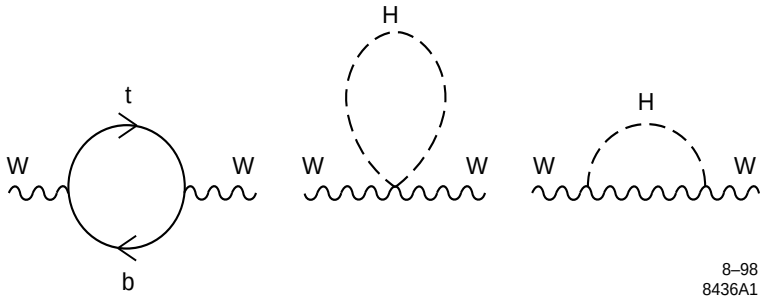

Figure 17: One-loop heavy fermion and Higgs-boson corrections to the W self-energy.

contributions to Δr are also computed, as are the two-loop Higgs dependent non-leading m_t terms.[44,48]

These sophisticated calculations lead to precise predictions for M_W and to uncertainties in $\sin^2\theta_w$ of only $\sim 3\times 10^{-5}$ for a fixed set of input parameters. In both cases these uncertainties are far smaller than those associated with the error on the top-quark mass measurement. Given the uncertainties in G_F and $\alpha(M_Z)$ discussed above, together with the determinations from LEP of $M_Z = 91186.7 \pm 2.1$ MeV and $\alpha_s(M_Z) = 0.119 \pm 0.005$, the uncertainty on M_W for $m_t = 173.8 \pm 5.0$ GeV is 32 MeV from $\delta(m_t)$ and 5 MeV from all other sources for a fixed value of m_H.

We now examine how well these predictions match the experimental results. The Tevatron value of $m_t = 173.8 \pm 5.0$ GeV is shown in Fig. 18 along with the combined W-boson mass as directly measured by CDF/D0/UA2 and LEPII, *i.e.*, $M_W = 80.390 \pm 0.064$ GeV. Also displayed in the figure is the prediction for M_W in the SM as a function of m_t for various values of the Higgs-boson mass; the widths of the bands for different Higgs masses shows an exaggerated $\pm 2\sigma$ uncertainty in the SM prediction. Given the measured value of m_t, it is clear that the combined measurements of the W mass prefer somewhat lighter Higgs boson masses; this result is common with other indirect determinations of the Higgs mass as will be discussed below.

4.4 Radiative Corrections II: Precision Measurements on the Z-Pole

At tree-level the process $e^+e^- \to f\bar{f}$ occurs through γ and Z exchange. At one-loop (and higher) order one needs to include, as in the case of μ-decay,

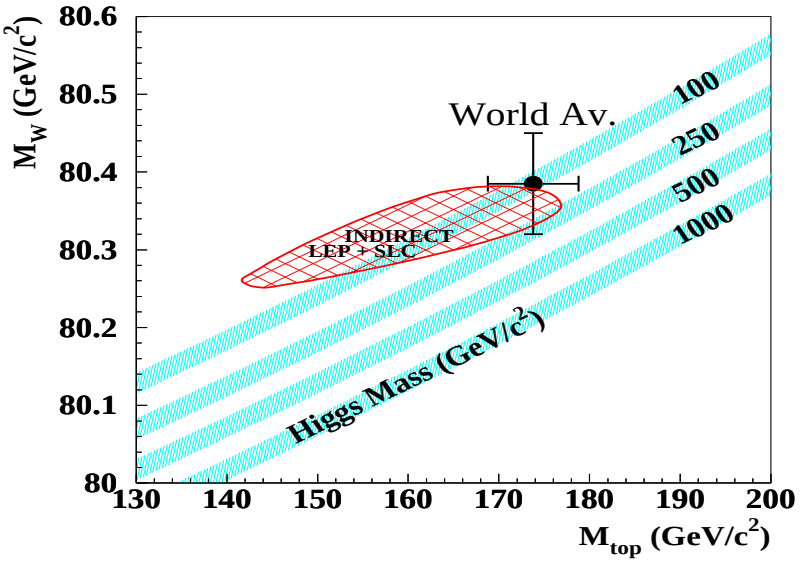

Figure 18: The comparison of the indirect determinations (from LEP and SLD) and the world average of direct measurements of M_W and m_t. Also displayed is the SM relationship for the masses as a function of the Higgs mass. From [49].

vertex corrections, external wave function renormalization, gauge boson self-energies, bremsstrahlung, and box diagrams; the last of which are very small numerically in the region of the Z-pole. In this region the γ exchange amplitude can be approximated by a factorized form

$$A_\gamma = 4\pi\alpha(s)\frac{Q_e Q_f}{s}[(1+F_V^e)\gamma_\mu - F_A^e\gamma_\mu\gamma_5]\times[(1+F_V^f)\gamma^\mu - F_A^f\gamma^\mu\gamma_5]\,, \quad (92)$$

with $\alpha(s) \simeq \alpha(M_Z)$ and $F_{V,A}^{e,f}$(s) representing form factors which vanish as $s \to 0$ and are numerically small, $\sim 10^{-3}$ at $s = M_Z^2$. Similarly one has for the Z piece (note the s-dependent width terms in the propagator)

$$A_Z = \frac{\sqrt{2}G_F M_Z^2\sqrt{\rho_e\rho_f}}{(s-M_Z^2)+i\frac{s}{M_Z^2}M_Z\Gamma_Z}[(T_{3L}^e - 2Q^e\kappa_e s_w^2)\gamma_\mu - T_{3L}^e\gamma_\mu\gamma_5] \quad (93)$$
$$\times[(T_{3L}^f - 2Q^f\kappa_f s_w^2)\gamma_\mu - T_{3L}^f\gamma_\mu\gamma_5]\,,$$

such that it appears that the Z has effective couplings to any fermion of

$$(\sqrt{2}G_F M_Z^2)^{1/2}[g_V^f\gamma_\mu - g_A^f\gamma_\mu\gamma_5]\,, \quad (94)$$

with

$$g_V^f = \sqrt{\rho_f}(T_{3L}^f - 2s_f^2 Q_f)\,, \qquad g_A^f = \sqrt{\rho_f}T_{3L}^f\,, \quad (95)$$

where the weak mixing angle is rescaled, $s_f^2 \equiv \kappa_f s_w^2$, due to $Z-\gamma$ mixing. The quantities ρ_f and κ_f absorb all vertex and self-energy corrections, have both universal and flavor dependent pieces, and are generally complex. The imaginary part of these corrections, which arises from absorptive parts, is generally neglected. This is known as the Effective Born Approximation, which is excellent numerically. For most fermions the universal terms dominate, with the exception being the case of the $b\bar{b}Z$ coupling, where potentially large m_t enhanced graphs such as those depicted in Fig. 19 contribute. Compared to the $d\bar{d}Z$ coupling, these effects can be approximated at one-loop as

$$\sqrt{\rho_b} = \sqrt{\rho_d}(1-2x_t)\,, \qquad s_b^2 = \frac{s_d^2}{1-2x_t}\,, \quad (96)$$

with $x_t \equiv G_F m_t^2/8\sqrt{2}\pi^2$. This leads to a strong m_t dependence in the $Z \to b\bar{b}$ width, which is not seen in the decays to other fermion pairs. This special correction is completely computed at one-loop as are the leading two-loop $O(G_F^2 m_t^4)$ and $O(\alpha G_F m_t^2)$ terms. The correction factors $\rho_f\,, \kappa_f$ for the other flavors are also known beyond leading order. Note that although κ_f and s_w^2 are

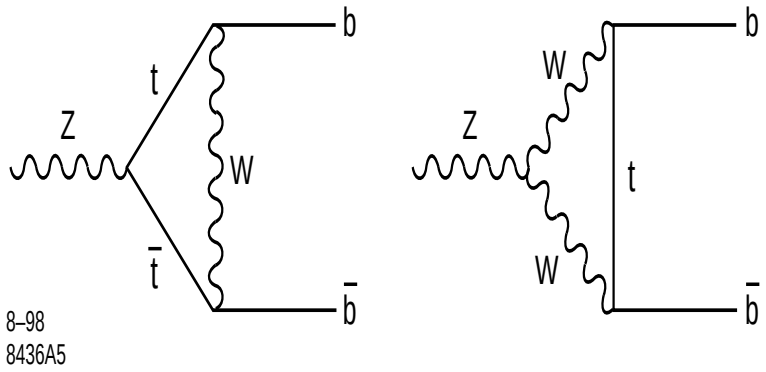

Figure 19: Feymann diagrams depicting heavy m_t one-loop corrections to the $Z \to b\bar{b}$ vertex.

scheme dependent, the combination $s_f^2 = \kappa_f s_w^2$ is scheme independent. $\Delta\kappa_f$ is especially small ($\kappa_f = 1 + \Delta\kappa_f$) in the $\overline{\rm MS}$ scheme, *e.g.*, $s_\ell^2 = \sin^2\theta_{\overline{\rm MS}} + 0.00029$.

Near the Z-pole, the cross section can be written as $\sigma \sim |A_\gamma + A_Z|^2$, so that

$$\sigma(s) = \frac{12\pi\Gamma_e\Gamma_f}{|s - M_Z^2 + i\frac{s\Gamma_Z}{M_Z}|^2}\left[\frac{s}{M_Z^2} + R_f\frac{s - M_Z^2}{M_Z^2} + I_f\frac{\Gamma_Z}{M_Z} + \cdots\right] + \frac{4\pi\alpha^2(s)}{3s}Q_f^2 N_c(1 + \delta_{QED} + \delta_{QCD})\,, \tag{97}$$

with $R_f\,, I_f$ representing the $\gamma - Z$ interference terms and the last terms being due to pure photon exchange. The pure Z resonance term is usually written as

$$\sigma_{res} = \sigma_0\frac{s\Gamma_Z^2}{(s - M_Z^2) + \frac{s^2\Gamma_Z^2}{M_Z^2}}\,, \qquad \sigma_0 = \frac{12\pi}{M_Z^2}\frac{\Gamma_e\Gamma_f}{\Gamma_Z^2}\,. \tag{98}$$

Due to the small size of the box graphs and the ability to at least approximately factorize the $e^+e^- \to f\bar{f}$ amplitude, initial and final state QED (and QCD) corrections can be handled separately. While final state corrections are best performed using perturbation theory, initial state radiation (ISR) (real and virtual) is best accounted for by the convolution approach,

$$\sigma_{obs}(s) = \int dz\; R(z)\sigma(s(1 - z))\,, \tag{99}$$

with $R(z)$ being a radiator function. $R(z)$ is known through $\mathcal{O}(\alpha^2)$ and all LL and NLL terms have been resummed. ISR reduces the value of the peak cross section by $\approx 25\%$ and shifts the peak position by ≈ 90 MeV. The effects of ISR must be deconvoluted from the data before it can be compared with the SM predictions.

There are several classes of observables on the Z-pole:

(i) Z partial widths

The partial widths of the Z-boson can be written as (defining $\beta \equiv 1 - 4m_f^2/M_Z^2$)

$$\Gamma_f = N_c \frac{G_F M_Z^3}{6\sqrt{2}\pi} \beta_f \left[\frac{3-\beta_f^2}{2} |g_V^f|^2 + \beta_f^2 |g_A^f|^2 \right] (1 + \delta_{QED} + \delta_{QCD}) \,, \qquad (100)$$

with the corrections δ_{QED} being known through $O(\alpha^2)$ and δ_{QCD} through $O(\alpha_s^3, \alpha\alpha_S)$. Commonly defined ratios of widths are $R_{had} \equiv \Gamma_{had}/\Gamma_\ell \,, R_{b,c} \equiv \Gamma_{b,c}/\Gamma_{had}$.

(ii) Forward-Backward Asymmetries

The fermion forward-backward asymmetries are defined by

$$A_{FB}^f \equiv \frac{\sigma_F^f - \sigma_B^f}{\sigma_F^f + \sigma_B^f} \,, \qquad (101)$$

with

$$\sigma_{F,B}^f = \int_{\cos\theta \gtrless 0} \frac{d\sigma^f}{d\cos\theta} d\cos\theta \,. \qquad (102)$$

Here, the pure γ terms are subtracted and final state QED and QCD corrections are normally deconvoluted from all asymmetries, so that

$$A_{F,B}^f = \frac{3}{4} A_e A_f \,, \qquad (103)$$

with

$$A_f = \frac{2\beta_f g_V^f g_A^f}{\frac{3-\beta_f^2}{2}|g_V^f|^2 + \beta_f^2 |g_A^f|^2} \,. \qquad (104)$$

(iii) Left-Right Asymmetry

The left-right polarization asymmetry, A_{LR}, requires a polarized electron

beam and is only measured by SLD. It is given by

$$A_{LR} = \frac{\sigma_L^f - \sigma_R^f}{\sigma_L^f + \sigma_R^f} = PA_e \,, \tag{105}$$

where $\sigma_{L,R}^f$ are the cross sections for left- or right-handed polarized electron beams with P being the degree of beam polarization. A_{LR} probes the leptonic Z couplings directly and is independent of the final state f.

(iv) Polarized Forward-Backward Asymmetry

The polarized forward-backward asymmetry, $A_{FB}^{pol}(f)$, also requires polarized initial beams and hence is also only measured by SLD. It is defined by

$$A_{FB}^{LR}(f) = A_{FB}^{pol}(f) = \frac{(\sigma_L^f - \sigma_R^f)_F - (\sigma_L^f - \sigma_R^f)_B}{(\sigma_L^f + \sigma_R^f)_F + (\sigma_L^f + \sigma_R^f)_B} = \frac{3}{4} PA_f \,, \tag{106}$$

and thus directly probes the final state fermion couplings to the Z-boson.

(v) Final State τ Polarization

In the decay $Z \to \tau^+\tau^-$ the polarization of the final state taus can be measured as a function of their production angle using the tau decay modes $\mu\bar{\nu}_\mu\nu_\tau$, $e\bar{\nu}_e\nu_\tau$, $\pi\nu_\tau$, $\rho\nu_\tau$, and $a_1\nu_\tau$. Assuming that taus decay with the Lorentz structure of the SM, this inventive observable can be written as

$$P_\tau(\cos\theta) = -\frac{A_\tau(1+\cos^2\theta) + 2A_e\cos\theta}{1+\cos^2\theta + 2A_eA_\tau\cos\theta} \,. \tag{107}$$

This clearly provides a measurement of both $A_{e,\tau}$.

All of these observables are well understood in the SM with uncertainties due to uncalculated higher order corrections being below the level of 0.01%. This is comparable to that due to the corresponding errors in the input parameters. Note that ISR corrections to the various asymmetries can also be performed by the convolution technique discussed above by using various radiating functions.

Next we examine how well the SM predictions agree with the enormous amount of Z-pole data collected at LEPI and SLC/SLD. Figs. 20 and 21 display the comparison between the SM expectations and the data. As can be seen, there is generally very good agreement between the two if all the values of the input parameters (including m_t and m_H) are allowed to vary within their

allowed ranges. The SM best fit to the data is obtained[49] by allowing the values of the input parameters to vary and minimizing the overall χ^2 distribution. Figure 22 shows the 'pull' for each observable, *i.e.*, the number of standard deviations that each measurement is away from the SM fit. Note the high level of precision of the measurements of the various observables, with many being at the 0.1% level. This provides a quantum level test of the SM predictions, and the agreement between theory and data is amazingly good. We also note that there is generally good agreement amongst the various experiments for each of the Z-pole observables. The LEPI and SLD Z-pole data set can be used by itself to predict the correlated values of M_W and m_t; this allowed region is presented in Fig. 18. Here, the overlap with the direct measurements for both quantities is good and the preference for light Higgs masses is again observed.

The results of the electroweak fits to the leptonic data are presented in Fig. 23. Here we see that the fits for the leptonic couplings g_V and g_A are in good agreement with the SM predictions. There is also good agreement with the assumption of universality.

One interesting derived result is that of the number of light neutrinos, which is obtained from the invisible width of the Z, *i.e.*, $\Gamma_{inv} = \Gamma_Z - \Gamma_{had} - \Gamma_{e,\mu\tau}$. Γ_Z is determined from a fit to the lineshape, and Γ_{had}/Γ_Z and $\Gamma_{e,\mu\tau}/\Gamma_Z$ are obtained from the cross section at the Z peak for each of these final states. The data yield $\Gamma_{inv} = 500.1 \pm 1.9$ MeV. The number of light neutrino generations is then given by $N_\nu = (\Gamma_{inv}/\Gamma_\ell)/(\Gamma_\nu/\Gamma_\ell)_{SM} = 2.994 \pm 0.011$, which is extremely close to the value of three! This error will be reduced even further when the new luminosity error analysis presently underway is completed.

There are a few observables that are worth special attention and should be watched as data analysis progresses further. The first is $x_\ell = \sin^2\theta^{\rm lept}_{eff} \equiv (1 - g^\ell_V/g^e_A ll)/4$ which is defined in the effective renormalization scheme. Figure 24 compares the values of x_ℓ obtained from 8 different observables, with the single most precise determination being from A_{LR} as measured by SLD. The second most precise determination is from the LEPI measurement of A^b_{FB}; this yields $x_\ell = 0.23223 \pm 0.00038$, which is somewhat high compared to that obtained from the purely leptonic measurements. These leptonic observables, $A_{LR}\,, A^{pol}_{FB}(\ell)\,, A^\ell_{FB}\,, A_\tau$, and A_ℓ yield the combined value of $x_\ell = 0.23129 \pm 0.00022$. Hence the average value of x_ℓ extracted from the leptonic measurements disagrees with that from A^b_{FB} by roughly 3σ. However,

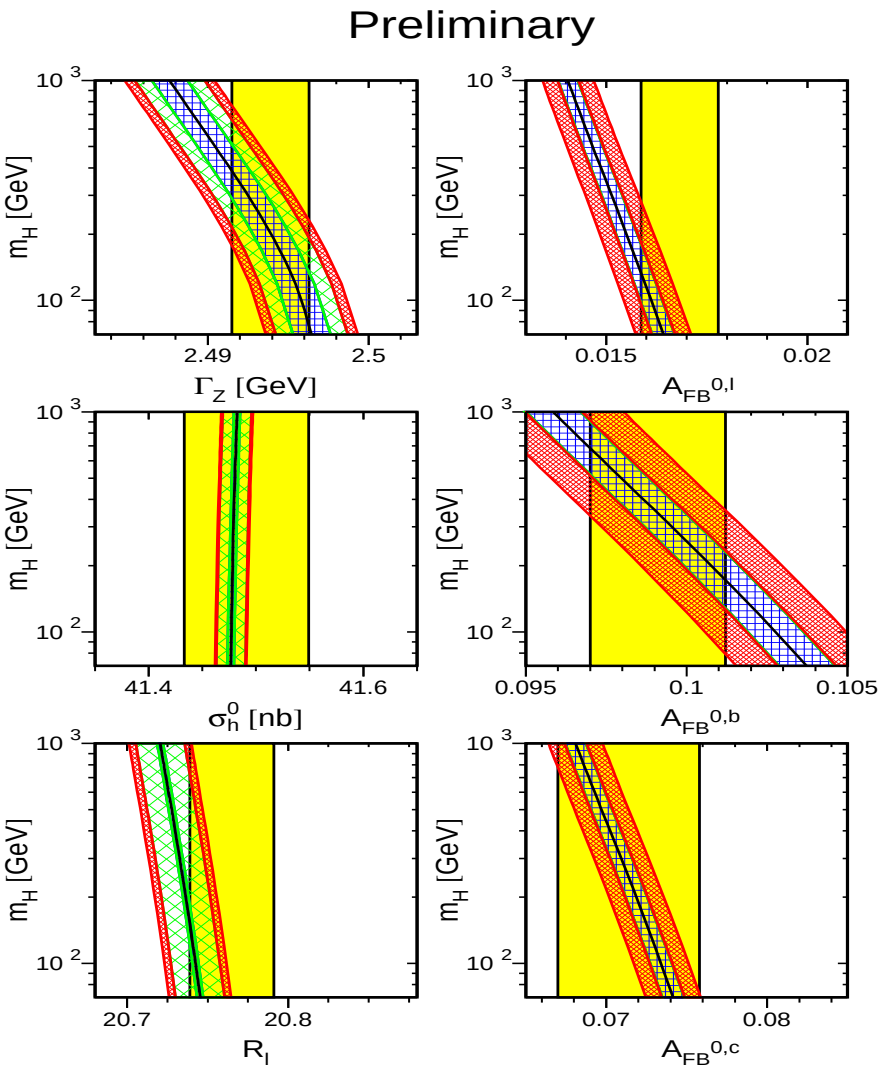

Figure 20: Comparison of LEPI measurements (represented by the vertical band) with the SM expectations as a function of the Higgs mass. The width of the SM band is due to uncertainties in $\alpha(M_Z^2)$, $\alpha_s(M_Z)$, and m_t. From [49].

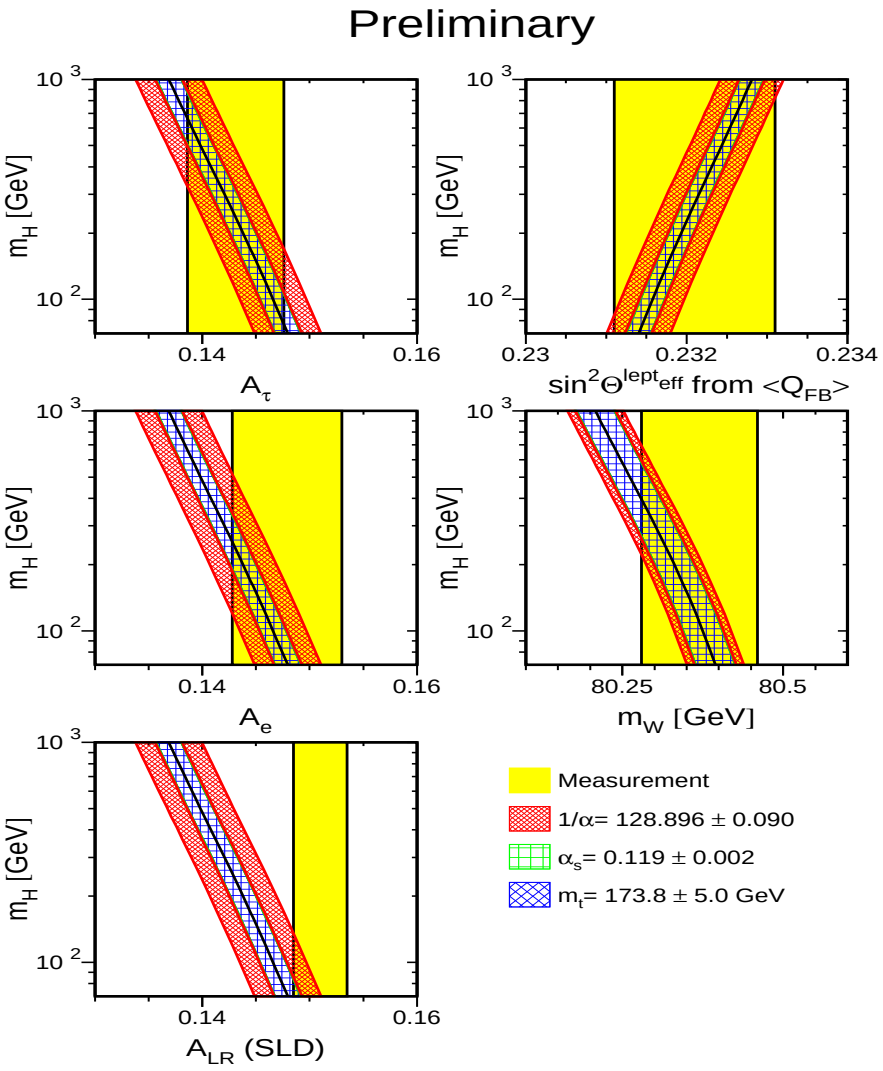

Figure 21: Comparison of LEPI and SLD measurements with the SM expectations as a function of the Higgs mass. The width of the SM band is due to uncertainties in $\alpha(M_Z^2)$, $\alpha_s(M_Z)$, and m_t. From [49].

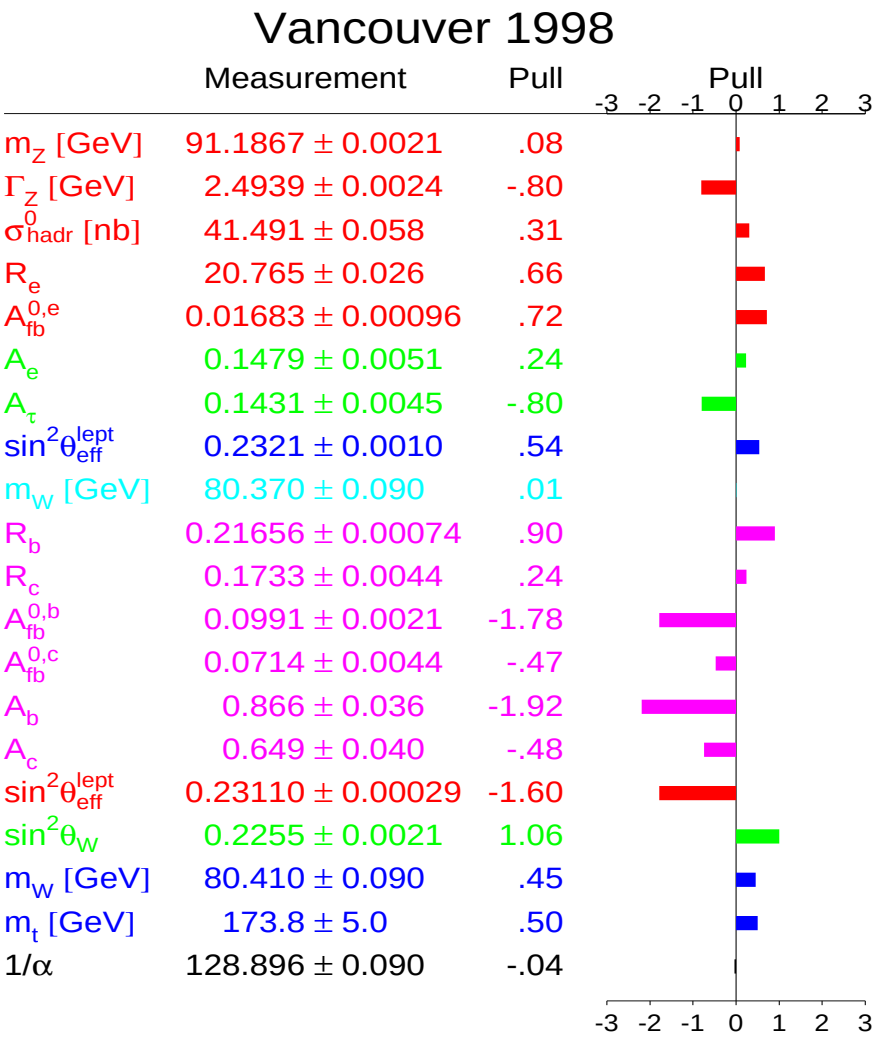

Figure 22: Compilation of the world's electroweak data as of summer 1998, and the deviation (in number of σ) of each measurement from the SM fit. From [49].

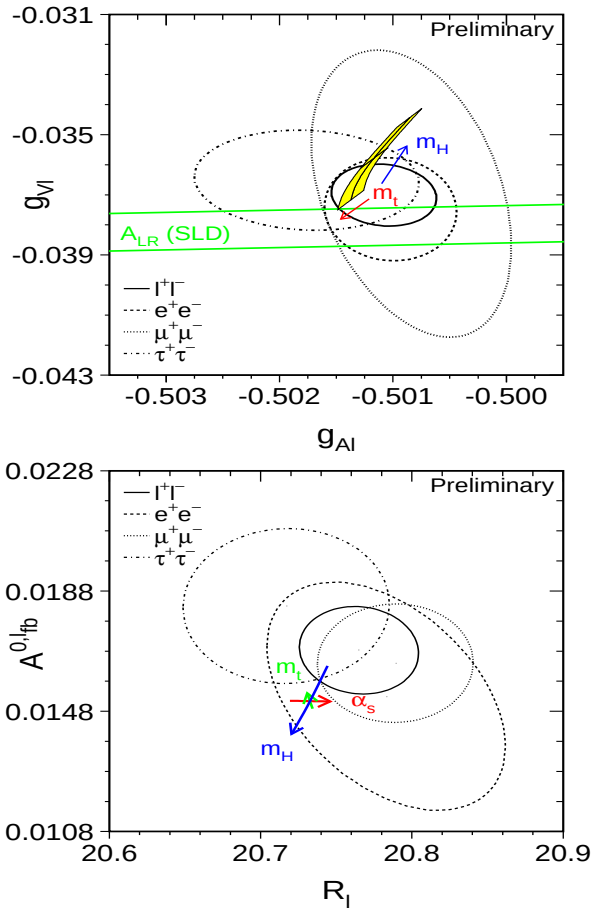

Figure 23: (a) 1σ contours in the $g_{V\ell} - g_{A\ell}$ plane from LEPI measurements and from A_{LR} from SLD. (b) 1σ contours in the $A^{0,\ell}_{FB} - R_\ell$ plane. In both figures, the solid contour represents the fit assuming lepton universality. The lines with arrows (or banana shaped region) represent the variation in the SM prediction when the parameters are varied in the intervals $m_t = 174.1 \pm 5.4\,\mathrm{GeV}$, $m_H = 300^{+700}_{-240}\,\mathrm{GeV}$, and $\alpha_s(M_Z) = 0.118 \pm 0.003$. From [49].

when x_ℓ is extracted from $A_{FB}^{b,(c)}$, the SM values of $A_{b,(c)}$ are assumed and used as input (recall that $A_{FB}^f = \frac{3}{4} A_e A_f$). Meanwhile, note that both A_{FB}^b and A_b are roughly 2σ low in comparison with the best fit SM expectations as shown in Fig. 22. Perhaps there should be some suspicion that there is some new physics in the $Zb\bar{b}$ vertex and the following analysis should be employed: (i) Use the combined leptonic measurements of LEPI and SLD to determine x_ℓ or A_ℓ. (ii) Determine the value of A_b for LEPI using the relation given above, so that A_b^{LEP} and A_b^{SLD} can be combined directly and compared with the SM expectation. This procedure implies that $A_b^{ave} = 0.882 \pm 0.019$, which is 3σ below the SM prediction of 0.925. The results of the fits to the heavy quark data is summarized in Fig. 25. In order to explicitly display the discrepancy with the SM, Fig. 26 shows the results of fitting the values of $\delta g_{L,R}^b$ to the $Z \to b\bar{b}$ data set, where these quantities are defined as $g_{L,R}^b = g_{L,R}^b|_{SM} + \delta g_{L,R}^b$. As can be seen from the figure, the SM prediction (which uses $m_t = 173.8\,\mathrm{GeV}, m_H = 300\,\mathrm{GeV}, \alpha_s(M_Z) = 0.119$) lies on the 99% C.L. exclusion contour. The best fit to these quantities yields $g_R^b = 0.027$ and $g_L^b = 0.0048$. This represents a $30-40\%$ shift in the right-handed b-quark coupling! One should not be overly concerned with these 3σ discrepancies at present, but they should be watched carefully in the future.

4.5 Radiative Corrections III: Low-Energy Precision Measurements

Deep Inelastic Neutrino Scattering

Data on cross sections from $^{(\bar{\nu})}N$ charged and neutral current (CC, NC) cross sections at modest values of Q^2 have been used for over 20 years [24] to obtain information on the u and d quark couplings to the Z-boson. (Here, N represents an isoscalar nuclear target.) Such measurements are easily influenced by systematic effects as well as uncertainties in the parton density functions and are thus conventionally quoted in terms of cross section ratios,

$$R^{\nu,\bar{\nu}} = \sigma_{NC}^{\nu,\bar{\nu}} / \sigma_{CC}^{\nu,\bar{\nu}}\,, \tag{108}$$

where many potentially dangerous effects cancel. However, possibly large uncertainties remain in these ratios due to sea quark contributions.

The most recent measurements of this type was performed by the NuTeV Collaboration [50] who have made use of the Paschos-Wolfenstein [51] relations, which we now describe. These relations greatly reduce the uncertainties due

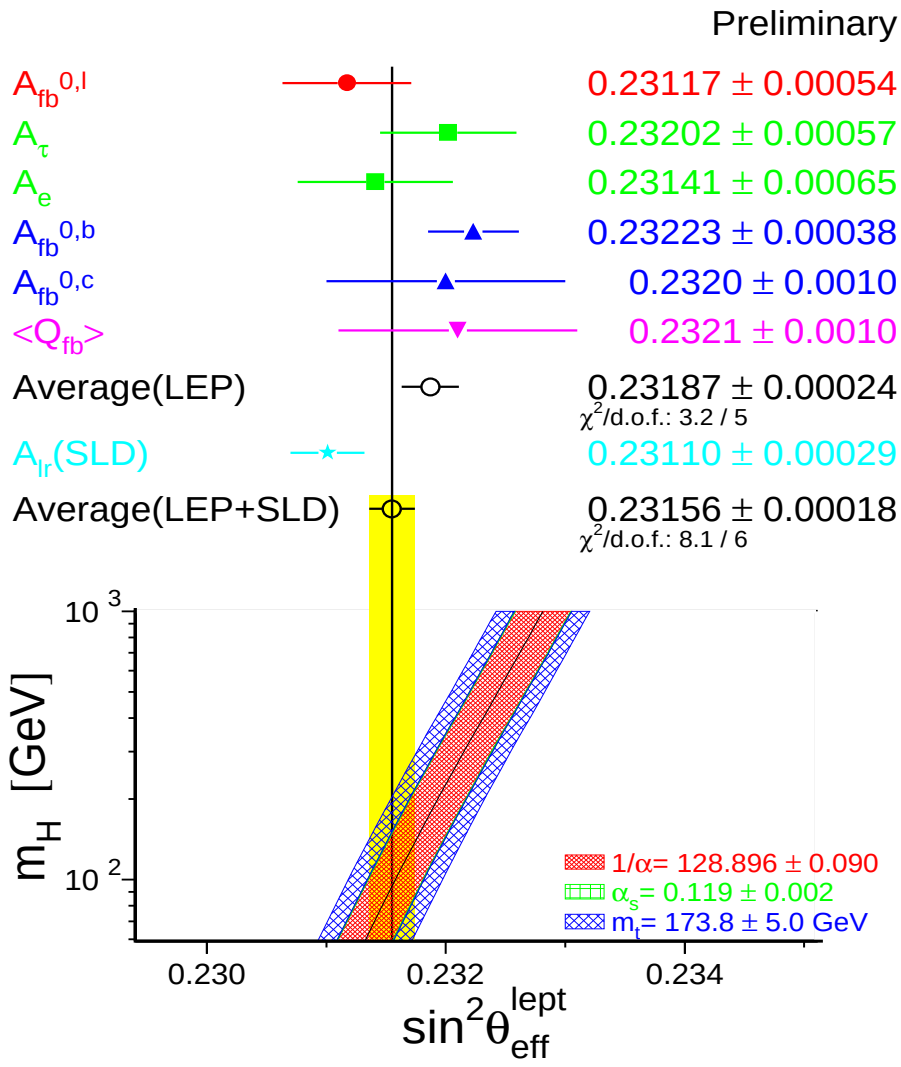

Figure 24: Compilation of various determinations of $\sin^2\theta_w$ $^{\rm lept}_{\rm eff}$. Also shown is the SM prediction as a function of the Higgs mass. From [49].

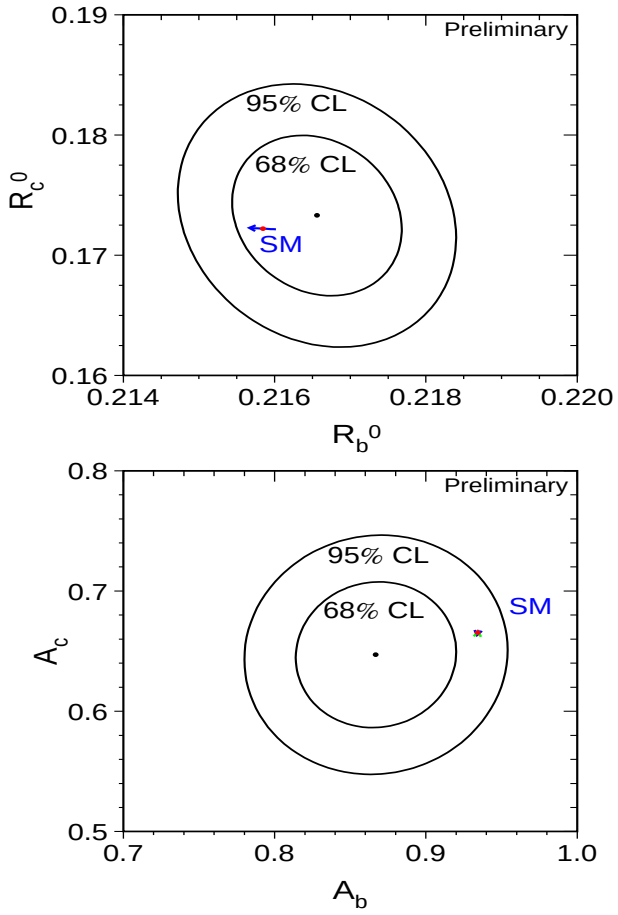

Figure 25: Contours in the (a) $R_b - R_c$ from LEPI and SLD data and (b) $A_b - A_c$ planes from and SLD data alone. The SM prediction for $m_t = 174.1 \pm 5.4$ GeV is also shown. From [49].

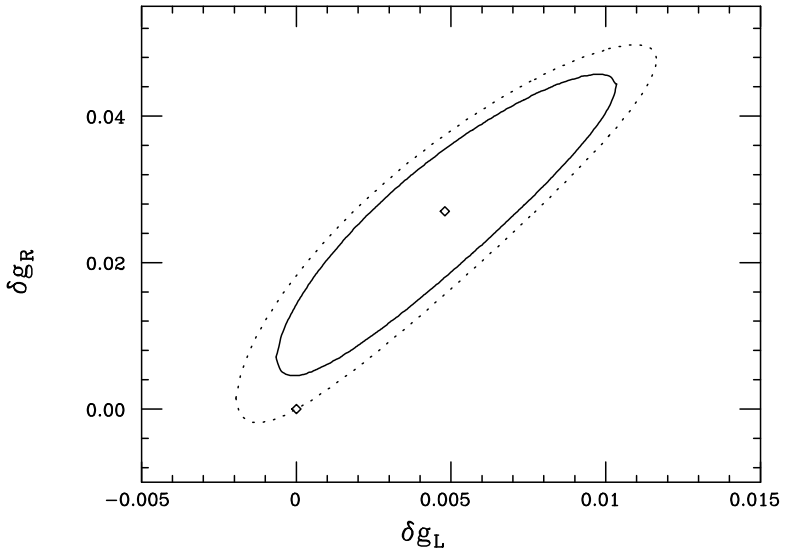

Figure 26: 95% (solid curve) and 99% C.L. (dashed) fit to the parameters $\delta g^b_{L,R}$ using the full LEPI/SLD $Z \to b\bar{b}$ data set. The diamond at the center (edge) represents the best fit (SM prediction).

to both sea quark contributions and the excitation of charm. Neglecting the contributions of the initial state b and t quarks, the integrated charged current $(\bar{\nu})N$ cross sections can be written in LO as

$$\sigma^{\nu}_{CC} \sim (u+d)[1-s^2_\theta(f-1)] + 2s[1+c^2_\theta(f-1)] + \frac{1}{3}(\bar{u}+\bar{d}+2\bar{c})\,,$$
$$\sigma^{\bar{\nu}}_{CC} \sim \frac{1}{3}(u+d+2c) + 2\bar{s}[1+c^2_\theta(f-1)] + (\bar{u}+\bar{d})[1-s^2_\theta(f-1)]\,, \quad (109)$$

where the $q/\bar{q}$ symbol represents the integrated contribution of that particular parton density function to the cross section, $s_\theta = \sin\theta_c\,, c_\theta = \cos\theta_c$ (where θ_c is the Cabbibo angle), and f represents a penalty factor for the excitation of charm off the light quark sea, which we will discuss below. Since the parton densities are integrated (over x and y), it is assumed that $s = \bar{s}$ and $c = \bar{c}$. In this case,

$$\sigma^{\nu}_{CC} - \sigma^{\bar{\nu}}_{CC} \sim (u+d-\bar{u}-\bar{d})[\frac{2}{3} - s^2_\theta(f-1)]\,, \quad (110)$$

and all sea quark terms cancel.

Similarly, the corresponding difference for the NC processes can be calculated, giving (the sea quark terms cancel here as well)

$$\sigma^{\nu}_{NC} - \sigma^{\bar{\nu}}_{NC} \sim \frac{2}{3}(u + d - \bar{u} - \bar{d})[g^2_L(u) + g^2_L(d) - g^2_R(u) - g^2_R(d)]\,, \qquad (111)$$

so that the ratio can be defined

$$R^- \equiv \frac{\sigma^{\nu}_{NC} - \sigma^{\bar{\nu}}_{NC}}{\sigma^{\nu}_{CC} - \sigma^{\bar{\nu}}_{CC}} = \frac{\frac{1}{2} - \sin^2\theta_w}{1 + \frac{3}{2}s^2_\theta(f-1)}\,, \qquad (112)$$

where the SM expressions for $g_{L,R}(u,d)$ have been inserted. This ratio, in the limit $f \to 1$, is the Paschos-Wolfenstein relation. In LO, one sees that a measurement of R^- will determine $\sin^2\theta_w$ if f is known. Experimentally, f is determined by measuring the charm production cross section in CC reactions via the dimuon final state and then parameterizing it in terms of the slow rescaling formalism.

Of course, both the QCD and electroweak radiative corrections need to be performed. The electroweak corrections have both universal and non-universal contributions, *e.g.*,

$$g_L(u) = \frac{1}{2} - \frac{2}{3}\sin^2\theta_w \quad \to \quad \rho_{\nu N}[\frac{1}{2} - \frac{2}{3}\kappa_{\nu N}\sin^2\theta_w] + \lambda_{Lu}\,, \qquad (113)$$

with similar redefinitions for the remaining couplings. These corrections are known in both the OS and $\overline{\rm MS}$ schemes. NuTeV chooses the OS scheme and extracts the preliminary value of $\sin^2\theta_w|_{\rm OS}$ at one-loop (taking $m_t = 175$ GeV and $m_H = 150$ GeV)

$$\sin^2\theta_w|{\rm OS} = 0.2253 \pm 0.0019 \pm 0.0010\,, \qquad (114)$$

which relates to

$$M_W = 80.26 \pm 0.11\,{\rm GeV}\,. \qquad (115)$$

This is in good agreement with the direct M_W measurements performed at LEPII and the Tevatron.

Atomic Parity Violation

Atomic parity violation occurs through the parity violating terms in the Z-boson exchange between the electrons and the nucleus of an atom. The effective Hamiltonian shows that there are two possible contributions due to the g_V and g_A couplings; $g^e_V g^{\rm nucl}_A$ and $g^e_A g^{\rm nucl}_V$. A short analysis shows that atomic

	Data	SM Prediction
$Q_w(Cs)$	-72.41 ± 0.84	-73.12 ± 0.06
$Q_w(Th)$	-114.8 ± 3.6	-116.7 ± 0.1

Table 4: Comparison of measurements of the atomic weak charge in Cesium and Thallium with the SM predictions.

parity violating effects are coherent so that the $g_A^e g_V^{\rm nucl}$ contribution would be enhanced in heavy nuclei. In addition, the claimed uncertainties in the atomic wave function for Cesium and Thallium, for which the most precise data is available, is of order $\sim 1\%$. The size of atomic parity violation is described by what is called the weak charge,

$$Q_w \sim -2[g_A^e g_V^u N_u + g_A^e g_V^d N_d]\,, \tag{116}$$

where $N_{u,d}$ represents the number of u- and d-quarks in the relevant nucleus and $g_{V,A}^{e,u,d}$ are the relevant $Zf\bar{f}$ couplings. In leading order one finds directly

$$Q_w = Z(1 - 4\sin^2\theta_w) - N\,. \tag{117}$$

Including the weak corrections entails making the replacements

$$\begin{aligned} g_A^e g_V^u &\to \rho_{eq}\left[-\frac{1}{2} + \frac{4}{3}\kappa_{eq}\sin^2\theta_w\right] + \lambda_u'\,, \\ g_A^e g_V^d &\to \rho_{eq}\left[\frac{1}{2} - \frac{2}{3}\kappa_{eq}\sin^2\theta_w\right] + \lambda_d'\,, \end{aligned} \tag{118}$$

with the corrections being known in both the OS and $\overline{\rm MS}$ schemes. The most precise data,[24] in comparison to the SM predictions are listed in Table 4, where the error on the SM prediction arises from varying m_t and m_H. We see that there is excellent agreement at the 1σ level.

4.6 Radiative Corrections IV: Higgs Mass Bounds

Assuming the SM describes all of the present data, the Z-pole results and the low-energy data, combined with direct measurements of $M_W\,, m_t$, and α_s, can be used to constrain the Higgs mass since it is the only remaining free parameter. Presently, direct searches at LEP have bounded the Higgs mass from below, with the current preliminary limit [52] being $m_H > 93.6$ GeV.

Figure 27 displays the m_H dependent $\Delta\chi^2$ distribution for all of the above data. The best fit is obtained for

$$m_H = 84^{+91}_{-51}\,\mathrm{GeV}\,, \tag{119}$$

with a 95% C.L. upper limit of 280 GeV. Much of the weight toward lower values is driven by the Z-pole leptonic asymmetries and the determinations of M_W. If one includes the experimental lower bound from direct searches in the fit, the one-sided 95% C.L. upper limit on m_H is not much affected. Note that these bounds would change if new physics were present. This result has generally led to the speculation that the discovery of the Higgs may not be too far in the distant future.

4.7 $S\,,T\,,U$ Formalism

A convenient parameterization which describes potential new physics contributions to electroweak radiative corrections is given by the $S\,,T\,,U$ formalism of Peskin and Takeuchi.[53] These parameters are defined such that they vanish for a reference point in the SM (*i.e.*, a specific value for the top-quark and Higgs masses) and deviations from zero would then signal the existence of new physics. We note that an alternative set of parameters, ϵ_i, also exist [54] which not require a reference point for the SM.

These parameters are only sensitive to new physics which contributes to the so-called oblique corrections. As discussed in the previous sections, there are three classes of radiative corrections to 4 fermion processes: vacuum polarization corrections, vertex corrections, and box corrections. The vacuum polarization corrections are usually referred to as oblique corrections, as they only affect the propagation and mixings of the gauge bosons and do not change the form of the interaction itself. They are thus independent of the final state fermions and affect all processes with electroweak gauge boson exchange universally. Whereas the direct corrections, *i.e.*, the vertex and box corrections, are clearly dependent on the final state fermions and are specific to each process. For new physics to affect the direct corrections, it must couple directly to the light external fermions. Such couplings are expected to be suppressed in most cases, with one exception being the $Zb\bar{b}$ vertex.

The assumptions inherent in the $S\,,T\,,U$ formalism about the nature of the new physics are:

1. The electroweak gauge group is given by $SU(2)_L \times U(1)_Y$, and thus there are no additional electroweak gauge bosons beyond the $\gamma\,Z$ and W.

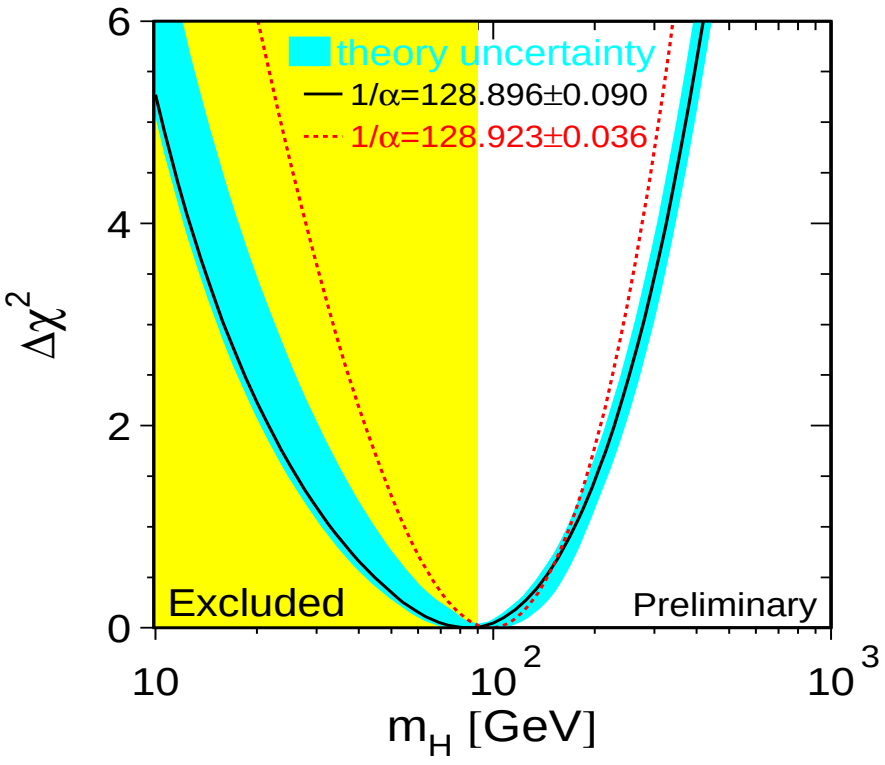

Figure 27: The $\Delta\chi^2$ fit using all data as a function of the Higgs mass. The vertical band displays the 95% C.L. exclusion limit on m_H from the direct search. From [49].

2. New physics couplings to light fermions are suppressed, and hence only oblique corrections need to be considered.

3. The new physics scale is large compared to the electroweak scale.

The first two assumptions indicate that only four vacuum polarization functions need to be considered, namely the self-energies of the γ, Z, and W, and $\gamma - Z$ mixing. Defining the notation

$$\int d^4x e^{iq\cdot x}\langle J_X^\mu(x) J_Y^\nu(0)\rangle = ig^{\mu\nu}\Pi_{\rm XY}(q^2) + (q^\mu q^\nu \text{term}), \tag{120}$$

where J_X is the current that couples to gauge boson X, these four vacuum polarization functions can be denoted as $\Pi_{\gamma\gamma}(q^2)(q^2)\,\Pi_{\rm ZZ}(q^2)(q^2)\,\Pi_{\rm WW}(q^2)(q^2)$ and $\Pi_{\gamma{\rm Z}}(q^2)(q^2)$. Note that the $q^\mu q^\nu$ terms of the vacuum polarization tensors are neglected here as they only correct the longitudinal components of the gauge boson propagators and are thus suppressed by $m_f^2/M_{W/Z}^2$.

The third assumption allows for the expansion of the new physics contributions to the self-energies in powers of q^2/M_{new} about $q^2 = 0$, where M_{new} represents the heavy scale of the new interactions. Keeping only constant and linear terms in q^2 thus yields

$$\begin{aligned}
\Pi_{\gamma\gamma}(q^2) &= q^2\Pi'_{\gamma\gamma}(0) + \cdots \\
\Pi_{{\rm Z}\gamma}(q^2) &= q^2\Pi'_{{\rm Z}\gamma}(0) + \cdots \\
\Pi_{\rm ZZ}(q^2) &= \Pi_{\rm ZZ}(0) + q^2\Pi'_{\rm ZZ}(0) + \cdots \\
\Pi_{\rm WW}(q^2) &= \Pi_{\rm WW}(0) + q^2\Pi'_{\rm WW}(0) + \cdots
\end{aligned} \tag{121}$$

for the part of the vacuum polarization functions which arise solely from the new interactions. This approximation thus allows us to express the new contributions in terms of six parameters. Three of these may be absorbed into the renormalization of the input parameters $\alpha\, G_F$, and M_Z, leaving three that are measurable. One choice for these parameters is given by [53]

$$\begin{aligned}
\alpha S &= 4s_w^2c_w^2\left[\Pi'_{\rm ZZ}(0) - \frac{c_w^2 - s_w^2}{s_w c_w}\Pi'_{{\rm Z}\gamma}(0) - \Pi'_{\gamma\gamma}(0)\right], \\
\alpha T &= \frac{\Pi_{\rm WW}(0)}{M_W^2} - \frac{\Pi_{\rm ZZ}(0)}{M_Z^2}, \\
\alpha U &= 4s_w^2\left[\Pi'_{\rm WW}(0) - c_w^2\Pi'_{\rm ZZ}(0) - 2s_w c_w\Pi'_{{\rm Z}\gamma}(0) - s_w^2\Pi'_{\gamma\gamma}(0)\right].
\end{aligned} \tag{122}$$

This definition ensures that the parameters T and U vanish if the new physics observes custodial isospin symmetry. In fact T represents the shift of the ρ

parameter due to new physics,

$$\rho = 1 + \delta\rho_{\rm SM} + \alpha T \,. \tag{123}$$

The electroweak observables can be expressed in terms of the parameters $S\,, T\,, U$ in a straightforward fashion [55] given the input values for $\alpha\,, G_F$, and M_Z and a reference value for m_H. These relations are

$$\begin{aligned} M_Z^2 &= M_{Z0}^2 \frac{1-\alpha T}{1 - G_F M_{Z0}^2 S/2\sqrt{2}\pi}\,, \\ M_W^2 &= M_{W0}^2 \frac{1}{1 - G_F M_{W0}^2 (S+U)/2\sqrt{2}\pi}\,, \\ \Gamma_Z &= \frac{1}{1-\alpha T}\frac{M_Z^3 \Gamma_{Z0}}{M_{Z0}^3}\,, \\ A_i &= \frac{1}{1-\alpha T} A_{i0}\,, \end{aligned} \tag{124}$$

where A_i represents a neutral current amplitude and $M_{Z0}\,, M_{W0}\,, \Gamma_{Z0}\,, A_{i0}$ are the Standard Model expressions in the $\overline{\rm MS}$ scheme. Note that the Z-pole measurements do not depend on U, and that this parameter only affects the W-boson mass. A global fit [24] to the precision electroweak data presented in Fig. 22 yields the determination

$$\begin{aligned} S &= -0.16 \pm 0.14 \quad (-0.10)\,, \\ T &= -0.21 \pm 0.16 \quad (+0.10)\,, \\ U &= 0.25 \pm 0.24 \quad (+0.01)\,, \end{aligned} \tag{125}$$

taking $m_t = 175 \pm 5$ GeV. The central values assume $m_H = M_Z$ while the numbers in parentheses describe the change for $m_H = 300$ GeV. These parameters are all consistent with their Standard Model values of zero within roughly 1σ. The corresponding 68% C.L. allowed region [56] (with updated data from the 1998 summer conferences) in the $S - T$ plane is displayed in Fig. 28. Also shown are the 68% C.L. bands in this plane from the measurements of A_{LR}, $\sin^2\theta_w^{\rm eff}$ from LEP, Γ_Z, M_W (assuming $U = 0$), and the ratio of charged to neutral current cross sections. The Standard Model prediction is represented by the banana shaped region, where the right-hand edge of this area corresponds to $m_H = 88$ GeV and $m_t = 173.9 \pm 5.2$ GeV. Increasing the Higgs mass to 1 TeV sweeps out the bounded area. The predictions of the Minimal Supersymmetric Standard Model (MSSM) from Bagger *et al.*,[57] are also shown as a series of small circular points, where each point corresponds to a separate

choice for the 5 MSSM parameters. We see that again the global fit is consistent with the SM, and that in the absence of the LEP $\sin^2\theta_w^{\rm eff}$ measurements the remaining measured bands would overlap in the region of negative S.

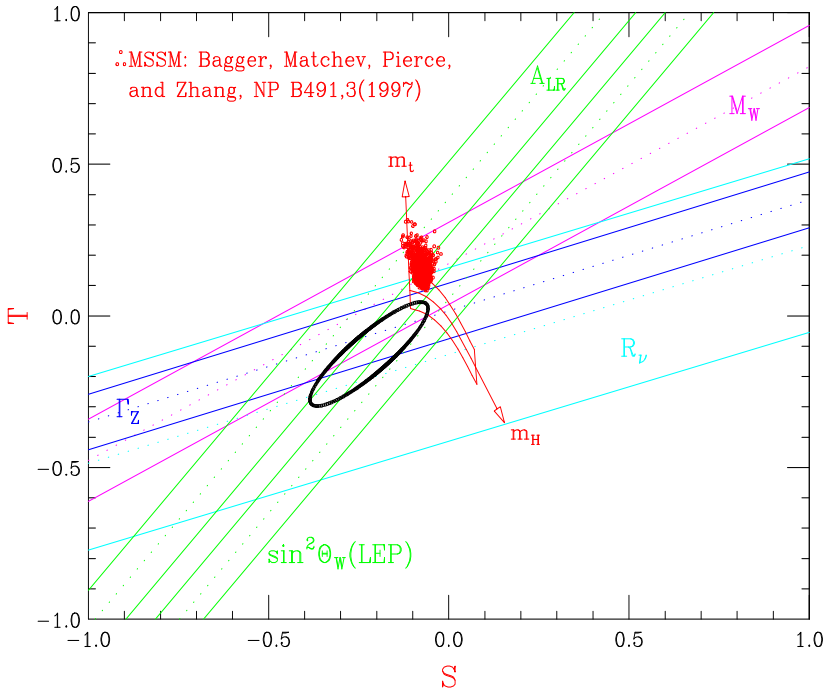

Figure 28: The 68% C.L. regions in the $S-T$ plane determined by various measurements as labeled. Also shown are the results from a global fit to the world's electroweak data which yields the 68% elliptical confidence region. The area predicted by the SM as described in the text is shown as the banana shaped region, while the MSSM expectations are denoted by the series of small circular points.

As an example of how new physics can affect these parameters, let us consider the case of a new color-singlet heavy fermion $SU(2)_L$ doublet, $(N\,,E)$,

with $m_{N,E} \gg M_Z$. The contribution of this doublet to $S\,, T\,, U$ is given by

$$\begin{aligned} S &= \frac{1}{6\pi}\left[1 - Y\ln\left(\frac{m_N^2}{m_E^2}\right)\right]\,, \\ T &= \frac{1}{16\pi s^2 c^2 M_Z^2}\left[m_N^2 + m_E^2 - \frac{2m_N^2 m_E^2}{m_N^2 - m_E^2}\ln\left(\frac{m_N^2}{m_E^2}\right)\right]\,, \\ U &= \frac{1}{6\pi}\left[-\frac{5m_N^2 - 22m_N^2 m_E^2 + 5m_E^2}{3(m_N^2 - m_E^2)^2}\right. \\ &\qquad \left. + \frac{m_N^6 - 3m_N^4 m_E^2 - 3m_N^2 m_E^4 + m_E^6}{(m_N^2 - m_E^2)^3}\ln\left(\frac{m_N^2}{m_E^2}\right)\right]\,, \end{aligned} \tag{126}$$

where Y represents the hypercharge of the doublet. The expression for T is just the familiar contribution of a fermion $SU(2)_L$ doublet to the ρ parameter and restricts the size of the mass splitting within the doublet. The experimental bounds on T, or ρ, tightly constrain the mass splitting to be very small within any new fermion doublet, *i.e.*, $\Delta m \equiv |m_N - m_E| \ll m_{N,E}$. In fact, any new doublets must be nearly degenerate! In this case the above expressions simplify to

$$\begin{aligned} S &\approx \frac{1}{6\pi} \approx 0.05\,, \\ T &\approx \frac{1}{12\pi s^2 c^2}\left[\frac{(\Delta m)^2}{M_Z^2}\right]\,, \\ U &\approx \frac{2}{15\pi}\left[\frac{(\Delta m)^2}{m_N^2}\right]\,. \end{aligned} \tag{127}$$

This conflicts with the global fit value for S at the $1.5 - 2\,\sigma$ level. A generalization of the contribution to S from a multiplet of heavy degenerate chiral fermions is given by

$$S = C\sum_i [T_{3L}^i - T_{3R}^i]^2/3\pi\,, \tag{128}$$

where $T_{3L,R}$ is the third component of left-,right-handed weak isospin of fermion i and C is the number of colors. This is a serious problem for theories which contain a large number of extra fermion doublets, such as technicolor models. For example, in technicolor models with QCD-like dynamics, a full technigeneration yields [58] $S \sim 1.62$, which is clearly excluded! However, models of walking technicolor can avoid these difficulties and can yield smaller or even negative values of S.[59] Consistency with the values of S and T has now become a standard viability test in constructing theories beyond the Standard Model.

If the third assumption above is relaxed and the scale of the new physics is near the electroweak scale, then the linear approximation in Eq. (120) no longer applies and more parameters need to be introduced. In this case, Burgess *et al.*[60] have shown that it is sufficient to introduce three additional parameters, bringing the total number to six. The definitions of S and U become slightly modified, T is unchanged, and the additional parameters are denoted as V, W, X. The revised set of parameters are defined by

$$\begin{aligned}
\alpha S &= 4s_w^2 c_w^2 \left[\frac{\Pi_{\rm ZZ}(M_Z^2) - \Pi_{\rm ZZ}(0)}{M_Z^2} - \frac{c_w^2 - s_w^2}{s_w c_w} \Pi'_{\rm Z\gamma}(0) - \Pi'_{\gamma\gamma}(0) \right] , \\
\alpha T &= \frac{\Pi_{\rm WW}(0)}{M_W^2} - \frac{\Pi_{\rm ZZ}(0)}{M_Z^2} , \\
\alpha U &= 4s_w^2 \left[\frac{\Pi_{\rm WW}(M_W^2) - \Pi_{\rm WW}(0)}{M_W^2} - c_w^2 \frac{\Pi_{\rm ZZ}(M_Z^2) - \Pi_{\rm ZZ}(0)}{M_Z^2} \right. \\
&\qquad \left. -2s_w c_w \Pi'_{\rm Z\gamma}(0) - s_w^2 \Pi'_{\gamma\gamma}(0) \right] , \\
\alpha V &= \Pi'_{\rm ZZ}(M_Z^2) - \frac{\Pi_{\rm ZZ}(M_Z^2) - \Pi_{\rm ZZ}(0)}{M_Z^2} , \\
\alpha W &= \Pi'_{\rm WW}(M_W^2) - \frac{\Pi_{\rm WW}(M_W^2) - \Pi_{\rm WW}(0)}{M_W^2} , \\
\alpha X &= -s_w c_w \left[\frac{\Pi_{\rm Z\gamma}(M_Z^2)}{M_Z^2} - \Pi'_{\rm Z\gamma}(0) \right] ,
\end{aligned} \tag{129}$$

Clearly in the limit $M_{new} \to \infty$, S and U coincide with their original definitions and V, W, X vanish.

It is interesting to note that some types of new physics may be quite close to the electroweak scale and yet make little contribution to the oblique parameters. As an example we consider the low-energy sector of string-inspired SUSY E_6 theories wherein the particle spectrum of the MSSM is augmented by three generations of vector-like fermions and their supersymmetric partners. If, for simplicity, the small mixing between these states and the SM fields is neglected and they are taken to be degenerate, then the new contributions to T vanish automatically due to the vector-like nature of the exotic fields. The corresponding contributions to the other oblique parameters are presented in Fig. 29 and are seen to be small ($\lesssim 0.1$) for $m \gtrsim 150$ GeV. This example demonstrates that new physics may be lurking nearby without manifesting itself in the oblique corrections.

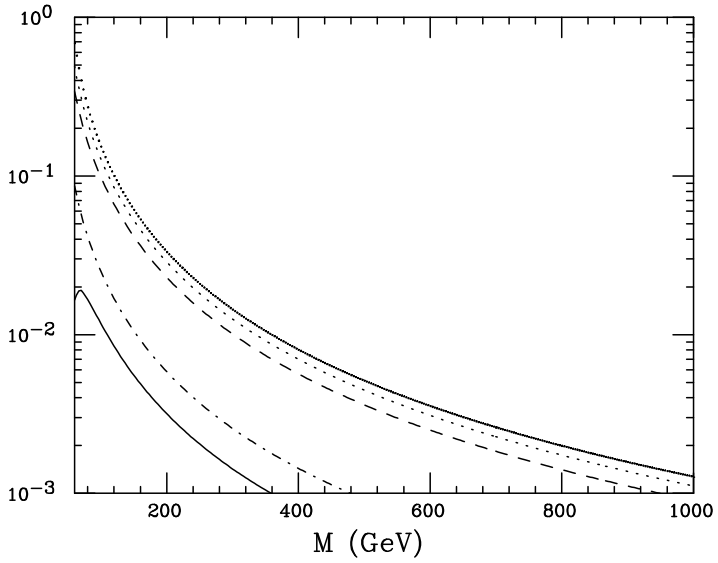

Figure 29: Contribution of 3 generations of degenerate E_6 exotic fermions of mass M and their SUSY partners to the oblique parameters. From top to bottom the curves correspond to the parameter $-V, -W, -S, X$, and $-U$, respectively.

4.8 Gauge Boson Pair Production

One element of the SM remains to be directly tested with significant precision, namely the non-Abelian self-couplings of the weak gauge bosons. Deviations from the SM gauge theory predictions for the Yang-Mills self-interactions would clearly signal the existence of new physics, possibly arising from, *e.g.*, loop corrections of new particles, substructure in the gauge boson sector, or additional interactions involving new gauge bosons. In addition, precise measurements of the WWV three-point function (where $V = \gamma$ or Z) can provide information on the nature of electroweak symmetry breaking.

The pair production of gauge bosons in e^+e^- or $q\bar{q}$ annihilation efficiently probes the structure of the trilinear couplings. In particular, the energy dependence of the cross section for the reaction $e^+e^- \to W^+W^-$ is critically dependent on the gauge cancellations. For example, the contribution of the neutrino exchange diagram depicted in Fig. 30(a) grows very rapidly with

energy,

$$\sigma_{\nu\nu} \simeq \frac{\pi\alpha^2 s}{96 x_w^2 M_W^4}\,, \tag{130}$$

and violates the optical theorem. This presented a serious problem for the Fermi theory of weak interactions, which was resolved only when gauge theories were introduced for the electroweak interactions. Including the SM s-channel gauge boson exchange diagrams of Fig. 30(b) yields the behavior

$$\sigma_{\rm total} \simeq \frac{\pi\alpha^2}{2x_w^2 s} \ln\frac{s}{M_W^2} \tag{131}$$

for the total cross section. These gauge cancellations are explicitly illustrated in Fig. 31, where the energy dependence of each contribution as well as for the total cross section for $e^+e^- \to W^+W^-$ is shown. This energy dependence has just now been measured at LEPII over a limited energy range near and just above threshold, as shown in Fig. 32 from Ref. [49]. These measurements are preliminary, but are in complete agreement with the SM, *i.e.*, the slightly low data point at $\sqrt{s} = 189\,\text{GeV}$ is no cause for concern at present. A higher energy e^+e^- collider is necessary in order to get a better lever arm in determining the high $\sqrt{s}$ behavior displayed in Fig. 31.

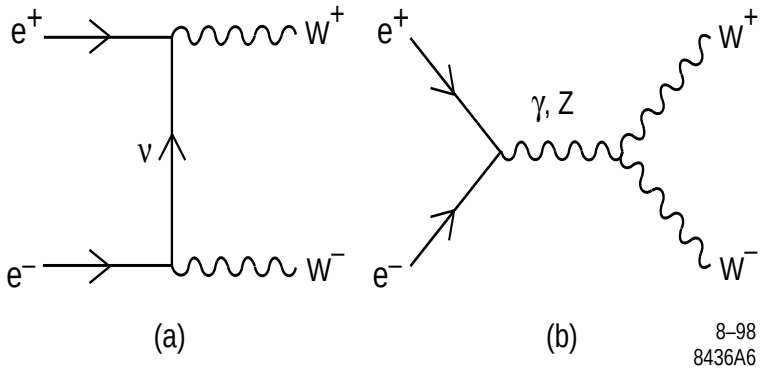

Figure 30: Feymann diagrams mediating the reaction $e^+e^- \to W^+W^-$.

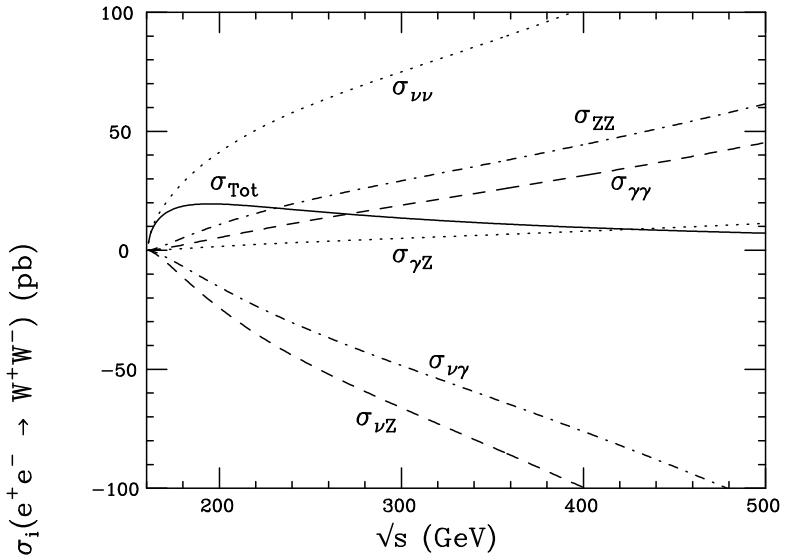

Figure 31: The energy dependence of each separate contribution as labeled, as well as the total cross section for W pair production in e^+e^- collisions.

The cross section for $e^+e^- \to W^+W^-$ is quite large, given roughly by 20 units of R where R is defined in Section 2.1, and presents a serious source of background for new physics signatures in high energy e^+e^- collisions. However, if polarized beams are available, this cross section can be substantially reduced by adjusting the initial electron beam polarization to be mainly right-handed. In addition, the angular dependence of this reaction is peaked in the forward direction due to the t-channel pole, with the W^+ being produced preferentially along the e^+ direction. This peaking sharpens with increasing center of mass energy and may also be used to differentiate W pair production from new physics.

Potential deviations from the SM form of the WWV trilinear couplings are parameterized in terms of the most general Lorentz invariant effective Lagrangian [61]

$$\mathcal{L}^{eff}_{WWV} = g_{WWV}\Big[ig_1^V(W^\dagger_{\mu\nu}W^\mu V^\nu - W^\dagger_\mu V_\nu W^{\mu\nu}) + i\kappa_V W^\dagger_\mu W_\nu V^{\mu\nu} + \frac{i\lambda_V}{M_W^2}W^\dagger_{\lambda\mu}W^\mu_\nu V^{\nu\lambda} - g_4^V W^\dagger_\mu W_\nu(\partial^\mu V^\nu + \partial^\nu V^\mu) \tag{132}$$

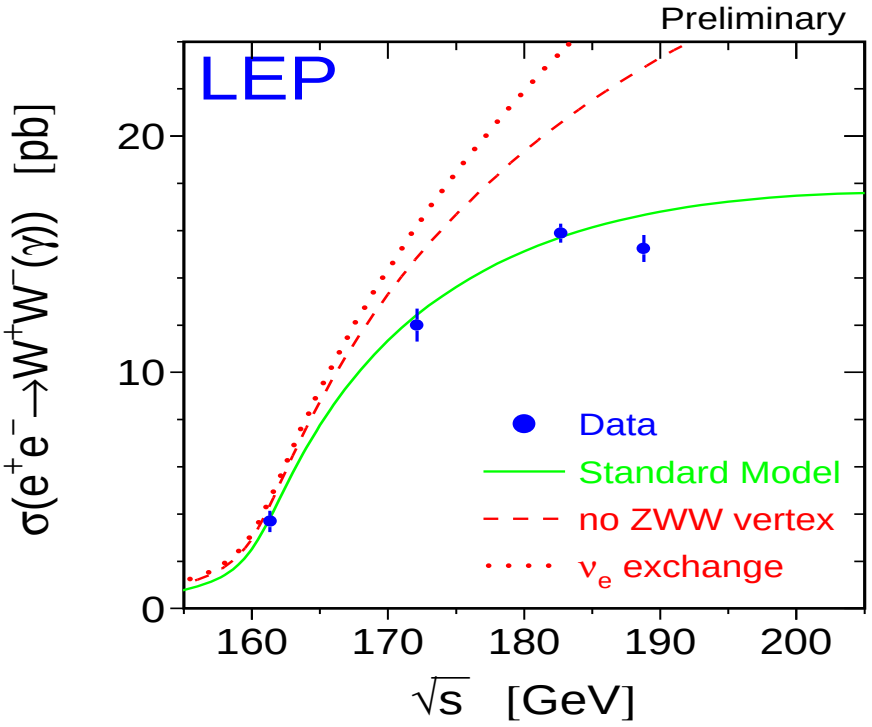

Figure 32: Energy dependence of the cross section for $e^+e^- \to W^+W^-$ as measured at LEP II. From Ref.[49].

$$+g_5^V \epsilon^{\mu\nu\rho\sigma}(W_\mu^\dagger \overset{\leftrightarrow}{\partial}_\rho W_\nu)V_\sigma + \tilde{\kappa}_V W_\mu^\dagger W_\nu \tilde{V}^{\mu\nu} + \frac{i\tilde{\lambda}_V}{M_W^2} W_{\lambda\mu}^\dagger W_\nu^\mu \tilde{V}^{\nu\lambda}\Big] ,$$

where $W_{\mu\nu} \equiv \partial_\mu W_\nu - \partial_\nu W_\mu$, $V_{\mu\nu} \equiv \partial_\mu V_\nu - \partial_\nu V_\mu$, $(A \overset{\leftrightarrow}{\partial}_\mu B) \equiv A(\partial_\mu B) - (\partial_\mu A)B$, and $\tilde{V}_{\mu\nu} \equiv \frac{1}{2}\epsilon_{\mu\nu\rho\sigma}V^{\rho\sigma}$. The overall normalization is defined such that $g_{WW\gamma} = -e$ and $g_{WWZ} = -e\cot\theta_w$. The coupling g_5^V violates C and P separately, while $g_4^V, \tilde{\kappa}_V$, and $\tilde{\lambda}_V$ are CP-violating. At tree-level within the SM the couplings take on the values $g_1^V = \kappa_V = 1$ and $\lambda_V = g_5^V = g_4^V = \tilde{\kappa}_V = \tilde{\lambda}_V = 0$. For on-shell photons, electromagnetic gauge invariance fixes $g_1^\gamma = 1$ and $g_5^V = 0$. Convention dictates that anomalous values of the CP-conserving couplings are denoted as $\Delta g_1^Z \equiv g_1^Z - 1$, $\Delta\kappa_V \equiv \kappa_V - 1$, λ_V, and g_5^Z. The C and P-conserving terms in the effective $WW\gamma$ interaction correspond to the lowest-order terms of an electromagnetic multipole expansion via

$$\begin{aligned} Q_W &= e g_1^\gamma , \\ \mu_W &= \frac{e}{2M_W}(g_1^\gamma + \kappa_\gamma + \lambda_\gamma) , \\ q_W &= -\frac{e}{M_W^2}(\kappa_\gamma - \lambda_\gamma) , \end{aligned} \tag{133}$$

where Q_W represents the charge, μ_W the magnetic dipole moment, and q_W the electric quadrupole moment of the W-boson. Whereas the two CP-violating couplings are related to the electric dipole moment, d_W, and magnetic quadrupole moment, $\tilde{Q}_W$, of the W by

$$\begin{aligned} d_W &= \frac{e}{2M_W}(\tilde{\kappa}_\gamma + \tilde{\lambda}_\gamma) , \\ \tilde{Q}_W &= -\frac{e}{M_W^2}(\tilde{\kappa}_\gamma - \tilde{\lambda}_\gamma) . \end{aligned} \tag{134}$$

It is important to keep in mind that these parameterized couplings are form factors and hence are functions of q^2, *e.g.*, $\lambda(q^2) = \lambda(1 + q^2/\Lambda^2)^{-n}$, where q is the momentum transfer, Λ is the form factor scale, and $n = 2$ for WWV couplings. Other parameterizations of these triple gauge boson couplings can be found in Ref. [62].

In any model with new physics that couples to the W, anomalous trilinear couplings will be induced. However, theoretical arguments suggest that the expected values of the induced couplings are small. Several general analyses have been performed [63] where the contributions of new physics to these couplings have been parameterized by both linear and non-linear effective Lagrangians. In either case, the resulting anomalous couplings are found to be suppressed

by factors of (M_W^2/Λ^2), where Λ is the scale of the new interactions. For new physics at the TeV scale or above, this leads to typical values of the anomalous couplings of 10^{-2} or less. In the SM, loop contributions generate these anomalous couplings at the level of $\sim 10^{-3}$,[64] and supersymmetric contributions yield [65] similarly small values.

Corresponding trilinear $ZZ\gamma$ and $Z\gamma\gamma$ couplings are not present in the SM, but may also arise from non-standard interactions. In this case, the most general Lorentz invariant Lagrangian involving one on-shell Z-boson and one on-shell photon is [61] (where $V = Z$ or γ is not necessarily on on-shell)

$$\mathcal{L}_{ZV\gamma} = -ie\left[\left(h_1^V F^{\mu\nu} + h_3^V \tilde{F}^{\mu\nu}\right) Z_\mu \frac{(\Box + M_V^2)}{M_Z^2} V_\nu \right. \\ \left. + \left(h_2^V F^{\mu\nu} + h_4^V \tilde{F}^{\mu\nu}\right) Z^\alpha \frac{(\Box + M_V^2)}{M_Z^2} \partial_\alpha \partial_\mu V_\nu \right], \qquad (135)$$

where $F^{\mu\nu}$ is the photon field strength tensor and clearly, $h_i^V = 0$ in the SM. $h_{1,2}^V$ are CP-violating. Here, the $(\Box - M_V^2)/M_Z^2$ factor is implied by Bose symmetry and indicates that these couplings arise from higher dimensional operators than in the WWV case. It is hence expected that they should be quite suppressed and take on very small values in any new physics scenario. These couplings are related to the magnetic and electric dipole and quadrupole transition moments of the Z by

$$\begin{aligned} \mu_Z &= -\frac{e}{\sqrt{2}M_Z}\frac{E_\gamma^2}{M_Z^2}(h_1^Z - h_2^Z)\,, \\ d_Z &= -\frac{e}{\sqrt{2}M_Z}\frac{E_\gamma^2}{M_Z^2}(h_3^Z - h_4^Z)\,, \\ Q_Z &= -\frac{2\sqrt{10}e}{M_Z^2}h_1^Z\,, \\ \tilde{Q}_Z &= -\frac{2\sqrt{10}e}{M_Z^2}h_3^Z\,, \end{aligned} \qquad (136)$$

where E_γ represents the photon energy. Due to the higher dimension operators in this case, $n = 3\,, 4$ for $h_3^V\,, h_4^V$, respectively, in the q^2 dependent form factor for these couplings.

We now examine the current and prospective bounds placed on the anomalous trilinear couplings by present and future experiments. In principle, all 14 free parameters in the Lagrangian of Eq. (131) are simultaneously present in W pair production at LEPII. It would be an impossible and meaningless

exercise to consider all these parameters at once and thus physical insights are employed to suggest which couplings are the most likely to have observable effects at LEPII. The data is then analyzed with the following assumptions: (i) Only the CP-conserving couplings are considered as bounds on the neutron electric dipole moment constrain combinations of the CP-violating interactions. (ii) Only the dimension 6 operators are considered as the higher dimension terms are more likely to be suppressed. (iii) The gauge boson self-interactions should resemble, at least approximately, those of the SM. Hence $\mathrm{SU}(2)_L \times \mathrm{U}(1)_Y$ gauge invariance is imposed and operators which would have produced large effects at LEPI/SLC are excluded. These assumptions reduce the set of free parameters to just three, Δg_1^Z , $\Delta\kappa_\gamma$, and λ_γ, with the constraints $\Delta\kappa_Z = \Delta g_1^Z - \Delta\kappa_\gamma \tan^2\theta_w$ and $\lambda_Z = \lambda_\gamma$. The preliminary combined results [66] from LEPII (including single W production as well) are presented in Fig. 33, where only one parameter is taken to be non-zero at a time. We see that all three couplings are consistent with zero at this level of sensitivity, which is $1-2$ orders of magnitude above the theoretical expectations. We also note that the momentum dependent form factors for these couplings are not numerically relevant at LEPII. The CP-conserving $ZV\gamma$ interactions are also constrained by LEPII via the reactions $e^+e^- \to q\bar{q}\gamma, \nu\bar{\nu}\gamma$. The current bounds [66] are $|h_3^\gamma| < 0.34$ and $|h_4^\gamma| < 0.55$, assuming a form factor scale of $\Lambda = 1$ TeV. We note that the $WW\gamma$ and WWZ couplings may be probed separately via the processes $e^+e^- \to \nu\bar{\nu}\gamma$ and $e^+e^- \to \nu\bar{\nu}Z$, respectively, if the possibility of anomalous $ZV\gamma$ interactions are neglected.

The trilinear gauge couplings are also constrained by diboson production at the Tevatron. The effect of these interactions is to increase the diboson production cross section and to enhance the p_T spectrum of the gauge bosons at large values of p_T. At hadron colliders it is important to include the form factor dependence of the couplings in order to preserve unitarity, taking $q^2 = \hat{s}$ where $\sqrt{\hat{s}}$ is the subprocess center of mass energy. The $WW\gamma$ self-interactions are cleanly measured in $W\gamma$ production, which has the advantage of being independent of the WWZ vertex. The 95% C.L. bounds obtained [67] by D0 from such events, $-0.93 < \Delta\kappa_\gamma < 0.94\,(\lambda_\gamma = 0)$ and $-0.31 < \lambda_\gamma < 0.29\,(\Delta\kappa_\gamma = 0)$ taking $\Lambda = 1.5$ TeV, are not as stringent as those obtained at LEPII, but are free of the assumptions discussed above. The results from the 2-parameter fit are displayed in Fig. 34(a). Also shown in the figure for comparison are the constraints from the observation of the rare inclusive decay $B \to X_s\gamma$ by CLEO.[68] We see that the case of $\lambda_\gamma = \kappa_\gamma = 0$ is excluded at the 95% C.L. The inclusion of the WW and WZ production channels with the $W\gamma$ events increases the statistical sensitivity, but necessarily introduces a dependence on the WWV vertex. Employing the same set of assumptions as used at LEPII

yields [67] the 95% C.L. bounds $-0.33 < \Delta\kappa_\gamma < 0.46$ and $|\lambda_\gamma| < 0.21$ from D0. Combining these results with those from LEPII gives

$$\begin{aligned} -0.15 < \Delta\kappa_\gamma < 0.41\,, \\ -0.16 < \lambda_\gamma < 0.10\,, \end{aligned} \tag{137}$$

at 95% C.L. We note that the Tevatron analysis is not very sensitive to Δg_1^Z. Similarly, the $ZV\gamma$ interactions are constrained via $Z\gamma$ production at the Tevatron. Combining the $e^+e^-\gamma/\mu^+\mu^-\gamma$ and $\nu\bar{\nu}\gamma$ channels, D0 finds [67]

$$|h_3^{Z,\gamma}| < 0.37\,, \qquad |h_4^{Z,\gamma}| < 0.05\,, \tag{138}$$

at 95% C.L., taking $\Lambda = 750\,\mathrm{GeV}$. The 95% C.L. allowed contours in the $h_3^{Z,\gamma} - h_4^{Z,\gamma}$ plane are presented in Fig. 34(b) for the various final states with $\Lambda = 500$ and 750 GeV. The increased sensitivity of the $\nu\bar{\nu}\gamma$ channel is illustrated in this figure.

A comparison from Ref. [69] of the anticipated level of sensitivity that can be reached on $\Delta\kappa_\gamma$ and λ_γ at 95% C.L. from a variety of processes at the Tevatron, LEPII, LHC, and NLC is presented in Fig. 35. We see from the figure that the region where one expects the effects of new physics to appear, as discussed above, will only start to be probed at the LHC, and the predicted level of the SM loop corrections can only be tested at a higher energy linear collider.

5 Summary

We have reviewed the basic components of the SM and the experiments which have probed them. However, due to time constraints there are many features of the SM which we have omitted, such as heavy quark decays, the GIM mechanism, and rare and forbidden processes. Such processes, as well as the precision measurements discussed here, provide powerful constraints on potential scenarios of new physics.[70]

In summary we see that all elements of the SM enjoy an outstanding agreement with an overwhelming set of experimental data, even at the quantum level. In fact searches for new physics is tightly constrained by the success of the SM. However, in light of the many questions that remain unanswered by the theoretical framework of the SM, we hope that unexpected discoveries reveal themselves in the near future!

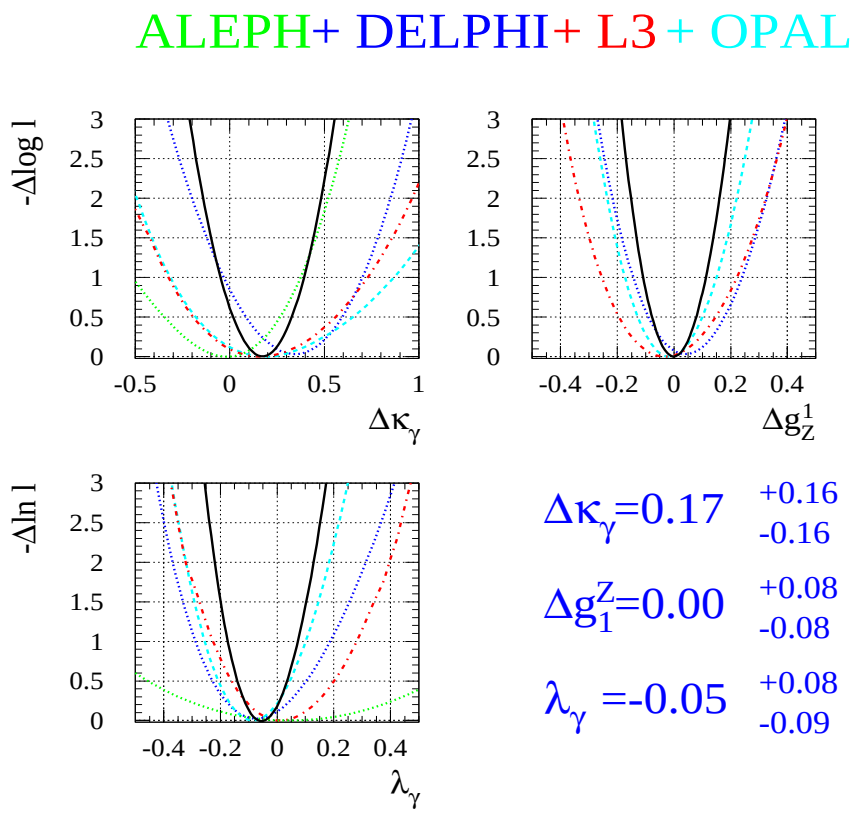

Figure 33: Log likelihood distributions and allowed ranges for the anomalous trilinear coupling parameters $\Delta\kappa_\gamma$, Δg_1^Z, and λ_γ as determined at LEPII. From Ref. [66].

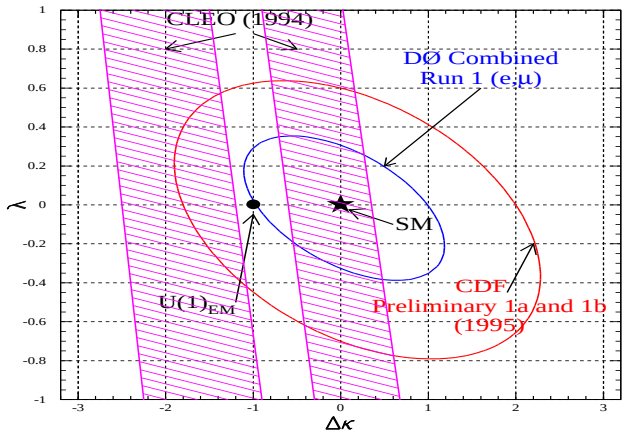

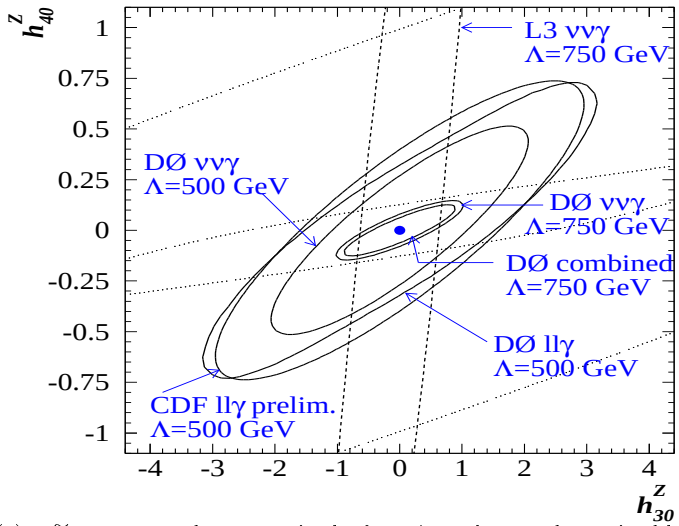

Figure 34: (a) 95% C.L. allowed contours in the $\lambda_\gamma - \Delta\kappa_\gamma$ plane as determined by CDF and D0 from $W\gamma$ production (taking $\Lambda = 1.5$ TeV). 95% C.L. allowed bands as determined by CLEO from $B \to X_s\gamma$. (b) 95% C.L. allowed contours in the $h_3^Z - h_4^Z$ plane for the various final state channels; the values of Λ and the experiments are as labeled. From Ref. [67].

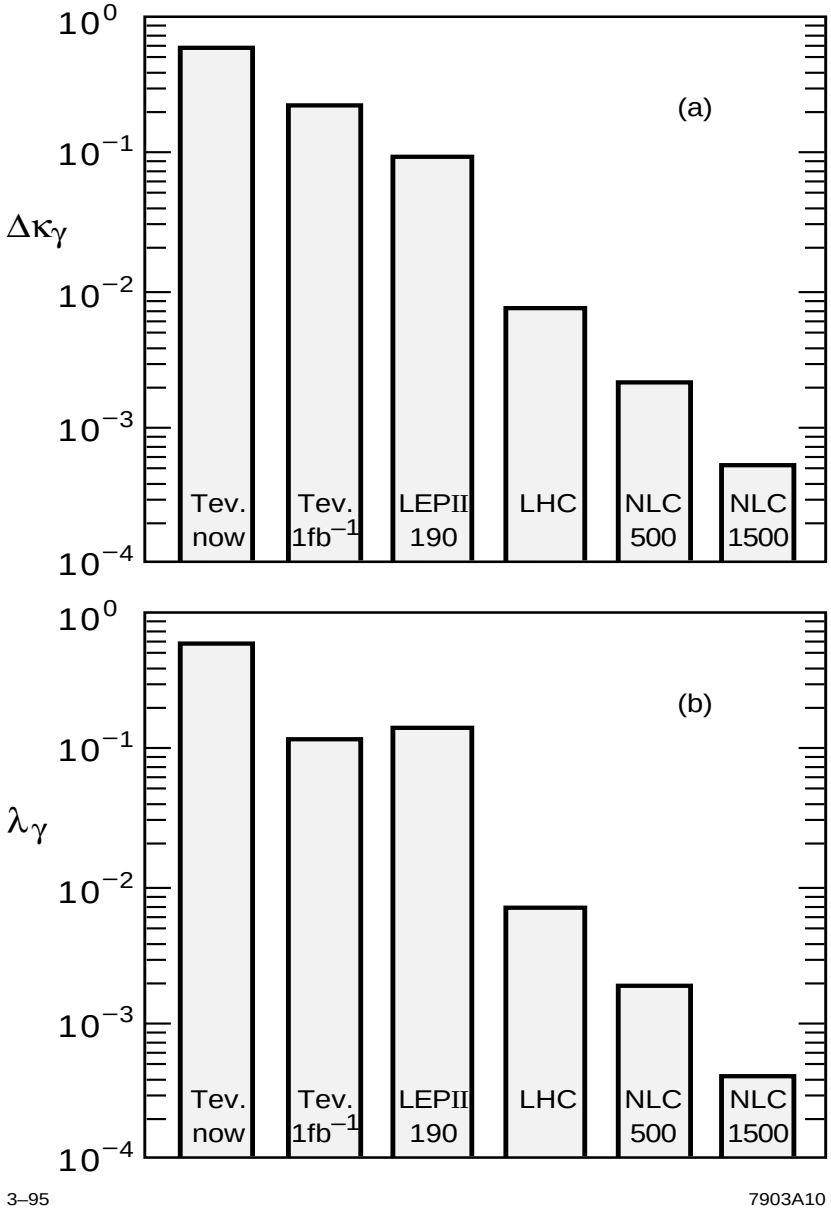

Figure 35: Comparison of 95% C.L. constraints on $\Delta\kappa_\gamma$ and λ_γ at present and future accelerators. From [69].

Acknowledgments

I thank P. Burrows and T. Rizzo for their assistance in preparing these lectures and J. Bagger, the TASI staff, and the students for providing a stimulating atmosphere for the school.

References

1. S. Weinberg, Phys. Rev. Lett. **19**, 1264 (1967); Phys. Rev. **D5**, 1412 (1972); A. Salam, in *Elementary Particle Theory: Relativistic Groups and Analyticity (Nobel Symposium No. 8*, ed. N. Svartholm (Almqvist and Wiksell, Stockholm, 1968); S. Glashow, Nucl. Phys. **22**, 579 (1961).
2. For some original work and reviews see, D.J. Gross and F. Wilczek Phys. Rev. **D8**, 3633 (1973); Phys. Rev. **D9**, 908 (1974); H.D. Politzer, Phys. Rep. **14C**, 129 (1974); F. Wilczek, Ann. Rev. Nucl. Part. Sci, **32**, 177 (1982).
3. M. Gell-Mann, Phys. Rev. **125**, 1067 (1962).
4. P.W. Higgs, Phys. Rev. Lett. **12**, 132 (1964); T.W.B. Kibble, Phys. Rev. **155**, 1554 (1967); G.S. Guralnik, C.R. Hagen, and T.W.B. Kibble, Phys. Rev. Lett. **13**, 585 (1956).
5. G. 't Hooft, Nucl. Phys. **B35**, 167 (1971); G 't Hooft and M.T. Veltman, Nucl. Phys. **B44**, 189 (1973); B.W. Lee and J. Zinn-Justin, Phys. Rev. **D5**, 3121 (1972).
6. N. Cabibbo, Phys. Rev. Lett. **10**, 531 (1963); M. Kobayashi and T. Maskawa, Prog. Theor. Phys. **49**, 652 (1973).
7. For reviews, see for example, A.S. Kronfeld and P.B. Mackenzie, Ann. Rev. Nucl. and Part. Sci. **43**, 793 (1993); H. Wittig, Int. J. Mod. Phys. **A12**, 4477 (1997).
8. For recent reviews see, P.N. Burrows, in lectures given at the *XXIVth SLAC Summer Institute*, Stanford, CA, August 1996, hep-ex/9705013; S. Bethke, in*QCD Euroconference 97*, Montpellier, France, July 1997, hep-ex/9710030.
9. G. Hanson *et al.*, Mark I Collaboration, Phys. Rev. Lett. **35**, 1609 (1975).
10. G. Sterman and S. Weinberg, Phys. Rev. Lett. **39**, 1436 (1977).
11. R.F. Schwitters *et al.*, Mark I Collaboration, Phys. Rev. Lett. **35**, 1320 (1975).
12. M. Althoff *et al.*, TASSO Collaboration, Z. Phys. **C22**, 307 (1984).
13. See, for example, V. Barger and R.J.N. Phillips, *Collider Physics*, Frontiers in Physics, Vol. 71 (Addison-Wesley, Redwood City, CA 1987).
14. R. Marshall, Z. Phys. **C43**, 595 (1989).

15. L.R. Surguladze and M.A. Samuel, Phys. Rev. Lett. **66**, 560 (1991); S.G. Gorishny, A. Kataev, and S.A. Larin, Phys. Lett. **B259**, 114 (1991).
16. R. Brandeik *et al.*, TASSO Collaboration, Phys. Lett. **86B**, 243 (1979); D.P. Barber *et al.*, Mark J Collaboration, Phys. Rev. Lett. **43**, 830 (1979); Ch. Berger *et al.*, PLUTO Collaboration, Phys. Lett. **86B**, 418 (1979); W. Bartel *et al.*, JADE Collaboration, Phys. Lett. **91B**, 142 (1980).
17. S.L. Wu, Phys. Rep. **107**, 59 (1984).
18. J. Ellis and I. Karliner, Nucl. Phys. **B148**, 141 (1979).
19. K. Abe *et al.*, SLD Collaboration, Phys. Rev. **D55**, 2533 (1997).
20. W. Braunschweig *et al.*, TASSO Collaboration, Z. Phys. **C42**, 17 (1989), **C44**, 365 (1989).
21. P.N. Burrows, talk presented at *XXIXth International Conference on High Energy Physics, ICHEP98*, Vancouver, CA, July 1998.
22. L. Dixon and A. Singer, Phys. Rev. Lett. **78**, 811 (1997), Phys. Rev. **D56**, 4031 (1997).
23. R. Barate *et al.*, ALEPH Collaboration, Z. Phys. **C76**, 1 (1997).
24. C. Caso *et al.*, Particle Data Group, E. Phys. J. **C3**, 1 (1998).
25. Y. Dokshitzer, talk presented at *XXIXth International Conference on High Energy Physics, ICHEP98*, Vancouver, CA, July 1998.
26. M. Albrow, in lectures given at the *XXIVth SLAC Summer Institute*, Stanford, CA, August 1996.
27. S. Ellis, Z. Kunszt, and D. Soper, Phys. Rev. Lett. **64**, 2121 (1990); F. Aversa *et al.*, Phys. Rev. Lett. **65**, 401 (1990); W.T. Giele, E.W.N. Glover, and D.A. Kosower, Nucl. Phys. **B403**, 633 (1993).
28. F. Abe *et al.*, CDF Collaboration, Phys. Rev. Lett. **77**, 438 (1996).
29. B. Abbott *et al.*, D0 Collaboration, Phys. Rev. Lett. **80**, 666 (1998).
30. J. Huston *et al.*, Phys. Rev. Lett. **77**, 444 (1996).
31. A. Jeffrey *et al.*, in *Conference on Precision Electroweak Measurements*, Branschweig, Germany, 1996.
32. J.H. Kühn and M. Steinhauser, hep-ph/9802241; M. Steinhauser, Phys. Lett. **B429**, 158 (1998).
33. K.G. Chetyrkin, J.H. Kühn, and M. Steinhauser, Phys. Lett. **B371**, 93 (1996); Nucl. Phys. **B482**, 213 (1996), **B505**, 40 (1997).
34. M. Davier and A. Höcker, hep-ph/9805470; A. Höcker, talk presented at *XXIXth International Conference on High Energy Physics, ICHEP98*, Vancouver, CA, July 1998.
35. For a recent update, see, A.I. Studenikin, hep-ph/9808219.
36. A. Czarnecki, B. Krause, and W. Marciano, Phys. Rev. Lett. **76**, 3267 (1996); Phys. Rev. **D52**, 2629 (1995); T. Kukhto *et al.*, Nucl. Phys.

B371, 567 (1992); S. Persis, M. Perrottet, and E. de Rafael, Phys. Lett. **B355**, 523 (1995).
37. P. Schwinberg, R. VanDyck, and H. Dehmelt, Phys. Rev. Lett. **59**, 26 (1987).
38. C. Timmermans, talk presented at *XXIXth International Conference on High Energy Physics, ICHEP98*, Vancouver, CA, July 1998.
39. J.P. Leveille, Nucl. Phys. **B137**, 63 (1978).
40. S.M. Berman and A. Sirlin, Ann. Phys. **20**, 20 (1962).
41. T. Kinoshita and A. Sirlin, Phys. Rev. **113**, 1652 (1959); S.M. Berman, Phys. Rev. **112**, 267 (1958).
42. T. van Ritbergen and R.G. stuart, hep-ph/9808283.
43. L. Michel, Proc. Phys. Soc. **A63**, 514 (1995); C. Bouchiat and L. Michel, Phys. Rev. **106**, 170 (1957).
44. G. DeGrassi, P. Gambino, and A. Sirlin, Phys. Lett. **B354**, 188 (1997); G. DeGrassi *et al.*, Phys. Lett. **B418**, 209 (1998); G. Weiglein, hep-ph/9807222.
45. See, M. Consoli and W. Hollik; in *LEP Yellow Book*, CERN 89-08 (1989); and G. Burgers and F. Jegelehner, *ibid.*
46. For details see, W. Hollik, hep-ph/9602380.
47. M. Veltman, Nucl. Phys. **B123**, 89 (1977); M.S. Chanowitz, M.A. Furman, and I. Hinchliffe, Phys. Lett. **B78**, 285 (1978).
48. See, W. Hollik, hep-ph/9711492, and references therein.
49. D. Karlen, talk presented at *XXIXth International Conference on High Energy Physics, ICHEP98*, Vancouver, CA, July 1998; The LEP Collaborations, the LEP Electroweak Working Group, and the SLD HEavy Flavor and Electroweak Groups, CERN-PPE/97-154 (1997).
50. K.S. McFarland *et al.*, (NUTEV Collaboration) hep-ex/9806013.
51. E.A. Paschos and L. Wolfenstein, Phys. Rev. **D7**, 91 (1973).
52. D. Trielle, talk presented at *XXIXth International Conference on High Energy Physics, ICHEP98*, Vancouver, CA, July 1998.
53. M.E. Peskin and T. Takeuchi, Phys. Rev. Lett. **65**, 964 (1990); Phys. Rev. **D46**, 381 (1992); W. Marciano and J. Rosner, Phys. Rev. Lett. **65**, 2963 (1990); D. Kennedy and P. Langacker, Phys. Rev. Lett. **65**, 2967 (1990); Phys. Rev. **D44**, 1591 (1991).
54. G. Altarelli and R. Barbieri, Phys. Lett. **B253**, 161 (1990).
55. D.C. Kennedy and B.W. Lynn, Nucl. Phys. **B322**, 1 (1989).
56. K. Baird, talk presented at *XXIXth International Conference on High Energy Physics, ICHEP98*, Vancouver, CA, July 1998.
57. J.A. Bagger, K.T. Marchev, D.M. Pierce, and R.-J. Zhang, Nucl. Phys. **B491**, 3 (1997). For details see, D. Pierce, these proceedings.

58. M. Golden and L. Randall, Nucl. Phys. **B361**, 3 (1991).
59. R. Sundrum and S. Hsu, Nucl. Phys. **B391**, 127 (1993); R. Sundrum, Nucl. Phys. **B395**, 60 (1993); M. Luty and R. Sundrum, Phys. Rev. Lett. **70**, 529 (1993); T. Applequist and J. Terning, Phys. Lett. **B315**, 139 (1993); E. Gates and J. Terning, Phys. Rev. Lett. **67**, 1840 (1991).
60. I. Maksymyk, C.P. Burgess, and D. London, Phys. Rev. **D50**, 529 (1994); C.P. Burgess *et al.*, Phys. Lett. **B326**, 276 (1994).
61. K. Hagiwara, K. Hikasa, R.D. Peccei, D. Zeppenfeld, Nucl. Phys. **B282**, 253 (1987); H Aihara *et al.*, in *Electroweak Symmetry Breaking and New Physics at the TeV Scale*, ed. T. Barklow *et al.* (World Scientific, Singapore 1996); J. Ellison and J. Wudka, hep-ph/9804322.
62. K. Hagiwara *et al.*, Phys. Rev. **D48**, 2182 (1993); G. Gounaris *et al.*, in *Proceedings of the CERN Workshop on LEP II Physics*, ed. G. Altarelli *et al.*, CERN 96-01 (1996).
63. A. De Rújula, M.B. Gavela, P. Hernández, and E. Massó, Nucl. Phys. **B384**, 3 (1992); K. Hagiwara, S. Ishihara, R. Szalapski, and D. Zeppenfeld, Phys. Lett. **B283**, 353 (1992), Phys. Rev. **D48**, 2182 (1993); C. Arzt, M. Einhorn, and J. Wudka, Phys. Rev. **D49**, 1370 (1994); Nucl. Phys. **B433**, 41 (1994); T. Applequist and G.-H. Wu, Phys. Rev. **D48**, 3235 (1993); S. Dawson and G. Valencia, Phys. Rev. **D49**, 2188 (1994); J. Bagger, S. Dawson, and G. Valencia, Nucl. Phys. **B399**, 364 (1993).
64. E.N. Argyres, Nucl. Phys. **B391**, 23 (1993); J. Papavassiliou and K. Philoppides, Phys. Rev. **D48**, 4255 (1993).
65. G. Couture, J.L. Hewett, J.N. Ng, and T.G. Rizzo, Phys. Rev. **D38**, 860 (1988), **D36**, 859 (1987); T.G. Rizzo, Phys. Rev. **D46**, 3894 (1992); E.N. Argyres, A.B. Lahanas, C.G. Papadopoulos, V.C. Spanos, Phys. Lett. **B383**, 63 (1996); A Arhib, J.L. Kneur, and G. Moultaka, Phys. Lett. **B376**, 127 (1996); M. Kitahara, Eur. Phys. J. **C4**, 661 (1998).
66. H.T. Phillips, talk presented at *XXIXth International Conference on High Energy Physics, ICHEP98*, Vancouver, CA, July 1998.
67. H.T. Diehl, talk presented at *XXIXth International Conference on High Energy Physics, ICHEP98*, Vancouver, CA, July 1998, hep-ex/9810006; R.J. Madaras, talk given at *XVIII International Conference on Physics in Collision*, Frascati, Italy, June 1998, hep-ex/9808021.
68. M.S. Alam *et al.*, CLEO Collaboration, Phys. Rev. Lett. **74**, 2885 (1995).
69. T. Barklow *et al.*, in *Particle Physics: Perspectives and Opportunities*, ed. R. Peccei *et al.*(World Scientific, Singapore, 1995); S. Kuhlman *et al.*, *Physics and Technology of the Next Linear Collider: A Report Submitted to Snowmass '96*, hep-ex/9605011.

70. J.L. Hewett, T. Takeuchi, and S. Thomas, in *Electroweak Symmetry Breaking and New Physics at the TeV Scale*, (World Scientific, Singapore 1996), ed. T. Barklow *et al.*, hep-ph/9603391.